EXPLORING CONDUCTIVE, SELECTIVE AND STABLE POLYMERIC MEMBRANES FOR REDOX FLOW BATTERIES

by

Hao Wang

A dissertation submitted to the Faculty of the University of Delaware in partial fulfillment of the requirements for the degree of Doctor of Philosophy in Chemical Engineering

Fall 2019

EXPLORING CONDUCTIVE, SELECTIVE AND STABLE POLYMERIC MEMBRANES FOR REDOX FLOW BATTERIES

by

Hao Wang

Approved: _____
Eric M. Furst, Ph.D.
Chair of the Department of Chemical and Biomolecular Engineering

Approved: _____
Levi T. Thompson, Ph.D.
Dean of the College of Engineering

Approved: _____
Douglas Doren, Ph.D.
Interim Vice Provost for Graduate and Professional Education and Dean of the Graduate College

I certify that I have read this dissertation and that in my opinion it meets the academic and professional standard required by the University as a dissertation for the degree of Doctor of Philosophy.

Signed: _____

Yushan Yan, Ph.D.
Professor in charge of dissertation

I certify that I have read this dissertation and that in my opinion it meets the academic and professional standard required by the University as a dissertation for the degree of Doctor of Philosophy.

Signed: _____

Thomas H. Epps, III, Ph.D.
Member of dissertation committee

I certify that I have read this dissertation and that in my opinion it meets the academic and professional standard required by the University as a dissertation for the degree of Doctor of Philosophy.

Signed: _____

Arthi Jayaraman, Ph.D.
Member of dissertation committee

I certify that I have read this dissertation and that in my opinion it meets the academic and professional standard required by the University as a dissertation for the degree of Doctor of Philosophy.

Signed: _____

Erin Setzler, Ph.D.
Member of dissertation committee

ACKNOWLEDGMENTS

At the beginning, I would like to express my deepest gratitude to my advisor, Dr. Yushan Yan. He is always a great model for me. His passion for science, his earnest for work, and his kindness to students deeply influenced me in the past five years and will positively impact me in the future. I first met Dr. Yan when I was in China, which is long before I joined the University of Delaware. This encounter was about six years ago, but I still remember his presentation of chemically stable phosphonium cations for anion exchange membranes, his vision of future fuel cell vehicles, the whole picture of renewable energy sources and redox flow batteries for energy storage. Those were super cool to me as a young student in the bachelor stage. I am lucky to eventually become his student and work on these impactful phosphonium cations and redox flow batteries. Without his support and help, this dissertation would not be possible. Not only did Dr. Yan funded me, he also provided excellent guidance on my research. One thing, in particular, was that he carefully reviewed my experimental plan and walked me through the whole experiment when I was trying to operate a dangers Grignard reaction for the first time. He is also an open-minded advisor and always hopes the best for his student. He firmly supported me to pursue a successful career and a meaningful life.

I would also like to thank my group members for their company in my study and useful discussions on the research. In particular, Dr. Junhua Wang guided me through my early synthesis experiments; Dr. Yun Zhao shared his experience of reinforced membrane casting with me; Dr. Ke Gong and Dr. Bingzi Zhang conducted wonderful researches of double-membrane cerium redox flow battery and phosphonium cations

respectively for me to future investigate; Dr. Keda Hu and Dr. Lan Wang participated in the discussion of polymer degradation mechanism; and Dr. Brain Setzler provided meaningful insights on electrochemistry. Besides them, I would also like to thank Dr. Shuang Gu, Dr. Xuan Yang, Jared Nash, Dr. Marco Dunwell, Xiaoya Ma, Dr. Jie Zheng, Dr. Qianrong Fang, Dr. Mariah Woodroof, Dr. Santiago Rojas-Carbonell, Lin Shi, Dr. Reza Abbasi, Saisai Lin, Dr. Teng Wang, Dr. Hui Duan, Dr. Wenjuan Shi, Dr. Junwu Xiao, Dr. Robert Kaspar, Dr. Mingchuan Luo, Dr. Yan Wang, Dr. Zhongbin Zhuang, Dr. Jarrid Wittkopf, Dr. Stephen Giles, Dr. Andrew Tibbits, Dr. Hongxia Guo, Jon Wilson, Stephanie Matz, Catherine Weiss, Nick Oliveira for their support and hard work on research.

I would also like to thank Dr. Thomas H. Epps, III, Dr. Arthi Jayaraman, and Dr. Erin Setzler for being my dissertation committee members and providing me with useful feedback on my research.

At last, I would like to thank my family members. Their dedication and selfless supports are always there to comfort me, and their encouragement is always the greatest power for me to make progress.

TABLE OF CONTENTS

LIST OF TABLES xii
LIST OF FIGURES xiv
ABSTRACT xx

Chapter

1 INTRODUCTION 1

1.1 Renewable Energy and Redox Flow Batteries 1

1.1.1 Renewable Energy 1
1.1.2 Energy Storage 2
1.1.3 Redox Flow Batteries 4
1.1.4 Aqueous Redox Flow Batteries 6
1.1.5 Vanadium Redox Flow Batteries 8
1.1.6 Zinc Cerium Double Membrane Redox Flow Batteries 9

1.2 Ion-Exchange Membranes 11

1.2.1 Ion-Exchange Membranes for Redox Flow Batteries 11
1.2.2 Chemical Stability of Ion-Exchange Membranes 12
1.2.3 Conductivity of Ion-Exchange Membranes 13
1.2.4 Selectivity of Ion-Exchange Membranes 15
1.2.5 Cation-Exchange Membranes for Redox Flow Batteries 16
1.2.6 Anion-Exchange Membranes for Redox Flow Batteries 19

1.3 Research Aim and Objectives 22
1.4 Outline of the Dissertation 23

2 INVESTIGATION OF POLYMER BACKBONE DEGRADATION IN CERIUM ELECTROLYTES 26

2.1 Introduction 26
2.2 Materials and Methods 28

2.2.1 Materials 28
2.2.2 Experimental Methods 28

2.2.2.1 Synthesis of Hexafluoropropylidene Polybenzimidazole (F_6PBI) 28
2.2.2.2 Membrane Fabrication 28
2.2.2.3 Polymer Backbone Oxidative Stability Test in Cerium(IV) Solution 29
2.2.2.4 NMR Spectroscopy Characterization 29

2.3 Results and Discussion 29

2.3.1 Polymer Backbone Degradation in Cerium (IV) and $HClO_4$ Solution 29
2.3.2 Poly(p-phenylene oxide) Degradation Mechanism 32
2.3.3 Polysulfone Degradation Mechanism 36

2.4 Conclusion 39

3 INVESTIGATION AND DESIGN OF OXIDATIVELY STABLE MEMBRANES FOR CERIUM REDOX FLOW BATTERIES 40

3.1 Introduction 40
3.2 Materials and Methods 42

3.2.1 Materials 42
3.2.2 Synthesis 43

3.2.2.1 Synthesis of Hexafluoropropylidene Polybenzimidazole (F_6PBI) 43
3.2.2.2 Synthesis of Iodobutanol Tris(2,4,6-trimethylphenyl)phosphonium ($IBTTMePP^+$) 43
3.2.2.3 Synthesis of Butanol Tris(2,4,6-trimethylphenyl)phosphonium Functionalized Hexafluoropropylidene Polybenzimidazole (TTMePP-PBI) 43
3.2.2.4 Synthesis of (4-(chloromethyl)benzyl)tris(2,4,6-trimethoxyphenyl)phosphonium Chloride ($CBTTMPP^+Cl^-$) 44
3.2.2.5 Synthesis of Tris(2,4,6-trimethoxyphenyl)phosphonium Functionalized Hexafluoropropylidene Polybenzimidazole (TTMPP-PBI) 44

3.2.3 Experimental Methods 45

3.2.3.1 Polymer Backbone Screening Test in Cerium(IV) Electrolyte 45
3.2.3.2 Membrane Fabrication 45
3.2.3.3 Reinforced Membrane Fabrication 45
3.2.3.4 Ion Exchange Capacity (IEC) of Membranes 46
3.2.3.5 Water Uptake (WU) and Swelling Ratio (SR) of Membranes 46
3.2.3.6 Anion (OH^- and ClO_4^-) Conductivity Measurement 47
3.2.3.7 Oxidative Stability Test in Cerium (IV) Aqueous Solution 47

3.3 Results and Discussion 47

3.3.1 Polymer Backbone Stability in Cerium (IV) and $HClO_4$ Solution 47
3.3.2 Tris(2,4,6-trimethylphenyl)phosphonium Functionalized Polybenzimidazole (TTMePP-PBI) Membrane 48
3.3.3 Tris(2,4,6-trimethoxyphenyl)phosphonium Functionalized Polybenzimidazole (TTMPP-PBI) Membrane 52
3.3.4 Characterization of Phosphonium Functionalized Polybenzimidazole Membranes 58
3.3.5 Membrane Chemical Stability in Cerium (IV) Electrolyte 60

3.4 Conclusion 66

4 HIGHLY CONDUCTIVE AND STABLE PHOSPHONIUM POLYBENZIMIDAZOLE MEMBRANES FOR VANADIUM REDOX FLOW BATTERIES 68

4.1 Introduction 69
4.2 Materials and Methods 70

4.2.1 Materials 70
4.2.2 Synthesis 71

4.2.2.1 Synthesis of Hexafluoropropylidene Polybenzimidazole (F_6PBI) 71
4.2.2.2 Synthesis of (4-(chloromethyl)benzyl)tris(2,4,6-trimethoxyphenyl)phosphonium Chloride 71
4.2.2.3 Synthesis of Tris(2,4,6-trimethoxyphenyl)phosphonium Functionalized Polybenzimidazole 71

4.2.3 Experimental Methods 71

4.2.3.1 Membrane Fabrication 71
4.2.3.2 Composite Membrane Fabrication 71
4.2.3.3 Ion-Exchange Capacity (IEC) of Membranes 72
4.2.3.4 Water Uptake (WU) and Swelling Ratio (SR) of Membranes 72
4.2.3.5 Acid Doping Level (ADL) of Membranes 72
4.2.3.6 Area Specific Resistance of Membranes 73
4.2.3.7 Vanadium Permeability 73
4.2.3.8 Vanadium Redox Flow Battery Performance 74

4.3 Results and Discussion 75

4.3.1 Polymer Synthesis and Reinforced Membrane Casting 75
4.3.2 Membrane Acid Doping Behavior, Area Specific Resistance and Vanadium Permeability 77
4.3.3 Vanadium Redox Flow Battery (VRFB) Single Cell Test 84

4.4 Conclusion 88

5 STUDY OF HIGHLY CONDUCTIVE METHYLATED POLY(BENZIMIDAZOLIUM) MEMBRANES FOR VANADIUM REDOX FLOW BATTERIES 90

5.1 Introduction 90
5.2 Materials and Methods 92

5.2.1 Materials 92
5.2.2 Synthesis 92

5.2.2.1 Synthesis of Hexafluoropropylidene Polybenzimidazole (F_6PBI) 92
5.2.2.2 Synthesis of Methylated Hexafluoropropylidene Polybenzimidazole (DMF_6PBI) 93

5.2.3 Experimental Methods 93

5.2.3.1 Membrane Fabrication and Acid Doping 93
5.2.3.2 Area Specific Resistance (ASR) of Membranes 94
5.2.3.3 Mechanical Properties of Membranes 94
5.2.3.4 Viscosity Measurements of Polymer Solutions 94
5.2.3.5 Characterization of Chemical Structures 94
5.2.3.6 Sulfuric Acid Doping Level (ADL) of Membranes 94
5.2.3.7 VRFB Single Cell Test 95
5.2.3.8 Ex-situ Degradation Test 95

5.3 Results and Discussion 96

5.3.1 Preparation and Characterization of F_6PBI and DMF_6PBI Membranes 96
5.3.2 Vanadium Redox Flow Battery (VRFB) Single Cell Test 102
5.3.3 Degradation of DMF_6PBI Membrane 106

5.4 Conclusion 114

6 CONCLUSIONS AND FUTURE WORK 115

6.1 Conclusions 115
6.2 Future Work 118

6.2.1 Poly(2,5-benzimidazole) for Vanadium Redox Flow Batteries 118

6.2.1.1 Chemical Stability Issue of Polybenzimidazoles 118
6.2.1.2 Acid Doping Level of Polybenzimidazoles with Different Chemical Structures 119
6.2.1.3 Implementation of Poly(2,5-benzimidazole) for Vanadium Redox Flow Batteries 120

6.2.2 Investigation of the ePTFE reinforcement on ion-exchange membrane properties 120

6.2.2.1 Mechanical Properties of Ion-Exchange Membranes with Reinforcement 120
6.2.2.2 Water Uptake, Ion Exchange Capacity and Ion Conductivity of Ion-Exchange Membranes with Reinforcement 121
6.2.2.3 Tris(2,4,6-trimethoxyphenyl)phosphonium Functionalized Polybenzimidazole Membrane with Different Levels of ePTFE Reinforcement 121

REFERENCES 123

Appendix

A ABBREVIATIONS AND NOTATIONS 147

A.1 Abbreviations and notations 147

B BROMINATION OF METHYL-TRIS(2,4,6-TRIMETHYLPHENYL)PHOSPHONIUM 149

B.1 Bromination of Methyl-tris(2,4,6-trimethylphenyl)phosphonium 149

C SUPPLEMENTARY TABLES 154

C.1 Literature sources for Figure 4.4 154

LIST OF TABLES

Table 1.1: Commonly reported redox pairs in RFBs. The standard redox potential and typical electrolyte of each redox pair are also summarized. (This table is inspired by a published work of Dr. Ke Gong.[72]) 7

Table 1.2: Ionic mobilities of selected cations and anions at infinite dilution in water at 298 K. 14

Table 1.3: Selected list of reported cations for AEMs, some of these cation functionalized membranes were not implemented in RFB applications. (This table is inspired by a published work of Dr. Bingzi Zhang.[108]) ... 21

Table 3.1: Degree of substitution (DS), theoretical ion exchange capacity (IEC^{t}), titration measured ion exchange capacity (IEC^{md}), tensile strength, and elongation at break of pure F_6PBI membrane, TTMePP and TTMPP functionalized polybenzimidazole membranes. Error bars are standard errors of the measurements (n = 3). 60

Table 3.2: WU, OH^- conductivity, and ClO_4^- conductivity of pure F_6PBI membrane, TTMePP and TTMPP functionalized polybenzimidazole membranes. Error bars are standard errors of the measurements (n = 3). 60

Table 3.3: Accelerated membrane stability test of prepared TTMPP-PBI-3/PTFE membrane, F_6PBI membrane, Nafion 212, FAB-PK-130, and FAS-30 at 60 °C in 0.5 M cerium (IV) and 1.3 M $HClO_4$. 62

Table 4.1: Degree of substitution (DS), theoretical ion exchange capacity (IEC^{t}), titration measured ion exchange capacity (IEC^{md}), WU, tensile strength, and elongation at break of TTMPP-PBI membranes. Error bars are standard errors of the measurements (n = 3). (For reading convenience, partial data from Table 3.1 and Table 3.2 is re-used to construct this table.) 77

Table 4.2: ADL, acid weight percentage (W_A), water weight percentage (W_W), and water acid mole ratio (W/A) of F_6PBI and TTMPP-PBI-3/PTFE membranes in 1 M and 3 M sulfuric acid solution. Error bars are standard errors of the measurements (n = 3). 79

Table 5.1: ADL of DMF_6PBI (HSO_4^- form in acid) and F_6PBI in 3 M sulfuric acid. Error bars are standard errors of the measurements (n = 3). 101

Table 5.2: Properties of DMF_6PBI and F_6PBI membranes before and after VRFB cycling test. Error bars are standard errors of the measurements (n = 3). 109

Table 6.1. Tensile strength and elongation at break of TTMPP-PBI membrane and TTMPP-PBI membrane with ePTFE reinforcement. Error bars are standard errors of the measurements (n = 3). (For reading convenience, partial data from Table 3.1 is re-used to construct this table.) 121

Table B1: Partial list of investigated bromination conditions. 151

Table C1: Literature sources for Figure 4.4. Area specific resistance (ASR) are measured in different electrolytes, and the cell configurations are different for different literature. 154

LIST OF FIGURES

Figure 1.1: 2016 world power generation by source (Percentage of 24,973 TWh). Hydro sources (16.3 %) and non-hydro renewable sources (8 %) contributed 24.3 % in 2016 world power generation (Data source: 2018 key world energy statistics[8]). 2

Figure 1.2: Structure of a typical vanadium redox flow battery (VRFB), the most marketed RFB system. The negative electrolyte is comprised of V^{2+} and V^{3+} in sulfuric acid, the positive electrolyte is comprised of VO^{2+} and VO_2^+ in sulfuric acid. The middle IEM can be a proton exchange membrane (PEM) or an anion (SO_4^{2-}/HSO_4^-) exchange membrane (AEM). PEM is the most popular choice. 5

Figure 1.3: Schematic of Zn-Ce double-membrane RFB.[105] The negative electrolyte is comprised of $Zn(OH)_4^{2-}/Zn$ in NaOH solution; The middle electrolyte is a $NaClO_4$ solution; The positive electrolyte is comprised of Ce^{4+}/Ce^{3+} in $HClO_4$ solution. A CEM separates the negative electrolyte and middle electrolyte, while an AEM separates the middle electrolyte and positive electrolyte. 10

Figure 1.4: Chemical structure of Nafion series membranes. The membrane is composed of a perfluorinated polymer backbone and sulfonate functional groups. 17

Figure 1.5: Chemical structure of meta-polybenzimidazole(m-PBI). PBIs have electron pairs on the nitrogen of the benzimidazole group and can act as electron donators to form hydrogen bonds with protons or polyprotic acids. 19

Figure 2.1: Chemical structures of prepared polymer membranes: PS, PPO, PSF, and F_6PBI. While PS, PPO, and PSF were commercial polymers, F_6PBI was synthesized in our lab. 30

Figure 2.2: Remaining weight of four polymeric membranes during oxidative stability test in 0.5 M cerium (IV) and 1.3 M $HClO_4$ solution at 60 °C. Membranes were thoroughly washed and dried in a vacuum oven before weight measurements were taken. For each polymer, three membrane samples were measured, and the standard error of remaining weight is shown through the error bars. 31

Figure 2.3: HSQC spectroscopy of pristine PPO before chemical stability test in the cerium electrolyte, $CDCl_3$ as the solvent, TMS as the internal standard. 33

Figure 2.4: HSQC spectroscopy of decomposed PPO after chemical stability test in the cerium electrolyte, $CDCl_3$ as the solvent, TMS as the internal standard. 34

Figure 2.5: Stacked ^{1}H-NMR spectroscopy of (top) pristine PPO and (bottom) decomposed PPO polymeric membranes. 35

Figure 2.6: Proposed degradation mechanism of PPO polymeric membranes in cerium (IV) and $HClO_4$ electrolyte. 36

Figure 2.7: HSQC spectroscopy of pristine PSF before chemical stability test in the cerium electrolyte, $CDCl_3$ as the solvent, TMS as the internal standard. 37

Figure 2.8: HSQC spectroscopy of decomposed PSF after chemical stability test in the cerium electrolyte, $CDCl_3$ as the solvent, TMS as the internal standard. 38

Figure 2.9: Proposed degradation mechanism of PSF polymeric membranes in the cerium (IV) and $HClO_4$ electrolyte. 39

Figure 3.1: Model reactions between TTMePP and iodohexane, quaternization of TTMePP with alkyl iodide could only be achieved by adding copper as decomposition inhibitor and using high temperature to overcome the steric hindrance of TTMePP. 49

Figure 3.2: Synthesis of $IBTTMePP^+$ from TTMePP and diiodobutane. The mole ratio of TTMePP/1,4-diiodobutane was 1/29 to avoid couple linkage. Cu was added as an inhibitor to prevent alkyl iodide decomposition. 50

Figure 3.3: ^{1}H NMR spectroscopy and ^{31}P NMR spectroscopy of synthesized $IBTTMePP^{+}$ after purification. DMSO-d6 was used as the solvent. There is only one peak in ^{31}P NMR spectroscopy indicating that the purified $IBTTMePP^{+}$ was obtained. 50

Figure 3.4: Synthetic route for TTMePP-PBI polymer. $IBTTMePP^{+}$ and F_6PBI were synthesized before final linkage. The synthetic details are reported in Section 3.2.2.1, Section 3.2.2.2, and Section 3.2.2.3. 51

Figure 3.5: Picture of prepared TTMePP-PBI membrane. 52

Figure 3.6: Synthetic route for TTMPP-PBI polymer. TTMPP can be quaternized by a linker molecule. The synthetic details are reported in Section 3.2.2.1, Section 3.2.2.4, and Section 3.2.2.5. 54

Figure 3.7: ^{1}H NMR spectroscopy and ^{31}P NMR spectroscopy of purified $CBTTMPP^{+}Cl^{-}$, DMSO-d6 as the solvent. There is only one peak in ^{31}P NMR spectroscopy indicating that the purified $CBTTMPP^{+}Cl^{-}$ was obtained. 55

Figure 3.8: ^{1}H NMR spectroscopy of purified F_6PBI, DMSO-d6 as the solvent. 56

Figure 3.9: ^{1}H NMR spectroscopy of purified TTMPP-200-F_6PBI, DMSO-d6 as the solvent..... 57

Figure 3.10: Prepared TTMPP-PBI-3/PTFE reinforced membrane. ePTFE was used as reinforcement support. 58

Figure 3.11: Optical microscopy images of FAB-PK-130 and TTMPP-PBI-3/PTFE reinforced membrane before and after accelerated oxidation stability test in 0.5 M cerium (IV) and 1.3 M $HClO_4$ at 60 °C for 100 h. (a and b: FAB-PK-130 before and after; c and d: TTMPP-PBI-3/PTFE reinforced membrane before and after). 63

Figure 3.12: SEM images of TTMPP-PBI-3/PTFE membrane cross section and surface before (a) and after (b) 200 h accelerated chemical stability test (blue bar indicated the cross section; the ePTFE substrate is not suitable for freeze fracturing in liquid nitrogen, membrane samples are prepared by cut). 64

Figure 3.13: ClO_4^- conductivity of TTMPP-PBI-3/PTFE membranes before and after the accelerated stability test in 0.5 M cerium (IV) and 1.3 M $HClO_4$ at 60 °C. The conductivity of membrane samples was tested at different temperatures from 20 °C to 70 °C in DI water. Error bars are standard errors of the measurements (n = 3). 65

Figure 3.14: Infrared spectra of TTMPP-PBI-3/PTFE membranes before and after the accelerated stability test in 0.5 M cerium (IV) and 1.3 M $HClO_4$ at 60 °C. No noticeable change was observed. 66

Figure 4.1: (left) a schematic principle of the designed membrane with large phosphonium TTMPP-sulfuric acid conducting channel; (right) acid doping and proton conducting mechanism of TTMPP-PBI membranes. 75

Figure 4.2: ASR of TTMPP-PBI-3/PTFE (20 μm), F_6PBI (20 μm), and Nafion 115 (125 μm) in 1 M and 3 M sulfuric acid solutions respectively. Error bars are standard errors of the measurements (n = 3). 80

Figure 4.3: Concentration versus time at the deficiency side with TTMPP-PBI-3/PTFE (20 μm), F_6PBI (20 μm), and Nafion 115 (125 μm) membranes. Calculated permeabilities for TTMPP-PBI-3/PTFE (20 μm), F_6PBI (20 μm), and Nafion 115 (125 μm) were $(3.37 \pm 0.28)\times10^{-8}$ cm^2min^{-1}, $(3.00 \pm 1.53)\times10^{-9}$ cm^2min^{-1}, and $(1.09 \pm 0.13)\times10^{-6}$ cm^2min^{-1}, respectively. Error bars are standard errors of the measurements or calculation results (n = 3). 82

Figure 4.4: Plots of vanadium (IV) permeance (permeability/thickness) to ASR based on data obtained in this work and published literature (Details are shown in Appendix C). The red square is the prepared TTMPP-PBI-3/PTFE membrane in this work. For data collected in this work (hollow points), error bars are standard errors of the measurements or calculation results (n = 3). Some error bars are not visible, because they are very short. 84

Figure 4.5: VRFB single cell performance of TTMPP-PBI-3/PTFE (20 μm), F_6PBI (20 μm), and Nafion 115 (125 μm) membranes at various current densities (80-200 mA/cm^2): (up) coulombic efficiency, (middle) voltage efficiency, and (down) energy efficiency. Test conditions: 1.5 vanadium and 3 M sulfuric acid electrolyte 15 mL on both sides. 30 mL/min flow rate, 20 ℃ operating temperature, and cut off voltage 1.0 V – 1.7 V. At each current density, data of the last 4 cycles of the same sample was used, and 95 % confident intervals of t-distributions were calculated as error bars (n = 4). Some error bars are not visible, because they are very short. 88

Figure 5.1: Synthetic route of F_6PBI and DMF$_6$PBI polymer. 97

Figure 5.2: ^{1}H NMR spectroscopy of F_6PBI polymer, DMSO-d6 as the solvent..... 98

Figure 5.3: ^{1}H NMR spectroscopy of DMF$_6$PBI polymer, DMSO-d6 as the solvent. 99

Figure 5.4: ASR of DMF$_6$PBI (40 μm), F_6PBI (40 μm), and Nafion 115 (125 μm) in 3 M sulfuric acid. Error bars are standard errors of the measurements (n = 3). 101

Figure 5.5: VRFB single cell performance of DMF$_6$PBI (two membranes used, first membrane broke after 120 mA cm^{-2} test), F_6PBI (single membrane), and Nafion 115 (single membrane) membranes at various current densities (80-200 mA/cm^2): (up) coulombic efficiency, (middle) voltage efficiency, and (down) energy efficiency. Test conditions: 1.5 M vanadium and 3 M sulfuric acid electrolyte 15 mL on both sides. 30 mL/min flow rate, 20 ℃ operating temperature, and cut off voltage 1.0 V – 1.7 V. At each current density, data of the last 4 cycles of the same sample was used, and 95 % confident intervals of t-distributions were calculated as error bars (n = 4). Some error bars are not visible, because they are very short. 106

Figure 5.6: VRFB single cell performance of DMF$_6$PBI membrane at 120 mA/cm^2, with voltage limit from 1.0 V to 1.7 V, state of charge of the first cycle from 9 % to 74 %. The DMF$_6$PBI membrane broke after 46 cycles. (a) coulombic efficiency, voltage efficiency, and energy efficiency; (b) charge and discharge capacity decay..... 108

Figure 5.7: (a) acid doped pristine DMF$_6$PBI membrane and (b) DMF$_6$PBI membrane after 46-cycle VRFB degradation test, the active area became fragile. 108

Figure 5.8: FTIR spectra of DMF_6PBI membrane before and after 46-cycle in-situ VRFB degradation test. 110

Figure 5.9: ^1H NMR spectroscopy of DMF_6PBI membrane pristine, after 46-cycle VRFB, and after 500 h degradation test in 1.5 M vanadium (V) at 80 °C. 112

Figure 5.10: Proposed overall degradation of DMF_6PBI in VRFB application. 113

Figure 6.1: Chemical structure comparison between F_6PBI and ABPBI. ABPBI has the highest density of benzimidazole groups. 119

Figure B1: Proposed synthetic strategy of connecting TTMePP to a polymer backbone through bromination. F_6PBI polymer backbone was chosen as an example here. TTMePP cation must be single brominated to prevent crosslinking. 150

Figure B2: ^1H NMR spectroscopy of the products of entry 9 at a milligram scale. The peak at 4.71 ppm is attributed to the brominated methylene group. 152

Figure B3: ^{31}H NMR spectroscopy of the products of entry 9 at a larger gram scale. The peak at 9.71 ppm indicates multiple bromination $TTMePP^+$. 153

Figure B4: Mass spectrometry of bromination reaction products. m/z 403 was attributed to the non-brominated $TTMePP^+$, m/z 481 and 483 were attributed to the single brominated $TTMePP^+$, while m/z 561 was attributed the double brominated $TTMePP^+$ 153

ABSTRACT

Redox flow batteries (RFBs) are currently considered as the most appealing energy storage options for the large-scale grid integration of the intermittent renewable energy sources such as solar and wind. Favorable features of RFBs include higher cell voltage, which leads to higher power and energy density and thus lower capital costs, and redox couples based on the same element, which allows easy crossover remediation. At present, zinc-cerium double membrane RFBs have the highest reported cell voltage in aqueous electrolytes, while vanadium RFBs (VRFBs) are the only commercially demonstrated systems with redox couples based on the same element. The goal of this thesis research is to explore highly conductive, selective and stable ion-exchange membranes (IEMs) for RFB systems. For Zn-Ce double membrane RFBs, the focus is the oxidative resistance, while for VRFBs, it is the conductivity. The work began with the examination of four commercial polymers for oxidation resistance, and among the four aromatic polymers examined, hexafluoroisopropylidene polybenzimidazole (F_6PBI) showed the highest oxidative resistance in the cerium electrolyte. F_6PBI was then functionalized to provide anion conductivity with tris(2,4,6-trimethylphenyl)phosphonium ($TTMePP^+$) and tris(2,4,6-trimethoxylphenyl)phosphonium ($TTMPP^+$). The tris(2,4,6-trimethoxylphenyl)phosphonium-functionalized polybenzimidazole (TTMPP-PBI) membrane exhibited a good balance of oxidation resistance and anion conductivity. Anion-exchange membranes (AEMs) are also excellent proton exchangers in polyprotic acid electrolytes. The TTMPP-PBI membrane was acid doped, and an excellent acid

doping level was achieved due to the favorable acid-base interaction at the lone-pair nitrogen and oxygen sites, and cation-anion interaction at the positive cations. The high acid doping level led to low area specific resistance which was exploited in VRFBs for better voltage and energy efficiency compared with Nafion 115 and F_6PBI membranes. An alternative pathway to functionalize the F_6PBI was also explored by using methyl iodide to produce methylated hexafluoroisopropylidene polybenzimidazolium (DMF_6PBI) membrane. The DMF_6PBI membrane showed higher acid doping level and higher voltage and energy efficiency than F_6PBI and Nafion 115 for VRFBs. However, the DMF_6PBI membrane was not chemically stable, and the degradation was investigated for the future design of robust membranes.

Chapter 1

INTRODUCTION

1.1 Renewable Energy and Redox Flow Batteries

1.1.1 Renewable Energy

With the increasing shortage of fossil fuels, exploring and utilizing renewable energy has become an urgent direction of research for sustainable development. Renewable energy is collected from renewable sources, which are naturally replenished in a human timescale, and include sources such as sunlight, wind, rain, tides, waves, and geothermal heat.[1-6]

As of 2015, 19.3 % of global energy consumption is contributed by renewable energy. Among this consumption, 8.9 % is from biomass; 4.3 % is from heat energy, 3.9 % is from hydro-electricity, and 2.2 % is electricity from wind, solar, geothermal, and biomass. Half of the new electricity capacity installed worldwide was renewable in 2015 worldwide.[7] In 2016, 24.3 % of electricity generation is contributed by renewable energy (Figure 1.1).[8]

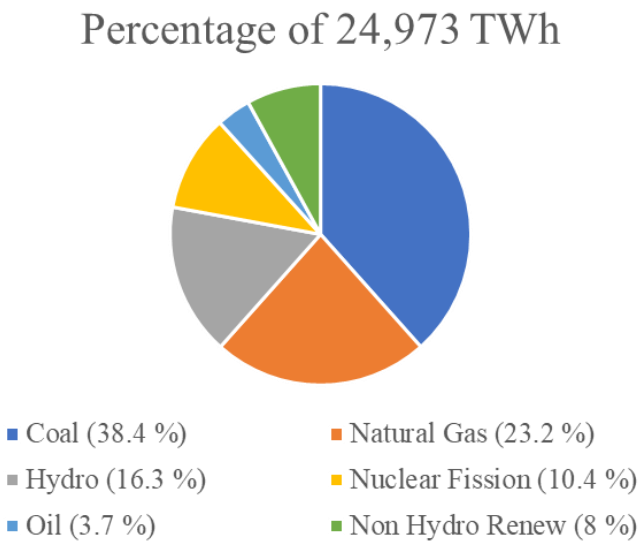

Figure 1.1: 2016 world power generation by source (Percentage of 24,973 TWh). Hydro sources (16.3 %) and non-hydro renewable sources (8 %) contributed 24.3 % in 2016 world power generation (Data source: 2018 key world energy statistics[8]).

In contrast to other energy sources that are limited to certain countries and areas, renewable energy resources exist over wide geographical areas.[9] Therefore, significant energy security, climate change mitigation and economic benefits are achieved by the rapid development of renewable energy. The percentage of renewable energies are projected to continue growing in the coming decades.[10-11]

1.1.2 Energy Storage

Solar and wind are two mostly public supported renewable resources indicated by the international public opinion surveys in 2011.[12] However, both solar and wind are intermittent and uncontrolled sources.[13-15] Sunlight usually peaks at noon and disappears at night, and wind greatly varies over hours, days and months. This inconsistency creates a great challenge for electric grid systems, and it is reported that

the electric grids will be destabilized if intermittent energy resources exceed 20 % of total electric generation without reliable energy storage systems.[16-18]

There are a variety of methods for energy storage,[19] which can be divided into mechanical storage, such as pumped hydroelectricity storage,[20-21] compressed air,[22-23] flywheels,[24-25] etc., electrical storage, such as capacitors,[26-27] supercapacitors,[28-29] etc., chemical storage, such as biofuels,[30] hydrogen,[31-32] etc., thermal storage, such as steam accumulators,[33-34] liquid air energy storage,[35-36] etc., electrochemical storage, such as redox flow batteries (RFBs),[37-42] rechargeable batteries,[43-46] etc. and so on. As of 2012, pumped hydroelectricity storage, which uses the gravitational potential energy of water by pumping water from lower reservoir to higher reservoir to store energy and generates electricity from turbine when water flows down, accounts for over 99% of bulk energy storage capacity worldwide.[47] The pumped hydroelectricity storage exhibits decent energy efficiency (70 % to 87 %) and low cost (around $ 100/kWh).[48] However, it is limited by geographical conditions as two water reservoirs at different altitudes are needed in close proximity. As an alternative to pumped hydroelectricity storage, electrochemical storage stands out as an excellent energy storage method for intermittent renewable resources due to its flexible design and reasonable cost.

Electrochemical storage is mostly based on reversible electrochemical reactions. Rechargeable batteries, which have a lower total cost of use and lower environmental impact than a non-rechargeable batteries, are commonly used.[43-46] Lead-acid batteries,[49-50] nickel-metal hydride batteries,[51-52] and lithium-ion batteries[53-55] all belong to this category. These batteries rely on the liquid or solid electrolyte to transport support ions to balance redox reactions on positive and negative electrodes and are mostly composed of solid electrodes. Due to repeated solid deposition/dissolution,[56-58]

rechargeable batteries exhibit limited cycle life and are generally not suitable for grid energy storage, which requires a services life of more than 10 years.

RFBs on the other hand, are composed of soluble redox pair in the fluid electrolyte and are much more suitable for grid electricity storage.

1.1.3 Redox Flow Batteries

RFBs are electrochemical energy storage systems which are suitable for grid storage of intermittent renewable energy resources. The chemical energy is stored in two redox pairs dissolved in liquids, and the two redox pairs are separated by an ion-exchange membrane (IEM). Because the redox pairs are dissolved in liquids, RFBs employ heterogeneous electron transfer rather than solid-state diffusion or intercalation, which other rechargeable batteries rely on. This allows RFBs to have more reliable charge and discharge reactions for long cycle life.[59-60] As shown in Figure 1.2, the electrolyte containing electroactive elements flows through the cell component and reversibly converts chemical energy to electricity, while additional electrolytes are stored in external tanks. This independent layout of the power unit (reactor cell component) and energy unit (external tanks) gives us the flexible design for RFB systems. RFBs also have the advantages of quick response time, no harmful emissions, and low maintenance required. For aqueous RFB systems, it is also non-flammable. These technical features make RFBs an appealing choice for large-scale energy storage.

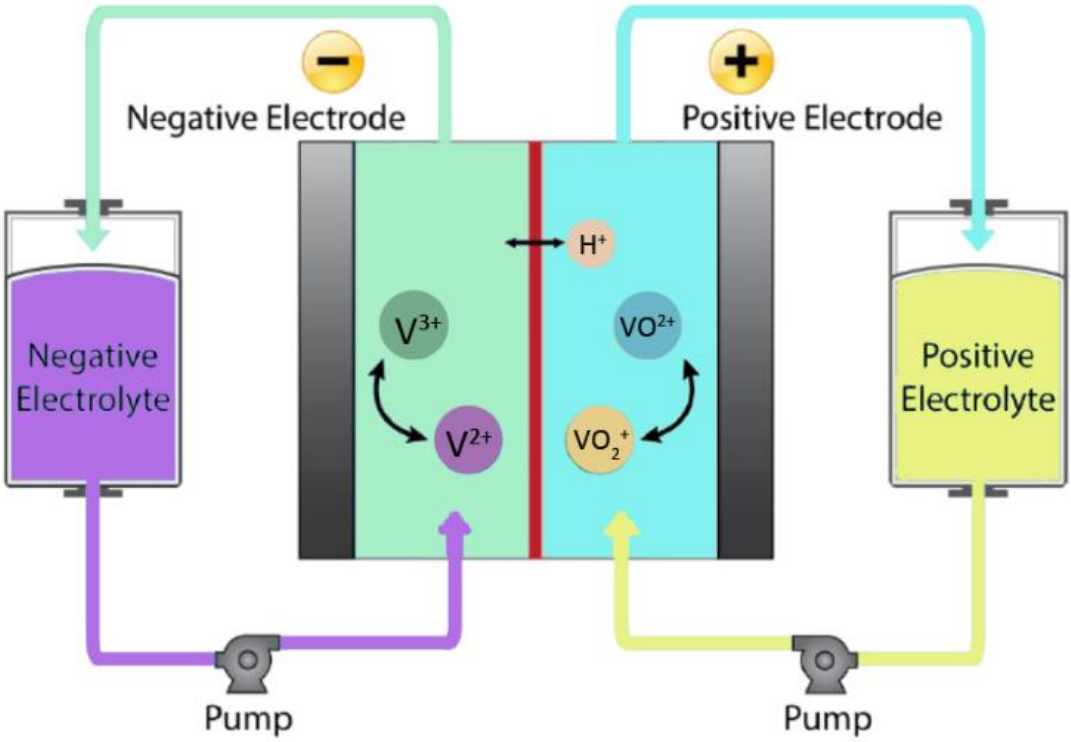

Figure 1.2: Structure of a typical vanadium redox flow battery (VRFB), the most marketed RFB system. The negative electrolyte is comprised of V^{2+} and V^{3+} in sulfuric acid, the positive electrolyte is comprised of VO^{2+} and VO_2^+ in sulfuric acid. The middle IEM can be a proton exchange membrane (PEM) or an anion (SO_4^{2-}/HSO_4^-) exchange membrane (AEM). PEM is the most popular choice.

At present, RFBs can be categorized based on the supporting electrolyte. There are two major types: aqueous RFBs[61-63] and nonaqueous RFBs.[64-66] Although nonaqueous RFBs have advantages of larger electrochemical windows and extended temperature ranges of operation,[67] they suffer from high internal resistance associated with organic solvents and generally slower kinetics during cycling compared to aqueous RFBs.[67] The investigation of nonaqueous RFBs are still in the very early stage, and the industrial implementation of nonaqueous RFBs still faces challenges.[67] On the other

hand, aqueous RFB technologies are more mature, and some aqueous RFBs are already commercially successful today, such as zinc-bromine RFBs[68-69] and vanadium RFBs.[70-71] The emphasis of this dissertation is aqueous RFBs.

1.1.4 Aqueous Redox Flow Batteries

Compared to nonaqueous RFBs, aqueous RFBs, in general, have the advantages of faster kinetics during cycling, much better voltage efficiency due to the lower internal resistance, and safer operation because the electrolyte is non-flammable.[39]

As stated before, RFBs feature flexible design due to the independence of the power units and energy units. Besides the flexible design of RFBs, the large selection of available redox pairs allows for tunable cell standard voltage, kinetics constant and electroactive component solubility.

In practice, two redox pairs are chosen to optimize the economy of the RFB, create adequate large standard cell voltage, and meet the general requirements of similar pH aqueous electrolytes, facile kinetics, and high solubilities. Table 1.1 summarizes commonly implemented redox pairs.

Table 1.1: Commonly reported redox pairs in RFBs. The standard redox potential and typical electrolyte of each redox pair are also summarized. (This table is inspired by a published work of Dr. Ke Gong.[72])

Redox pair	Standard redox potential (V)	Typical electrolyte
$Zn(OH)_4^{2-}/Zn$ [73]	−1.22 [74]	NaOH
$Cr(edta)^-/Cr(edta)^{2-}$ [75]	−0.96	NaAc
Zn^{2+}/Zn [76-80]	−0.76	NaBr, $ZnCl_2$, CH_3SO_3H
S_4^{2-}/S_2^{2-} [81]	−0.45	NaBr, NaOH
Fe^{2+}/Fe [82]	−0.45	HCl
Cr^{3+}/Cr^{2+} [83-85]	−0.41	H_2SO_4, HCl
V^{3+}/V^{2+} [86-88]	−0.26	H_2SO_4, HCl
$Fe(C_2O_4)_3^{3-}/Fe(C_2O_4)_3^{4-}$ [89]	−0.12 †	NaAc
Ti^{4+}/Ti^{3+} [83-84]	−0.06	HCl
Co^{3+}/Co^{2+} [78]	+1.95	CH_3SO_3H
Ce_2O^{6+}/Ce^{3+}	+1.86 [90]	$HClO_4$
Ce^{4+}/Ce^{3+} [79, 91]	+1.74	CH_3SO_3H, H_2SO_4
$Mn^{3+}/Mn2+$ [92]	+1.54	H_2SO_4
$Cr_2O_7^{2-}/Cr^{3+}$ [85]	+1.23	HCl
$Cr(edta)^+/Cr(edta)^-$ [75]	+1.14 †	NaAc
NpO_2^{2+}/NpO_2^+ [93]	+1.14	HNO_3
$ClBr_2^-/Br^-$ [77, 86]	+1.07 *	HCl, $ZnBr_2$
Br_3^-/Br^- [76, 81, 84, 89]	+1.05 *	NaBr, H_2SO_4
VO_2^+/VO^{2+} [80, 88, 94]	+0.99	H_2SO_4, CH_3SO_3H
Fe^{3+}/Fe^{2+} [82-83, 87, 94]	+0.77	HCl
$Fe(CN)_6^{3-}/Fe(CN)_6^{4-}$ [73]	+0.36 †	NaOH
Cu^{2+}/Cu [94]	+0.34	H_2SO_4
$Fe(C_6H_4O)^-/Fe(C_6H_4O)^{2-}$ [89]	+0.21 †, ‡	NaBr
$Fe(edta)^-/Fe(edta)^{2-}$ [75]	+0.18 †	NaAc
Np^{4+}/Np^{3+} [93]	+0.15	HNO_3
Sn^{4+}/Sn^{2+} [94]	+0.15	H_2SO_4

Standard redox potentials are calculated from standard Gibbs free energies or cited directly from standard redox potential tables [95] unless otherwise noted. Note that, when H^+ or OH^- are involved, unity was used as its activity unless otherwise noted.
* Calculated from Gibbs free energies in the reference[96]
† Calculated from formation constant of the complex in the reference[97]
‡ The complex structure was taken at pH = 6 from the reference.[98]

Among the various redox pairs available for RFB designs, this dissertation will focus on vanadium RFBs and zinc-cerium double-membrane RFBs.

1.1.5 Vanadium Redox Flow Batteries

As shown in Figure 1.2, VRFBs are rechargeable RFBs that utilize vanadium ions in four different oxidation states to form both positive and negative reactions. The electrochemical reactions on the positive and negative electrode are shown below.

Negative electrode: $V^{3+} + e^{-} \leftrightarrow V^{2+}$

Positive electrode: $VO_2^{+} + 2H^{+} + e^{-} \leftrightarrow VO^{2+} + H_2O$

The first successfully demonstrated VRFB, which used vanadium in sulfuric acid as both electrolytes, was by Maria Skllas-Kazacos at the University of New South Wales in the 1980s.[99] Since then, VRFBs quickly became the most popular RFB systems for researches and industrial applications. Several emerging companies have successfully launched their VRFB systems, such as Primus Power and UniEnergy in the United States, Rongke Power and Prudent Energy in China, and Cellennium in Thailand.

VRFBs featured a unique regeneration advantage because both positive electrolyte and negative electrolyte are vanadium species in sulfuric acid solution. If the electrolytes are mixed accidentally or gradually crossed over during cycling, VRFBs can be recharged back to their normal operating state without permanent damages.[100] However, the regeneration will cost 50 % more capacity than a normal charging of VRFBs.

Among the intensive studies of VRFB membranes, catalysts, electrolytes, and flow field designs, some exciting improvements were achieved recently. Li et al. boosted the energy capacity of VRFB by 70 % using mixed acid electrolytes.[101] Besides the enhanced solubility, the sulfate-chloride mixed electrolyte also exhibited a wider temperature range of -5 °C to 50 °C compared to the traditional sulfuric acid electrolyte, which is only stable between 10 °C and 40 °C. Therefore, the temperature

control module in VRFB could also be saved. Mench et al. demonstrated a peak power density of 557 - 767 $mW \cdot cm^{-2}$ at a state of charge of 60 % by employing a zero-gap flow field cell architecture and non-wetproofed carbon paper electrodes in 2012.[102-103] Perry et al. from United Technologies Research Center achieved a peak power density of over 1300 $mW \cdot cm^{-2}$ with the improved cell design,[37] compared to the peak power density of only 150 $mW \cdot cm^{-2}$ in commercial VRFB systems. These high-power density achievements can significantly reduce the stack cost of the VRFB systems and facilitate the widespread adoption of VRFBs. Zhang et al. also reported a new type of sponge-like porous polybenzimidazole (PBI) membrane with much better performance and significantly lower cost than traditional Nafion membranes.[104]

1.1.6 Zinc Cerium Double Membrane Redox Flow Batteries

One approach to lower the overall capital cost of the RFB systems is to design RFBs with two redox pairs that exhibited a higher cell potential. From Table 1.1, $Zn(OH)_4^{2-}/Zn$ (-1.22 V) as one of the lowest potential pairs is a great candidate for the negative side, and Ce_2O^{6+}/Ce^{3+} (1.86 V) as one of the highest potential pairs is a great candidate for the positive side. The potential of 3.08 V voltage would be 2.5 times of the VRFB (1.25 V) and 2.6 times of the chromium-iron RFB (1.18 V).

However, the $Zn(OH)_4^{2-}/Zn$ requires a basic electrolyte, while Ce_2O^{6+}/Ce^{3+} requires an acidic electrolyte. A special design must be made to put these two redox pairs into one RFB. Yan et al. demonstrated a double-membrane design to put the required basic electrolyte and acidic electrolyte together in 2013.[105] A cation-exchange membrane (CEM) is used between the NaOH electrolyte and the middle neutral electrolyte to allow the passage of Na^+, and an AEM is used between the $HClO_4$ electrolyte and the middle neutral electrolyte to allow the passage of ClO_4^- during

cycling. The zinc-cerium double membrane RFB is shown in Figure 1.3, and redox reactions for the positive and negative sides are shown below:

Negative electrode: $Zn(OH)_4^{2-} + 2e^- \leftrightarrow Zn + 4OH^-$

Positive electrode: $Ce_2O^{6+} + 2e^- + 2H^+ \leftrightarrow 2Ce^{3+} + H_2O$

This zinc-cerium double membrane RFB exhibited the highest voltage in aqueous RFB systems. However, the commercial AEMs are not chemically stable in the oxidative cerium electrolyte. In this work, new polymeric membrane materials with better stability in the cerium electrolyte were investigated.

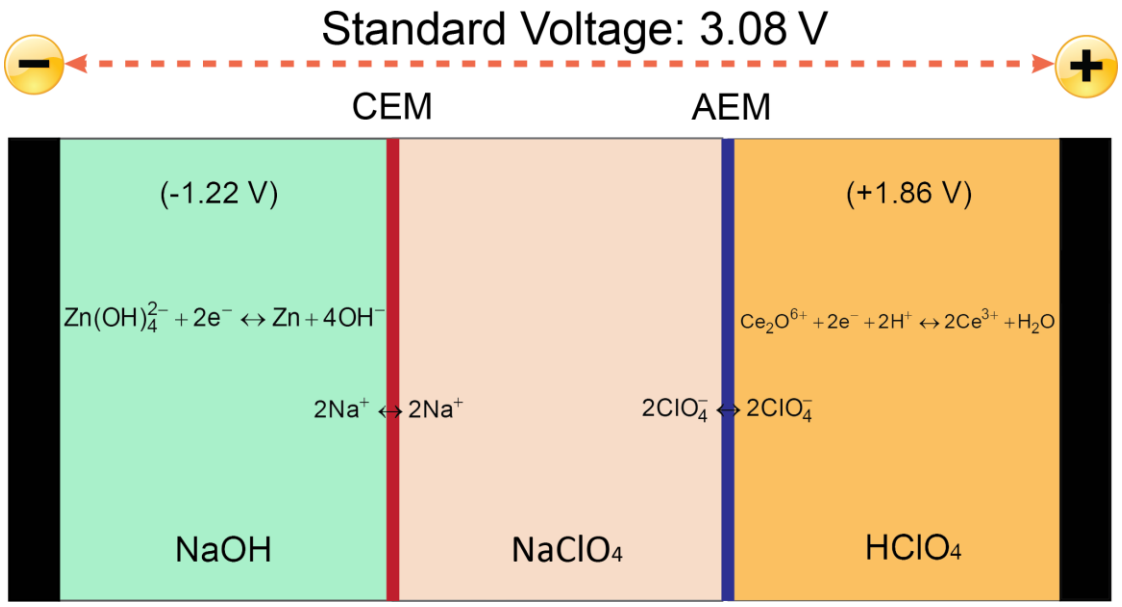

Figure 1.3: Schematic of Zn-Ce double-membrane RFB.[105] The negative electrolyte is comprised of $Zn(OH)_4^{2-}$/Zn in NaOH solution; The middle electrolyte is a $NaClO_4$ solution; The positive electrolyte is comprised of Ce^{4+}/Ce^{3+} in $HClO_4$ solution. A CEM separates the negative electrolyte and middle electrolyte, while an AEM separates the middle electrolyte and positive electrolyte.

1.2 Ion-Exchange Membranes

1.2.1 Ion-Exchange Membranes for Redox Flow Batteries

IEMs are semi-permeable membranes that can transport designed dissolved ions while blocking other ions and neutral molecules. Based on the functionality, IEMs are generally grouped into CEMs and AEMs. IEMs are generally made of organic polymers with charged ionic functional groups. For example, CEMs usually hold fixed anionic groups with mobile cations, and the conductivity of CEMs is attributed to the cation transport through the membrane. While AEMs usually hold fixed cationic groups with mobile anions.

The primary requirements for IEMs in RFB applications are:

1. Excellent chemically stability in RFB electrolytes
2. High conductivity of designed support ions
3. High selectivity of the supporting ions against the active redox ions
4. Good mechanical stability during manufacturing and operation
5. Low cost

As there are various designs for RFBs with different types of redox pairs, different electrolytes, and different operating conditions. The challenges and requirements of IEMs are different for different RFBs.

For VRFBs, which are the most marketed RFB systems as introduced in Section 1.1.5, the traditional choice of IEMs is the Nafion series, especially Nafion 115.[106] However, the costs of Nafion membranes are as high as 500-700 $ m^{-2}, and this cost has hampered the further implementation of the VRFBs.[104] Another disadvantage of the current Nafion membranes in VRFB systems is the low selectivity, and this low selectivity leads to a low coulombic efficiency during RFB operation.[107]

For the zinc-cerium double membrane RFB, a CEM between the $Zn(OH)_4^{2-}$/Zn electrolyte and the middle electrolyte and an AEM between the Ce^{4+}/Ce^{3+} electrolyte and the middle electrolyte are required. However, due to the limited chemical stability of current commercial AEMs, the first proposed zinc-cerium double membrane RFB by Yan et al.[105] only operated for 6 cycles before the AEM failed. The Ce^{4+}/Ce^{3+} redox pair in $HClO_4$ electrolyte has a potential of 1.86 V and poses a serious oxidative stability challenge to the AEM design.

In this dissertation, we will emphasize on the chemical stability, conductivity and selectivity of IEMs in RFBs.

1.2.2 Chemical Stability of Ion-Exchange Membranes

RFBs for grid energy storage require lifetimes of more than 10 years, thus, one of the biggest challenges for IEMs in RFBs is their chemical stability. Depending on the design and electrolytes of different RFBs, chemical stability can be referred to as acidic stability, alkaline stability, or oxidative stability. For example, in VRFBs, the electrolytes contain vanadium ions in generally 3 M sulfuric acid or high concentration of mixed acids, the acidic stability is the primary concern. In RFBs using $Zn(OH)_4^{2-}$/Zn in NaOH solution as the electrolyte, the alkaline stability is the primary concern. While in RFBs using Ce^{4+}/Ce^{3+} in $HClO_4$ solution as the electrolyte, the primary concern is the oxidative stability of the IEMs in strong oxidant Ce^{4+} in ClO_4^- aqueous solution.

For polymeric IEMs, a wise choice of organic chemical structures or a scientific design of new polymer structure are the ways to meet the chemical stability requirements. To fulfill the ion exchange function, IEMs are usually comprised of polymer backbones and functional groups (cations for AEMs or anions for CEMs). In most cases, the functional groups are the vulnerable parts of the polymeric IEMs.[108]

Because the functional groups are usually charged (positively charged cation for AEMs or negatively charged anion for CEMs), the functional groups are the hydrophilic part of the membrane in an aqueous environment and are usually easily attacked by species (such as OH^- in an alkaline environment) in the electrolytes. Due to the investigation of hydroxide exchange membrane fuel cell (HEMFC) systems, the alkaline stability of AEM functional groups is well studied. Many cationic functional groups with excellent alkaline stability were also proposed.[109-110] However, the functional group degradation related to oxidative stability is generally less investigated.

In terms of polymer backbones, they are traditionally considered to be chemically stable due to their hydrophobic nature. For example, even exposure to 40 % NaOH at 80 °C for 300 h, polysulfone (PSF) backbone was still reported to be chemically stable with no noticeable change in the membrane.[111] However, a recent study has proven that even though PSF is perfectly stable in a hot and corrosive alkaline environment, the PSF backbone can become vulnerable to OH^- attacks after functionalized by cations on aromatic rings.[112-114] These cation-triggered backbone degradation researches revealed new weak points of polymeric IEM chemical structures and inspired better designs of IEMs for electrochemical devices.

1.2.3 Conductivity of Ion-Exchange Membranes

The ionic conductivity of an IEM is proportional to the ionic mobility and ionic concentration.[108] As shown in Table 1.2, H^+ exhibits the highest ionic mobility in water, thus, for the same piece of CEM, proton usually shows the highest conductivity. Therefore, PEMs are often used to serve as IEMs for RFBs with acid electrolytes.

Table 1.2: Ionic mobilities of selected cations and anions at infinite dilution in water at 298 K.

Ion	Mobility ($10^{-8}m^2s^{-1}V^{-1}$)
H^+	36.23
Li^+	4.01
Na^+	5.19
K^+	7.62
Mg^{2+}	5.50
Ca^{2+}	6.17
NH_4^+	7.62
OH^-	20.64
F^-	5.74
Cl^-	7.92
Br^-	8.09
I^-	7.96
NO_3^-	7.41
ClO_4^-	6.98
SO_4^{2-}	8.29

Besides the intrinsic ionic mobility, another effective strategy to increase the IEM conductivity is to prepare the IEM with a high ion exchange capacity (IEC, i.e., the number of charged functional groups per unit mass of the membrane). However, there are trade-offs with high IECs. Because the charged functional groups are usually the vulnerable parts of IEMs, IEMs with higher IEC may be less chemically stable, and because of the increased water uptake and dimensional swelling, they may be less mechanically stable. Therefore, a careful decision is always required to pick the IEC of IEMs to balance the conductivity, mechanical strength, and chemical stability for the intended application.

The overall conductance of the IEM is proportional to its intrinsic conductivity but inversely proportional to its thickness. Just like the IEC of an IEM, the thickness of an IEM also requires mindful design. Thinner membranes generally show better conductance, but are less selective for the desired ions.[115] Lower selectivity leads to a

higher crossover rate and faster capacity decrease for RFB systems.[116] Besides the selectivity issue of thinner IEMs, a reasonable thickness of IEM (> 10 μm generally) is required for mechanical strength and RFB assembling.

Depending on the designs of RFBs and nature of the electrolytes, different supporting ions transport through IEMs to achieve charge balance. For the VRFB systems, the electrolytes are vanadium ions in sulfuric acid, and CEMs are commonly used to allow the transport of protons and to block the vanadium ions from crossover at the same time.[116] Due to the high ionic mobility of H^+, VRFBs with CEMs generally exhibit sufficient conductivity. However, the selectivity is generally sacrificed using CEMs. AEMs are also used in VRFBs to increase vanadium selectivity by Donnan exclusion (i.e., the intrinsic repulsion of positive charged functional groups in AEMs and vanadium cations). Although AEMs are functionalized with positively charged cations, protons could also pass through AEMs in a high concentration of sulfuric acid.[117] For zinc-cerium RFB systems, AEMs are required to allow the transport of ClO_4^- and to block the active cerium ions, and CEMs are also required to allow the transport of sodium ions and reject the zincate ions.

1.2.4 Selectivity of Ion-Exchange Membranes

In aqueous RFB systems, the electrolytes are composed of active redox pairs and supporting ions. The supporting ions are added to increase the conductivity of the electrolyte and to transport through IEMs to balance the reactions on both electrodes during cycling.[116] Using VRFB as an example, V^{2+}/V^{3+} are active redox pairs in the negative electrolyte, and VO^{2+}/VO_2^+ are active redox pairs in the positive electrolyte. These active redox pairs should be blocked by the IEM to prevent crossover and

capacity loss. While H^+, SO_4^{2-}, and HSO_4^- are supporting ions in the electrolyte that can transport through the IEM to balance the redox reactions on both sides.

Selectivity is used to compare the transport of two species through the membrane. For RFB membranes, a high permeability of designed supporting ions and a low permeability of active species are required. Ion selectivity of an IEM is primarily governed by the Donnan exclusion effect.[118] For CEMs, due to fixed negatively charged functional groups in the membranes, cations can pass through the membrane, while anions are rejected. For AEMs, due to the fixed positively charged functional groups in the membranes, anions can pass through while cations are rejected. The ion selectivity between ions of the same type of charge is generally governed by the differences in ionic mobility between the two ions. In VRFB systems, CEMs are traditionally used to separate positively charged protons and positively charged vanadium ions based on their ionic mobility.

As we mentioned in the previous section, the selectivity of an IEM is often counteracting with its conductance. For example, based on the same chemical structure of the IEM, a thinner membrane exhibits higher conductance, but a thicker membrane usually exhibits better selectivity.

1.2.5 Cation-Exchange Membranes for Redox Flow Batteries

Based on the types of materials, CEMs could be divided into three groups: perfluorinated membranes, partially fluorinated membranes, and nonfluorinated hydrocarbon membranes.[119]

The carbon-fluorine chemical bond is the strongest bond in organic chemistry,[120] thus perfluorinated membranes usually have great stability. Perfluorinated CEMs are currently the most commercially applied materials for RFBs,

such as the Nafion membranes developed in the late 1960s by Walther Grot of DuPont Inc,[121] and are currently products of the Chemours Company. The chemical structure of Nafion membranes is shown in Figure 1.4. Nafion membranes are comprised of perfluorinated polymer backbones and sulfonate functional groups. These perfluorinated CEMs feature excellent chemical stability and great ion conductivity. However, further development of RFBs with perfluorinated membranes is hampered by the high cost of perfluorinated membranes[122] (e.g., \$500 – \$700 per m^2 for Nafion series membranes[104, 116]) and low selectivity (e.g., high permeability of vanadium ions through Nafion series membranes in VRFB[116]).

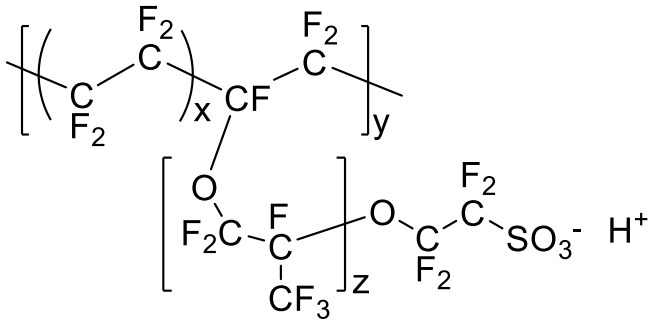

Figure 1.4: Chemical structure of Nafion series membranes. The membrane is composed of a perfluorinated polymer backbone and sulfonate functional groups.

Partially fluorinated materials have also been applied in RFBs.[123] For example, the pre-irradiation technique has been used to graft styrene and maleic anhydride onto polyvinylidene fluoride membranes for preparing partially fluorinated membranes for VRFBs.[124] The specific area resistance and properties of these grafted membranes can be controlled by the grafting ratio.[125] However, these partially fluorinated membranes

are generally less stable than perfluorinated membranes in relevant RFB electrolytes, and low-cost membranes are still unavailable due to the expensive fluorinated materials.[119]

Nonfluorinated hydrocarbon polymer backbones are cheaper alternatives to expensive fluorinated backbones. For example, sulfonated poly(tetramethydiphenyl ether ether ketone) (SPEEK) was prepared for VRFB applications.[126] Although some of these nonfluorinated CEMs exhibits better proton selectivity in VRFB,[126] their application in RFBs is still limited by their insufficient chemical stability.[116]

Since 2015, PBI membranes have been introduced for RFB applications.[127-131] PBI does not contain fixed anions as functional groups for cation transportation, while it featured benzimidazole groups that act as electron donators and form hydrogen bonds with acid molecules.[132] Especially in concentrated polyprotic acid solution (i.e., sulfuric acid solution in VRFBs and phosphoric acid in high-temperature fuel cells), PBIs can be doped with a large amount of acid, and these doped polyprotic acids form effective proton transportation channels in the membrane matrix.[133] Moreover, the PBI membranes exhibit excellent chemical stability and demonstrate more than 10,000 cycles of VRFB operation.[104] However, due to the relatively low concentration of sulfuric acid in VRFB electrolytes (i.e., 3 M sulfuric acid), the acid doping level and proton conductance are not adequate. Sponge-like porous PBI membranes were made to increase the proton conductance.[104]

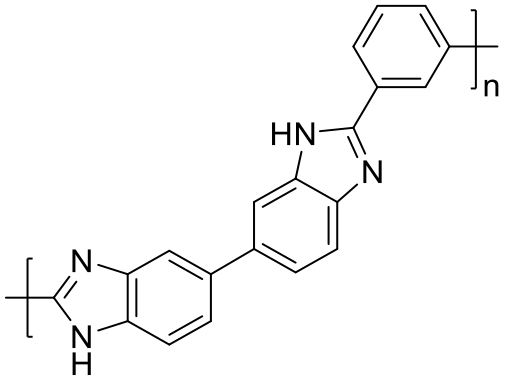

Figure 1.5: Chemical structure of meta-polybenzimidazole(m-PBI). PBIs have electron pairs on the nitrogen of the benzimidazole group and can act as electron donators to form hydrogen bonds with protons or polyprotic acids.

1.2.6 Anion-Exchange Membranes for Redox Flow Batteries

AEMs are membranes with fixed cations as functional groups and selectively allow the transportation of anions through the membrane matrix. Recent research demonstrated that in concentrated polyprotic acids (e.g., sulfuric acid or phosphoric acid), besides anion conductive, the AEMs are also good proton exchangers. For example, Jörissen et al. demonstrated that multiple charged anions can interact with fixed cations in AEMs and reduce the AEMs' ability to stop H^+ leakage.[117] Their experiments indicate that the majority of ion transportation through the AEM is proton transport in 30 % weight of sulfuric acid.[117] Kim et al. demonstrated that due to the formation of ammonium-biphosphate ion pairs, the ammonium functionalized membrane exhibited higher acid doping level than PBI membranes in concentrated phosphoric acid.[134]

In terms of the materials, AEMs are commonly made of nonfluorinated hydrocarbon polymers. A lot of research has been done towards the cations and polymer backbones. Chemical structures of selected cations for AEMs are listed Table 1.3, such

as: (1) quaternary ammoniums (e.g., tetramethyl-ammonium,[135-139] triethyl-methyl-ammonium,[136] 1,4-diazabicyclo[2.2.2]octane based ammonium,[140-141] 1,1-dimethyl-piperidinium,[142-143] 1,1-dimethyl-pyrrolidinium,[140, 144] 1,1,4-trimethyl-piperazinium[144]); (2) imidazoliums (e.g., 1,3-dimethyl-imidazolium,[138, 145-146] 1,2,3-trimethyl-imidazolium,[147] benzimidazolium,[148-150] 1,3-dimethyl-4,5-diphenyl-2-(2,4,6-trimethylphenyl)-imidazolium,[109] 1,3,4,5-tetramethyl-2-(2,4,6-trimethylphenyl)-imidazolium[109]); (3) guanidiniums (e.g., hexamethyl-guanidinium,[151-152] pentamethyl-alkyl-guanidinium[153-154]); (4) sulfoniums (e.g., trimethyl-sulfonium,[140, 155] triphenyl-sulfonium[156]); and (5) phosphoniums (e.g., methyl-tris(2,4,6-trimethoxylphenyl)phosphonium,[151, 157-159] methyl-tris(2,4,6-trimethylphenyl)phosphonium[110]). Quaternary ammoniums are the traditional choice in AEMs and have been widely used in RFBs, however, they are not chemically stable in corrosive environments. In 2015, Coates et al. published 1,3-dimethyl-4,5-diphenyl-2-(2,4,6-trimethylphenyl)-imidazolium and 1,3,4,5-tetramethyl-2-(2,4,6-trimethylphenyl)-imidazolium cations with exceptional alkaline stability in 5 M KOH at 80 °C for 30 days.[109] In 2016, Yan et al. demonstrated that methyl-tris(2,4,6-trimethylphenyl)phosphonium exhibited excellent alkaline stability in 1 M KOH at 80 °C.[110] To the best of our knowledge, the chemical stable phosphonium cations have not been implemented in RFBs before this work.

Table 1.3: Selected list of reported cations for AEMs, some of these cation functionalized membranes were not implemented in RFB applications. (This table is inspired by a published work of Dr. Bingzi Zhang.[108])

Cation	Chemical structure
Ammonium	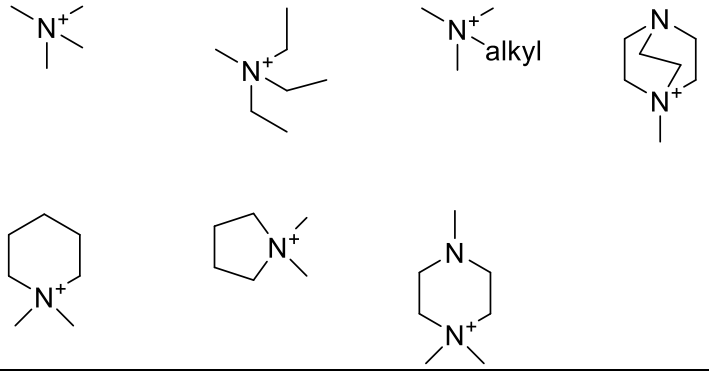
Imidazolium	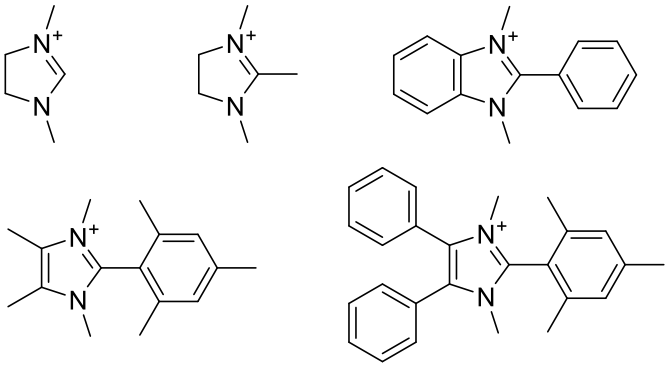
Guanidinium	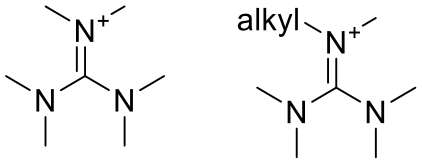
Sulfonium	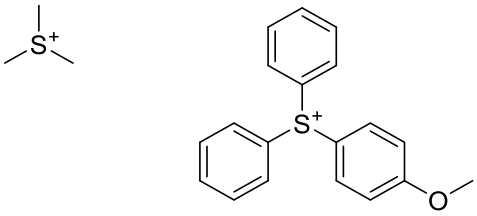
Phosphonium	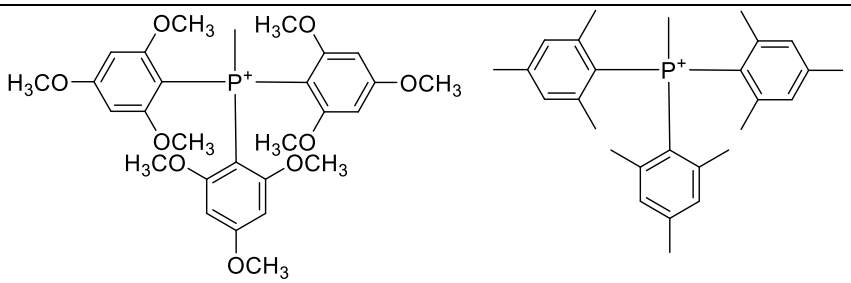

Polymer backbones control the mechanical strength of the IEMs and are generally hydrophobic and raise less chemical stability concerns than the functional groups. Common polymer backbones includes polystyrene (PS),[160-162] polyethylene,[163-165] PSF,[166-168] polyphenylene,[169-170] PBI,[149, 171-172] perfluorinated backbones,[173-174] poly(vinylbenzyl chloride),[175-177] polyphosphazene,[178] poly(vinyl alcohol),[179-181] poly(ether ketones),[182-185] poly(phenylene oxide),[186] and poly(ether imide).[187-189] Due to the uncharged nature of polymer backbones, they are usually considered chemically stable in most aqueous electrolytes. However, recent studies have demonstrated that tethering cations could trigger the degradation of polymer backbones in aqueous electrolytes.[190] These studies provided new prospects for chemically stable polymer backbone design.

1.3 Research Aim and Objectives

The overall research objective was to explore conductive, chemically stable and selective IEMs for various RFB applications.

The first project of my Ph.D. was to develop oxidative resistant AEMs for the zinc-cerium double membrane RFB system. Different aromatic polymer backbones were screened, and their degradation in cerium electrolytes was studied. The most stable PBI backbone was functionalized with chemical stable tris(2,4,6-trimethylphenyl)phosphonium ($TTMePP^+$). However, the prepared membrane showed trivial anion conductivity due to the hydrophobic functional group. Another tris(2,4,6-trimethoxylphenyl)phosphonium ($TTMPP^+$) functionalized polybenzimidazole membrane was prepared, and the TTMPP-functionalized polybenzimidazole membrane (TTMPP-PBI) provides decent conductivity with sufficient chemical stability in cerium electrolytes. Due to the nature of methoxy groups and large phosphonium cation, the

TTMPP-PBI membrane was an excellent platform for acid doping in the sulfuric acid electrolyte and very suitable for VRFBs. The TTMPP-PBI was then tested in a VRFB system and showed excellent energy efficiency compared with current membranes. To solve the low acid doping of the pure PBI in sulfuric electrolytes, a methylated polybenzimidazolium membrane (i.e., DMF_6PBI) was developed and first investigated (to the best of our knowledge) in VRFB systems. The prepared DMF_6PBI membrane showed excellent acid doping level and conductivity, but it was not stable enough in VRFB electrolytes. The membrane degradation in VRFB electrolytes was also investigated. Overall, the goal of this dissertation is to demonstrate novel membrane chemistries and their implementation into actual RFB devices.

1.4 Outline of the Dissertation

To achieve the goal of exploring conductive, chemically stable, and selective IEMs for various RFB applications, this dissertation is organized into the following chapters.

In chapter 2, in order to develop an oxidative resistant IEM for the zinc-cerium double membrane RFB, the selection of the polymer backbone was investigated. Cerium redox-pair (Ce^{4+}/Ce^{3+}) is one of most electronegative redox pair (1.74 vs. SHE) in water, while the degradation of organic polymers in cerium electrolyte was not well investigated. Four different commercial polymer backbones (PSF, PS, poly(2,6-dimethyl-phenylene oxide (PPO)), and hexafluoroisoproylidene polybenzimidazole (F_6PBI)) in the cerium electrolyte were examined. F_6PBI exhibited the lowest weight loss and was chosen as the polymer backbone for the membrane. The degradation mechanisms of the two unstable membranes (PSF and PPO) were also investigated in

detail using heteronuclear single quantum coherence (HSQC) spectroscopy for a deeper understanding of the oxidative resistance.

In chapter 3, to prepare an oxidative resistance AEM for the zinc-cerium double membrane RFB, taking advantage of the developed chemically stable phosphonium functional groups, the cation groups were linked them to the selected F_6PBI polymer backbone. At first, the F_6PBI was modified with TTMePP, while after great efforts devoted towards the synthesis, the obtained membrane showed trivial anion conductivity due to the hydrophobic nature of the TTMePP cation. The TTMPP cation was then linked to the F_6PBI, and the obtained membrane showed sufficient anion conductivity and chemical stability in the cerium electrolyte.

In chapter 4, the prepared TTMPP-PBI membrane from the previous chapter was further investigated in the vanadium sulfuric acid electrolyte for VRFB application. One TTMPP featured nine methoxy groups to form hydrogen bonds in concentrated sulfuric acid solution and one positively charged phosphonium to form phosphonium-bisulfate pairs for further acid doping. TTMPP-PBI membrane exhibited an acid doping level of 5.1 (mol acids per mol polymer repeat unit) in 3 M sulfuric acid which is much higher than pure F_6PBI, which showed an acid doping level of only 1.5 (mol acids per mol polymer repeat unit) in 3 M sulfuric acid. The specific area resistance of TTMPP-PBI membrane was even lower than Nafion 115 in 3 M sulfuric acid, and the prepared TTMPP-PBI membrane achieved the best voltage efficiency and energy efficiency in a single cell VRFB test compared with Nafion 115 and F_6PBI membranes.

In chapter 5, PBI membranes were used to form hydrogen bonds with acids and become proton conductive in polyprotic acid solutions (e.g., sulfuric acid). Inspired by the previous work of acid doping by forming cation-bisulfate in concentrated sulfuric

acid solution, the F_6PBI was modified with methyl iodide to form fixed benzimidazolium groups. The prepared methylated hexafluoroisoproylidene polybenzimidazolium (DMF_6PBI) membrane achieved higher acid doping level and a lower area specific resistance in a sulfuric acid electrolyte. However, after methylation, DMF_6PBI is not chemically stable in the vanadium electrolyte, and its degradation mechanism was investigated for the future design of chemically stable membranes.

Chapter 2

INVESTIGATION OF POLYMER BACKBONE DEGRADATION IN CERIUM ELECTROLYTES

Polymer backbones are the vital frame of ion-exchange membranes (IEMs) and control the mechanical strength of IEMs. In this chapter, the oxidative resistance of four polymer backbones was tested in the cerium (IV) electrolyte. Only hexafluoropropylidene polybenzimidazole (F_6PBI) membranes exhibited no significant weight loss and thus were chosen for further studies. For those polymers that are not stable, we attempted to probe the mechanisms of the polymer weight loss in this chapter.

Because of the unprecedented high cell voltage (1.87 V – 3.08 V)[105, 191-196] of cerium redox flow batteries (RFBs), cerium redox-pair (Ce^{4+}/Ce^{3+}) is extremely appealing. In order to achieve the highest-voltage (i.e., 3.08 V) of aqueous RFBs, a chemical stable AEM is required to operate with the oxidative cerium electrolyte. In this work, the stability of the common AEM backbones was tested. In addition, using heteronuclear single quantum coherence (HSQC) spectroscopy, their detailed degradation mechanisms were thoroughly investigated.

2.1 Introduction

RFB is a popular choice of renewable storage due to its reliability and scalability.[39, 118, 197] Due to the flexible design of RFB electrochemistry, various types of RFBs have been developed in the past century,[60, 198] for example: Zn-Br RFBs,[199-201] Fe-Cr RFBs,[202-205] all-V RFBs,[41, 99, 206] Zn-Ce RFBs,[192, 194-195] all-organic RFBs,[38, 40, 207-208] and all-polymer RFBs.[209-211] Among the numerous redox pairs used in different RFB systems, cerium redox-pair (Ce^{4+}/Ce^{3+}) is attractive because it is one of the most positive redox pair (1.74 vs. SHE) in water. The RFB designed with cerium

redox pair has unprecedented high cell voltage (1.87 V – 3.08 V).[105, 191-192] High cell voltage is important to achieve high energy and power densities, which leads to a lower storage cost of the RFB.[105]

The RFB with the highest voltage in an aqueous system was published by Yan et al., and the design requires an anion-exchange membrane (AEM) to work with cerium solution to prevent the cation crossover and allow the passing of selected anions.[105] However, due to the limited stability of existing AEMs, the RFB could only survive less than 20 cycles.[105] Ce^{4+} is a well-known oxidant, yet the influence of it on polymer membranes has not been systematically studied.

In this paper, I demonstrated that not only the hydrophilic AEMs can hardly survive in cerium (IV) electrolytes. Some membrane backbones which are traditionally considered to be acid and oxidative resistant can easily decompose in the strong oxidative and acidic environment of cerium (IV) electrolytes. This paper addresses the issue of membrane backbone stability in cerium electrolytes, and especially, the degradation mechanisms of poly(2,6-dimethyl-phenylene oxide) (PPO) and polysulfone (PSF).

1D ^{1}H nuclear magnetic resonance (NMR) spectroscopy and infrared spectroscopy have been the choices for elucidating polymer structure both for synthesized polymers and after degradation tests.[212-216] However, these methods lack the information on carbon and hydrogen correlation and are difficult to identify the specific chemical moieties present. Thus, the detailed degradation mechanism is always absent in polymer membrane studies. These degradation mechanisms are essential for designing future robust materials.

In this paper, HSQC spectroscopy is used to identify the moieties presented after cerium degradation test.[217-219] We introduced HSQC spectroscopy to study the polymer stability in RFB electrolytes, and the detailed degradation mechanisms are shown in the following sections.

2.2 Materials and Methods

2.2.1 Materials

All chemicals were obtained from Sigma-Aldrich and used as received unless otherwise stated. A rotary evaporator was used to concentrate 0.3 M cerium (IV) and perchloric acid solution purchased from Alfa Aesar to obtain 0.5 M Cerium(IV) in 1.3 M $HClO_4$ aqueous solution.

2.2.2 Experimental Methods

2.2.2.1 Synthesis of Hexafluoropropylidene Polybenzimidazole (F_6PBI)

F_6PBI was synthesized using a literature procedure.[133]

2.2.2.2 Membrane Fabrication

Polystyrene (PS), PSF, and PPO were used without further purification. F_6PBI was synthesized as described in Section 2.2.2.1. The polymer was completely dissolved before casting. The polymer solution was cast on a glass plate and dried in air at 60 °C for 24 h. After 24 h, the glass plate was immersed in DI water, and the membrane (thickness between 25 μm to 35 μm) was gently peeled from the glass.

2.2.2.3 Polymer Backbone Oxidative Stability Test in Cerium(IV) Solution

The obtained membranes were tested in 0.5 M Cerium(IV) and 1.3 M $HClO_4$ solution at 60 °C for dry-weight measurement at 0 h, 250 h, 500 h, 750 h, and 1000 h. Before each weight measurement, the membranes were immersed in 1 M $NaHCO_3$ solution for 48 h and then DI water for 24 h at room temperature to wash out residual salt and acid, and dried in a vacuum oven at 60 °C for 48 h.

2.2.2.4 NMR Spectroscopy Characterization

All NMR spectroscopy measurements were carried out by a Bruker AVIII 600 MHz NMR spectrometer. The solvent for NMR spectroscopy is deuterated chloroform ($CDCl_3$) with tetramethylsilane added as the internal standard.

2.3 Results and Discussion

2.3.1 Polymer Backbone Degradation in Cerium (IV) and $HClO_4$ Solution

Four commercially-available high-performance engineering aromatic polymer membranes, PS, PSF, PPO, and F_6PBI (chemical structures shown in Figure 2.1) were prepared with thicknesses between 25 μm to 35 μm. The remaining weights were measured in 0.5 M Cerium (IV) and 1.3 M $HClO_4$ solution at 60 °C. The results are shown in Figure 2.2.

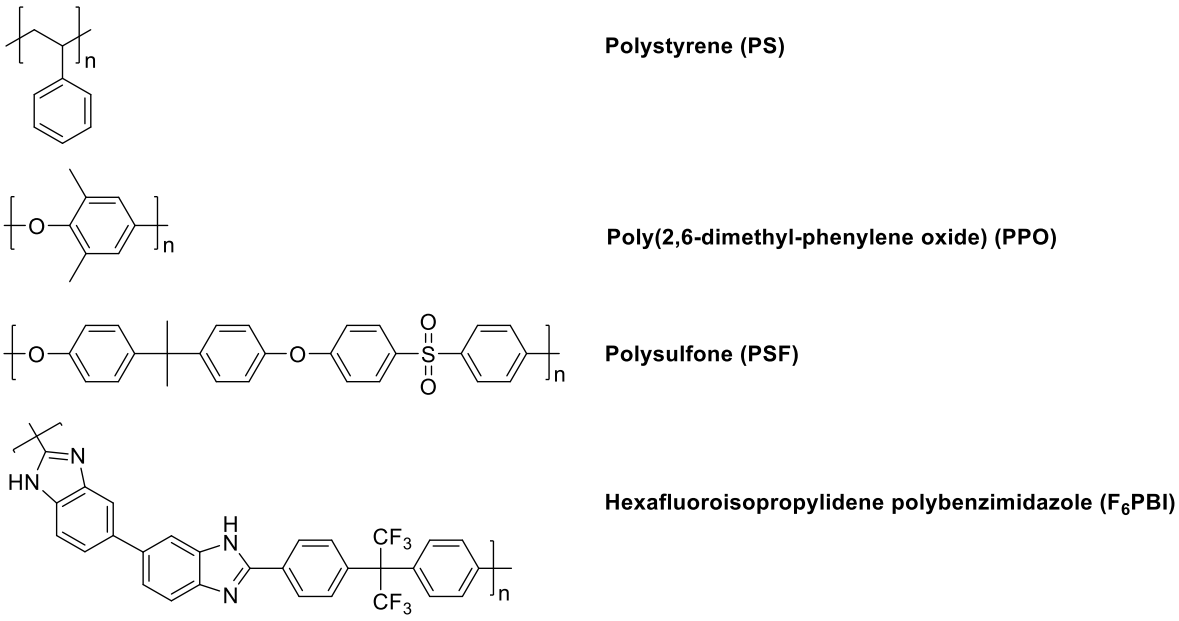

Figure 2.1: Chemical structures of prepared polymer membranes: PS, PPO, PSF, and F_6PBI. While PS, PPO, and PSF were commercial polymers, F_6PBI was synthesized in our lab.

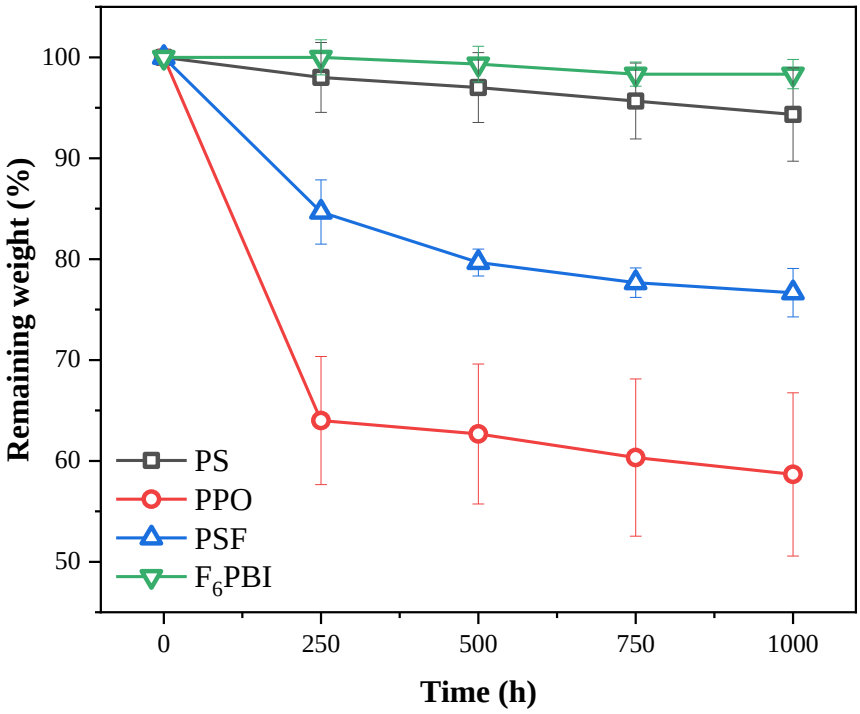

Figure 2.2: Remaining weight of four polymeric membranes during oxidative stability test in 0.5 M cerium (IV) and 1.3 M $HClO_4$ solution at 60 °C. Membranes were thoroughly washed and dried in a vacuum oven before weight measurements were taken. For each polymer, three membrane samples were measured, and the standard error of remaining weight is shown through the error bars.

As shown in Figure 2.2, F_6PBI membranes exhibited no noticeable weight loss during the cerium oxidation test, and PS membranes had less than 10 % weight loss on average after the oxidation test. However, PPO and PSF membranes presented 41 % and 23 % weight loss on average respectively after the oxidation test, and they both changed from strong and transparent to brittle and cloudy. A noticeable common feature of PPO and PSF is the ether linkage within the polymer structure (Figure 2.1). To our

best knowledge, the detailed degradation mechanisms of PPO and PSF in cerium (IV) and perchloric acid electrolyte have not been studied yet.

2.3.2 Poly(p-phenylene oxide) Degradation Mechanism

To investigate the degradation of PPO, ^{1}H NMR spectroscopy and HSQC spectroscopy of PPO before and after the 1000 h degradation in cerium solution. For comparison, the NMR spectroscopy results are shown in a stacked manner. From the HSQC spectroscopy in Figure 2.3 and Figure 2.4, clear degradation was observed through distinct emerging peaks at 4.6 ppm and 5.3 ppm in ^{1}H NMR spectroscopy, which are correlated with peaks at 68 ppm and 70 ppm in ^{13}C NMR spectroscopy, respectively. From the stacked ^{1}H NMR spectroscopy in Figure 2.5, the new peak at 10.3 ppm in ^{1}H NMR spectroscopy indicated the formation of well-known carboxylic acid after oxidation.

In Figure 2.4, the new blue peaks can only be $-CH_2$ groups due to the opposite color from the original red peaks ($-CH_3$ and -CH) in pristine PPO.[220] Based on their ^{1}H and ^{13}C chemical shifts, as well as the possible degradation of the PPO structure, the new peaks were most likely to be methylene ether linkage ($-CH_2-O-$). The methylene ether linkage was the product of decarboxylation after the oxidation ring opening of benzene. The oxidative aromatic ring opening and decarboxylation were facilitated by the positive charge delocalized in the system after protonation in a rich acid environment.

The overall proposed degradation mechanism is shown in Figure 2.6. The degradation started from the protonation of the ether bond in a rich acidic environment. After protonation of the ether bond, a nearby aromatic ring was activated and easily oxidized by Ce^{4+}. Due to the strong electron withdrawing effect of the delocalized

positive charge, the formed carboxylic acid went through decarboxylation and left a -CH_2-O- with the chemical shift at 5.3 ppm in ^{1}H NMR spectroscopy and 70 ppm in ^{13}C NMR spectroscopy. After the decarboxylation, the product went through a double bond cleavage due to the oxidation of Ce^{4+}. The further oxidation product with ether methylene carboxylic acid group (-O-CH_2-COOH) has the chemical shift at 4.6 ppm in ^{1}H NMR spectroscopy and 68 ppm in ^{13}C NMR spectroscopy, and the carboxylic acid is at 10.3 ppm in ^{1}H NMR spectroscopy in Figure 2.5.

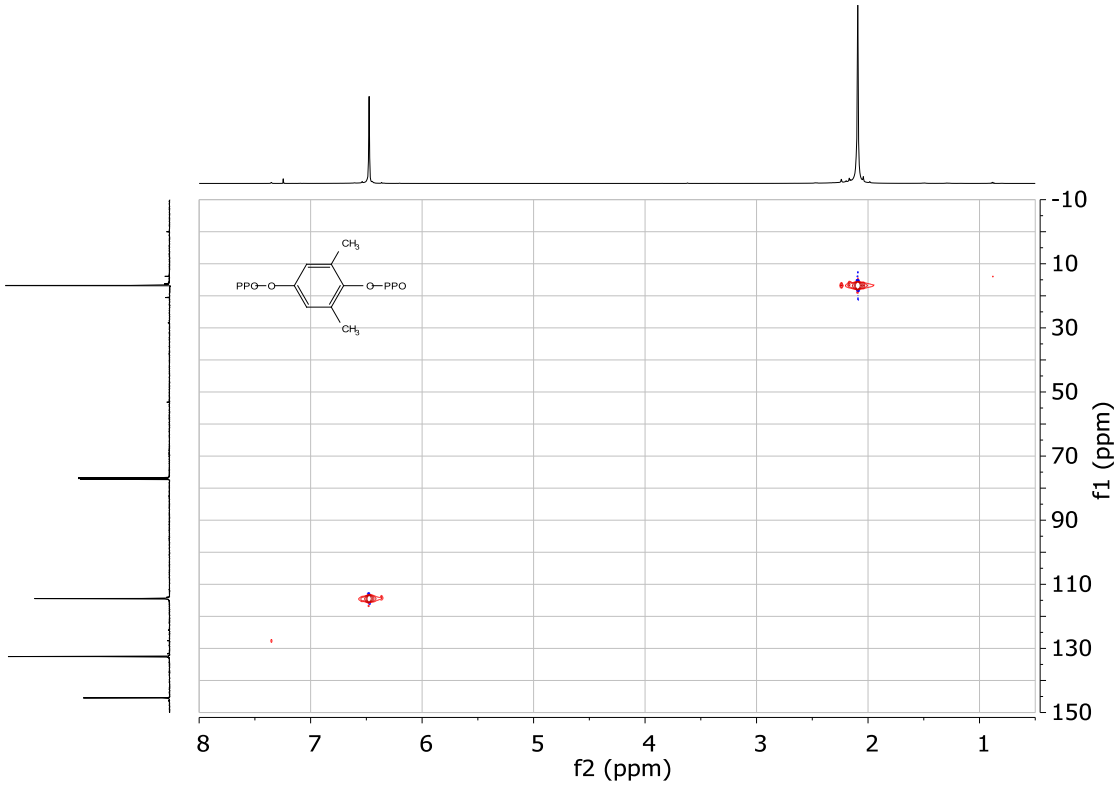

Figure 2.3: HSQC spectroscopy of pristine PPO before chemical stability test in the cerium electrolyte, $CDCl_3$ as the solvent, TMS as the internal standard.

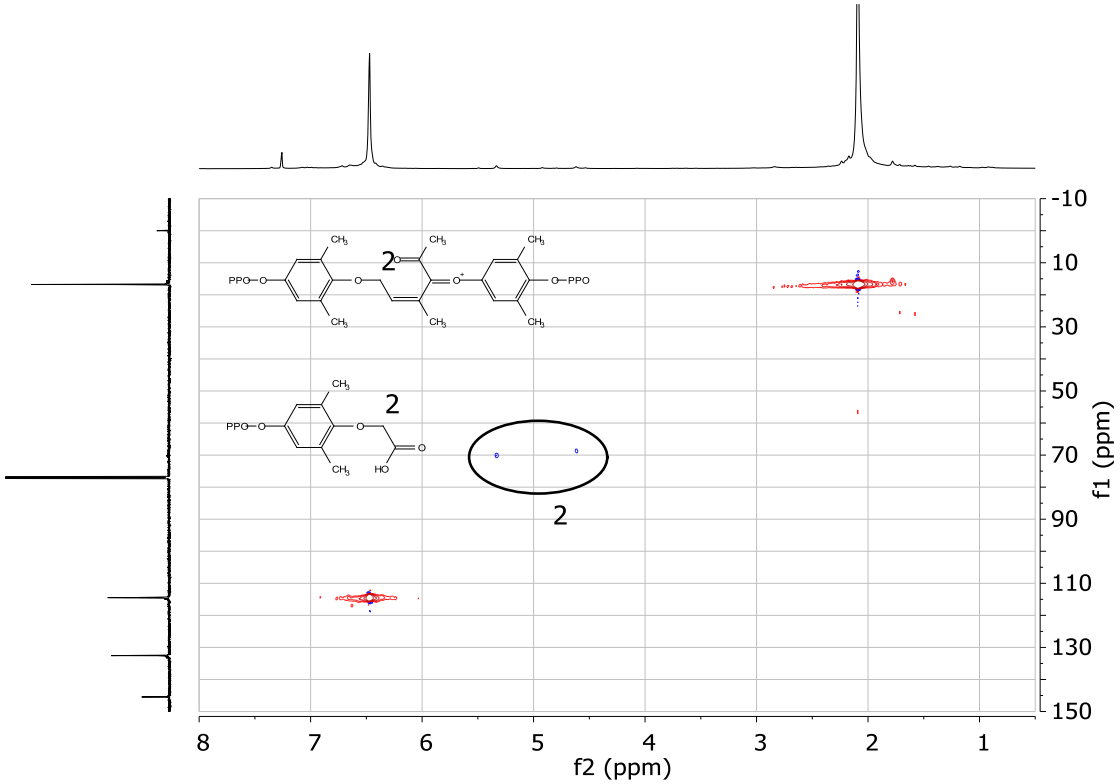

Figure 2.4: HSQC spectroscopy of decomposed PPO after chemical stability test in the cerium electrolyte, $CDCl_3$ as the solvent, TMS as the internal standard.

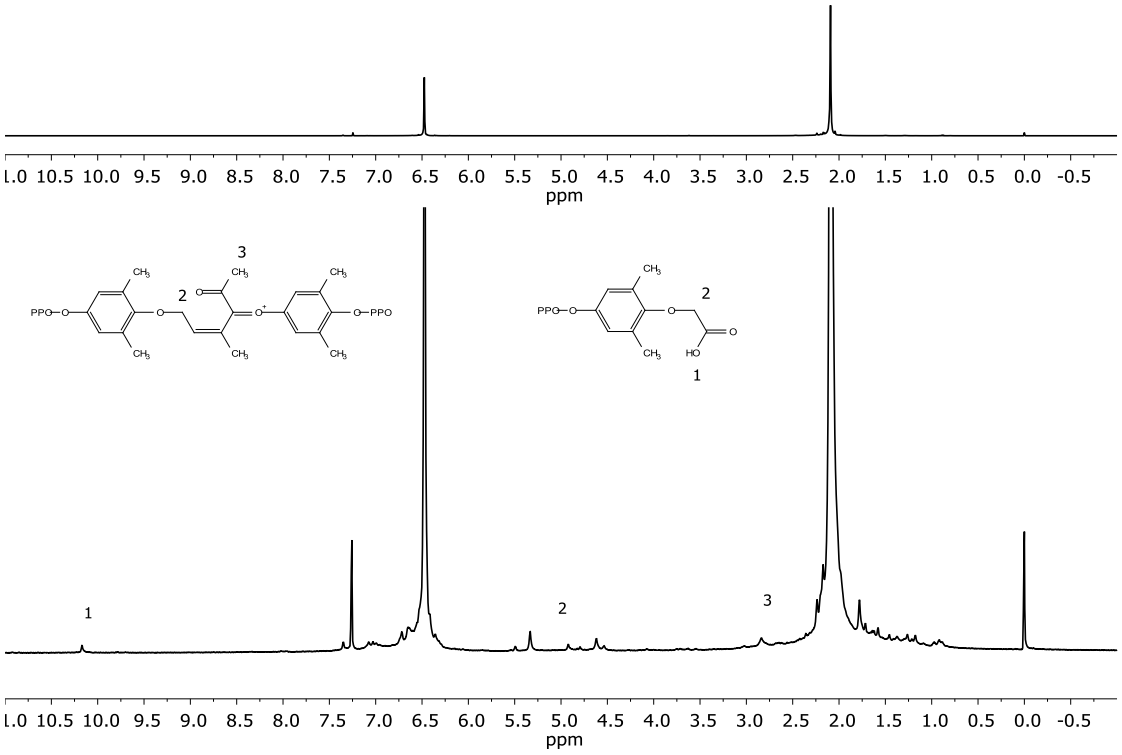

Figure 2.5: Stacked ^{1}H-NMR spectroscopy of (top) pristine PPO and (bottom) decomposed PPO polymeric membranes.

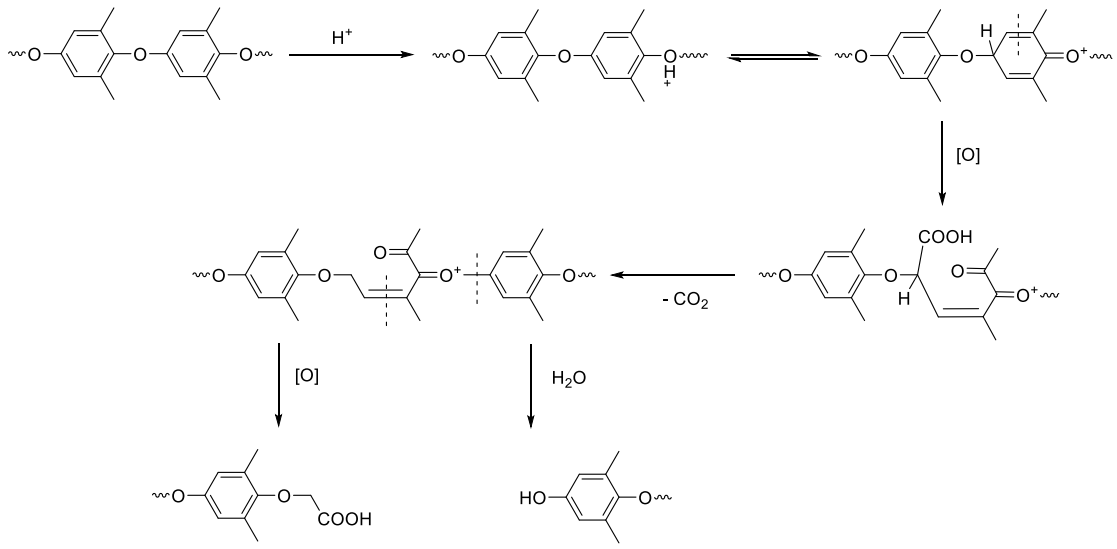

Figure 2.6: Proposed degradation mechanism of PPO polymeric membranes in cerium (IV) and $HClO_4$ electrolyte.

2.3.3 Polysulfone Degradation Mechanism

To investigate the degradation of PSF, HSQC spectroscopy of PSF was performed before and after the 1000 h degradation in cerium solution. From the HSQC spectroscopy in Figure 2.7 and Figure 2.8, clear degradation was shown by distinct emerging peaks at 2.7 ppm, 2.8 ppm, 3.0 ppm, and 3.4 ppm in ^{1}H NMR spectroscopy, which are correlated with peaks at 28 ppm, 30 ppm, 24 ppm, and 50 ppm in ^{13}C NMR spectroscopy, respectively. The color of these peaks indicates they could possibly be -CH, $-CH_2$, or $-CH_3$. Based on this information, these peaks most likely correlated with alkane groups linked to an aromatic ring.

These alkane groups are products from oxidation cleavage near the propylidene group in PSF backbone. The complexity of the alkane peaks is due to the decarboxylation after oxidation. The overall degradation mechanism is proposed in Figure 2.9. The degradation started from the protonation of the ether bond in a rich acid

environment. After protonation of the ether bond, the propylidene across an aromatic ring could be activated and oxidized by Ce^{4+}. Due to the delocalized positive charge, the formed carboxylic acid went through decarboxylation. Further oxidation and decarboxylation also occurred, thus multiple middle products M1, M2, and M3 (noted in Figure 2.9) were formed. M1, M2, and M3 were further oxidized by Ce^{4+}, and the adjacent aromatic ring was oxidized to benzoquinone, eventually causing the backbone to cleavage. The formed products had alkane groups with peaks from 2.0 ppm to 3.5 ppm in ^{1}H NMR spectroscopy and from 20 ppm to 50 ppm in ^{13}C NMR spectroscopy.

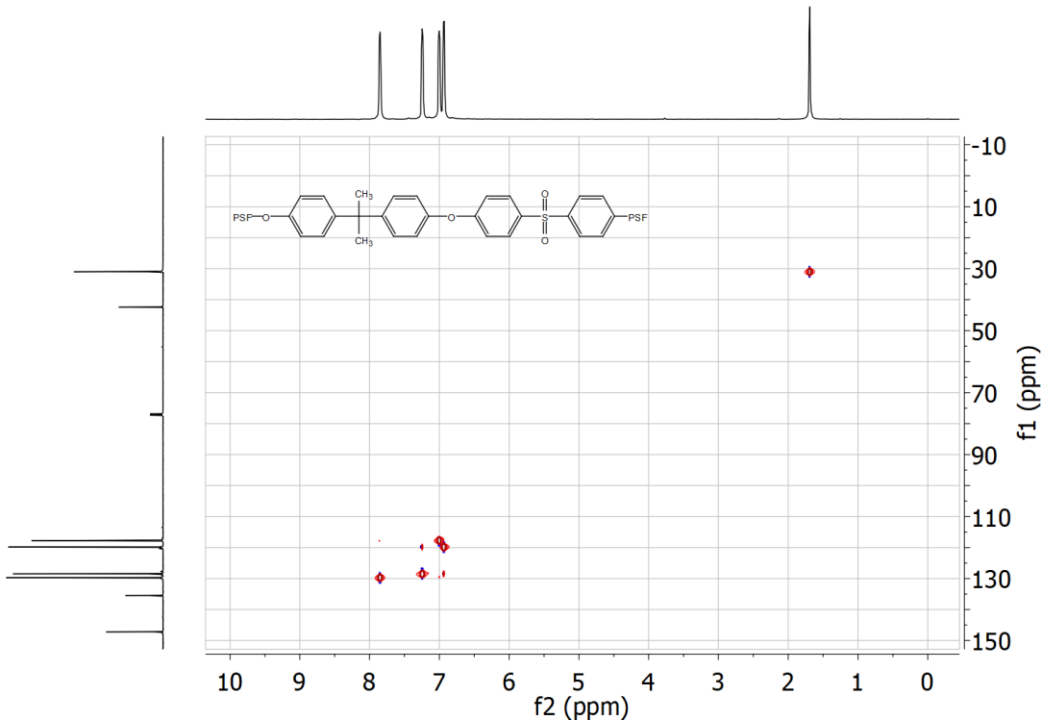

Figure 2.7: HSQC spectroscopy of pristine PSF before chemical stability test in the cerium electrolyte, $CDCl_3$ as the solvent, TMS as the internal standard.

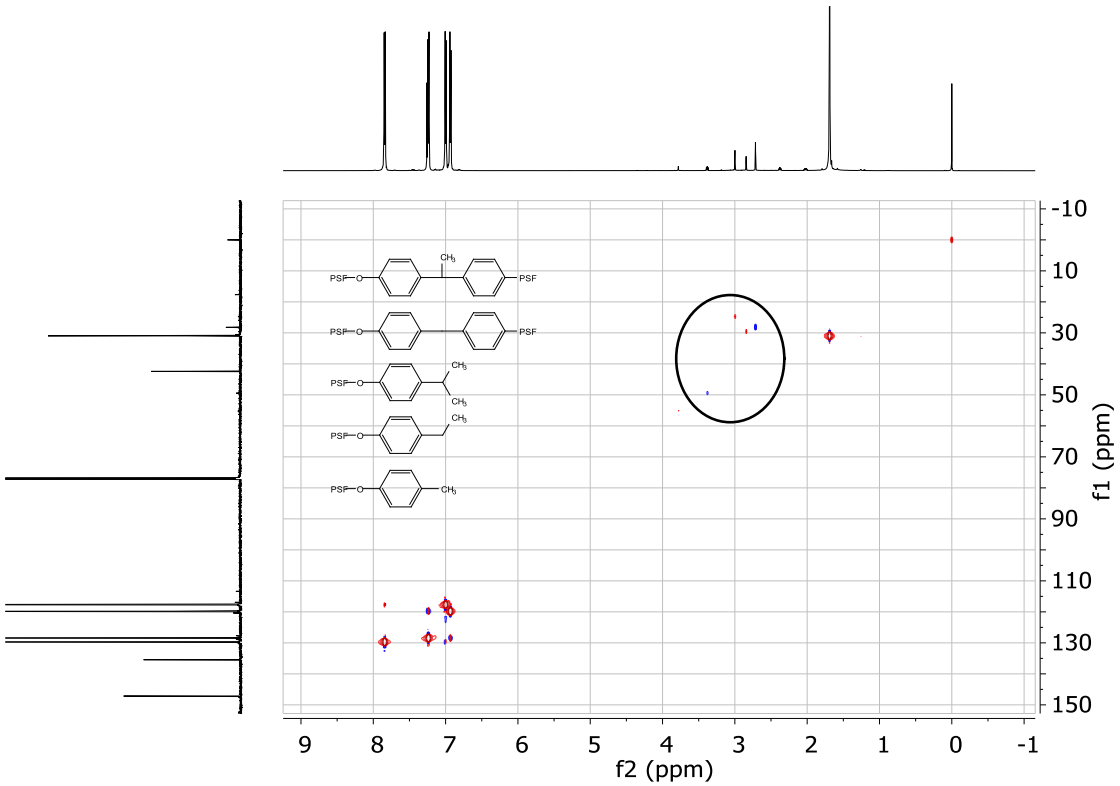

Figure 2.8: HSQC spectroscopy of decomposed PSF after chemical stability test in the cerium electrolyte, $CDCl_3$ as the solvent, TMS as the internal standard.

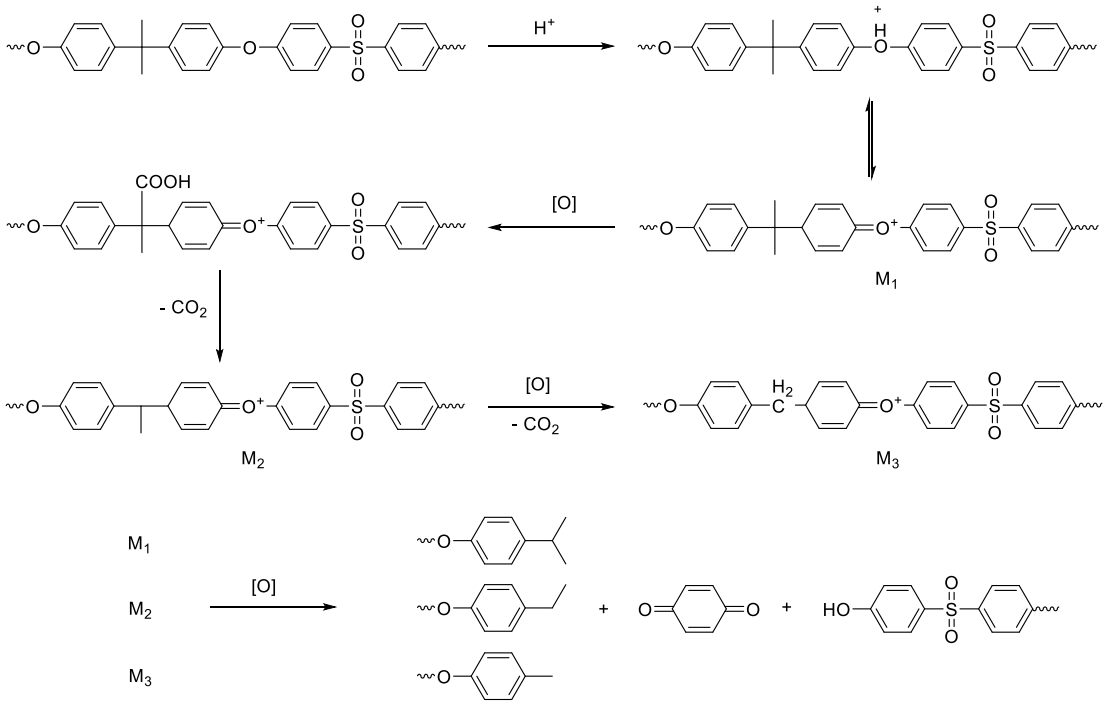

Figure 2.9: Proposed degradation mechanism of PSF polymeric membranes in the cerium (IV) and $HClO_4$ electrolyte.

2.4 Conclusion

HSQC spectroscopy was used to study the degradation of PPO and PSF in cerium solution, and the possible degradation mechanisms were illustrated. We demonstrated that for polymer membranes in cerium solution, aromatic ether structure should be avoided. The protonation of the ether bond will facilitate a further oxidation degradation that will eventually cause the backbone cleavage. To develop a chemically stable IEM for cerium RFB, the F_6PBI is the most suitable backbone choice among these four polymers.

Chapter 3

INVESTIGATION AND DESIGN OF OXIDATIVELY STABLE MEMBRANES FOR CERIUM REDOX FLOW BATTERIES

A double membrane zinc-cerium redox flow battery (RFB) with the highest voltage in the aqueous system was developed by Yan et al.[105] However, the RFB requires an anion-exchange membrane (AEM) with high oxidative resistance to work in the cerium electrolyte. Unfortunately, the commercial AEMs have limited oxidative stability and insufficient lifetime when working in cerium electrolytes.

As reported in Chapter 2, hexafluoropropylidene polybenzimidazole (F_6PBI) polymer backbone showed the highest oxidation resistance in cerium electrolytes. For the selection of cationic functional groups, two chemically stable phosphonium cations were tested, and their functionalized F_6PBI membranes were synthesized. The tris(2,4,6-trimethoxyphenyl)phosphonium functionalized polybenzimidazole (TTMPP-PBI) membrane exhibited desired anion conductivity and satisfactory oxidation stability.

3.1 Introduction

One of the hottest topics today is to investigate and utilize renewable energy sources. These renewable energy sources play an important role to reduce greenhouse gas emissions and solve fossil-fuel shortage.[221-225] In order to make renewable energy reliable and to overcome the intermittent nature of wind and solar, a large-scale energy storage system is necessary.[16-18, 226]

RFBs are well suited for energy storage purpose. The advantages of RFBs include flexible design, excellent scalability, and long cycle life. Aqueous RFB systems are also safer compared to flammable lithium-ion batteries and more reliable as the redox pairs are separated in different tanks during non-operation.[18, 116, 227-228]

As of today, various types of RFBs have been invented and are developed at different stages.[18, 227] A partial list includes: Zn-Br RFBs,[199-201] Fe-Cr RFBs,[202-205] all-V RFBs,[41, 99, 206] Zn-Ce RFBs,[192, 194-195] all-organic RFBs,[38, 40, 207-208] and all-polymer RFBs.[209-211] Among the numerous redox pairs used in different RFB systems, cerium redox-pair ($Ce(4^+)/Ce(3^+)$) is one of most positive redox pair (1.74 V vs. standard hydrogen electrode (SHE)) in water,[105] and its aqueous RFBs have unprecedented high cell voltage (1.87 V – 3.08 V).[105, 192] High cell voltage is crucial to achieve lower storage cost.[105]

Although possessing high energy density, compared to the widely used vanadium RFBs, cerium RFBs are still in the early research and development stage, and there are many scientific and technical challenges that must be overcome.[116, 192] The high standard potential of the $Ce(4^+)/Ce(3^+)$ redox pair (1.74 vs. SHE) poses a crucial threat to the stability of IEMs and causes decreased the conductivity and reduced mechanical integrity during operation.[105] The highest cell voltage (3.08 V) in aqueous RFB systems was achieved with a double-membrane zinc/cerium RFB by Gu et al. at 2014.[105] Unfortunately, this RFB could only operate for 6 complete cycles due to the failure of the Fumasep® AEM in the cerium electrolyte.[105]

With limited research in cerium stability, we first screened four kinds of polymeric backbones in cerium electrolyte and found F_6PBI exhibited the highest oxidation stability. F_6PBI's high thermo-oxidative stability and ease for further

processing and modification made it the best choice among the studied polymers for use in cerium RFB.[104, 133] For an AEM, the cation may be vulnerable to react with oxidative species resulting in chemical degradation. To design an AEM with strong oxidative resistance, we first chose one of the most chemically stable cation, tris(2,4,6-trimethylphenyl)phosphonium (TTMePP), which was published by Yan et al. in 2016,[110] as the functional group. However, we discovered that the TTMePP cation functionalized membrane has trivial anion conductivity in the aqueous system due to the hydrophobic nature of the cation. Another chemically stable phosphonium cation, tris(2,4,6-trimethoxyphenyl)phosphonium (TTMPP), developed earlier by Yan et al.[158] was then chosen as the functional group for this work. A series of TTMPP-PBI membranes were developed, and the oxidative resistance was examined.

3.2 Materials and Methods

3.2.1 Materials

All chemicals were obtained from Sigma-Aldrich and used as received unless otherwise stated. The 0.5 M Cerium (IV) in 1.3 M $HClO_4$ aqueous solution was concentrated by rotary evaporator from 0.3 M cerium (IV) and perchloric acid solution purchased from Alfa Aesar. Anhydrous Cerium (IV) sulfate was purchased from Alfa Aesar. Fumasep® FAS and FAB membranes were purchased from Fumatech. Nafion 212 membrane was purchased from FuelCellStore. Expanded polytetrafluoroethylene (ePTFE) was obtained from Xergy Inc.

3.2.2 Synthesis

3.2.2.1 Synthesis of Hexafluoropropylidene Polybenzimidazole (F_6PBI)

F_6PBI was synthesized using a literature procedure.[133]

3.2.2.2 Synthesis of Iodobutanol Tris(2,4,6-trimethylphenyl)phosphonium ($IBTTMePP^+$)

TTMePP (1.0 g) was fully dissolved in 1,4-diiodobutane (10 mL) at room temperature. Cu powder (1.5 g) was added into the reaction, and the reaction mixture stirred under a nitrogen purge. The reaction mixture was slowly heated to 150 °C and stirred for 48 h. During the reaction, the reaction mixture did not turn purple indicating no formation of iodine. Next, the reaction mixture was poured into 400 mL ethyl ether. The precipitate was collected and washed with ethyl ether twice. The precipitate was stirred in 500 mL ethanol covered at 60 °C for 1 day and filtered. The filtrate was collected, and then ethanol was removed by rotary evaporator. The yellow powder left was recrystallized by tetrahydrofuran (THF) and ethyl ether at 50 °C. While heating to 50 °C, the proper amount of THF was added to form a saturated solution at 50 °C. The same volume of ethyl ether was added later at 50 °C. After that, the mixed solution was allowed to cool over time to give precipitates. The $IB9MeTTP^+$ product was yellow powder, and this procedure attained a 50% yield.

3.2.2.3 Synthesis of Butanol Tris(2,4,6-trimethylphenyl)phosphonium Functionalized Hexafluoropropylidene Polybenzimidazole (TTMePP-PBI)

In a three-neck round flask with mechanical stirrer under nitrogen purge, F_6PBI polymer (0.25 g) was fully dissolved in n-methyl-2-pyrrolidone (10 mL). LiH (0.0035 g) was slowly added into the solution, and the reaction mixture stirred at 50 °C

overnight. NMP (20 mL) solution of IB9MeTTP$^+$ (0.50 g) was then added. The reaction was gently stirred at 80 °C for 2 days. After the reaction, the reaction mixture was concentrated by solvent evaporation and directly used for membrane casting.

3.2.2.4 Synthesis of (4-(chloromethyl)benzyl)tris(2,4,6-trimethoxyphenyl)phosphonium Chloride (CBTTMPP$^+$Cl$^-$)

In a 250 mL three-neck round bottom flask with nitrogen purge, 16.440 g (93.90 mmol) 1,4-bis(chloromethyl)benzene was dissolved in 60.0 mL THF at 60 °C. 10.000 g (18.78 mmol) (2,4,6-trimethoxyphenyl)phosphine was dissolved in 125.0 mL THF and slowly added into the flask through a dropping funnel over 14 h. White precipitation began to form after 30 minutes of adding (2,4,6-trimethoxyphenyl)phosphine solution. After all (2,4,6-trimethoxyphenyl)phosphine solution was added, the reaction mixture continued to stir for another 10 h. Next, the reaction mixture was filtered, and the white solid was washed with additional THF to remove remaining 1,4-bis(chloromethyl)benzene. The product was 12.621 g white powder (95 % yield).

3.2.2.5 Synthesis of Tris(2,4,6-trimethoxyphenyl)phosphonium Functionalized Hexafluoropropylidene Polybenzimidazole (TTMPP-PBI)

In a properly dried 250 mL three-neck round bottom flask equipped with a mechanical overhead stirrer under nitrogen purge, 2.000 g (3.54 mmol) F_6PBI powder was vigorously stirred in 80.0 mL anhydrous N-Methyl-2-pyrrolidone (NMP) at 100 °C for 12 h. The flask was cooled to room temperature after F_6PBI was completely dissolved. 0.169 g (21.3 mmol) 95 % LiH was then added to F_6PBI solution. The reaction mixture was then slowly heated to 50 °C. When gas was no longer released from the mixture, and the mixture became extremely viscous. CBTTMPP$^+$Cl$^-$ (2.504 g to 10.019 g, 3.54 mmol to 14.16 mmol) suspension in anhydrous NMP (20.0 mL to 80.0

mL) was added, and the reaction was slowly heated to 80 °C. The reaction mixture became less sticky afterward and then stirred at 80 °C for 24 h to 48 h. Next, the mixture was poured into 1500 mL of THF and filtered. The solid was TTMPP-F_6PBI and unreacted CBTTMPP$^+$Cl$^-$. The solid mixture was then washed with 2000 mL of DI water several times to remove remaining CBTTMPP$^+$Cl$^-$ until no further weight change was observed before and after the wash.

3.2.3 Experimental Methods

3.2.3.1 Polymer Backbone Screening Test in Cerium(IV) Electrolyte

The polymer backbone screening procedure is reported in Section 2.2.2.3.

3.2.3.2 Membrane Fabrication

The polymer was completely dissolved in dimethylacetamide (DMAc) to make a 2.5 w/v% solution. The solution was cast on a glass plate and dried in air at 60 °C for 24 h. After the solvent completely evaporated, the glass plate was immersed in DI water, and the membrane was gently peeled from the glass.

3.2.3.3 Reinforced Membrane Fabrication

10 mL ethanol was added to a 10 mL 2.5 w/v% solution of TTMPP-PBI-3 in DMAc. The 20 mL solution was then poured to ethanol infiltrated 10 cm × 10 cm porous ePTFE membrane in a glass frame. The solution was then heated to 40 °C for 24 h. After the solvent completely evaporated, the glass frame was immersed in DI water, and the composite membrane was gently removed from the frame.

3.2.3.4 Ion Exchange Capacity (IEC) of Membranes

The ion exchange capacity (IEC, unit: mmol g^{-1}) of membranes were determined by titration. A membrane sample was first immersed in 0.1 mol L^{-1} NaCl solution for 48 h at room temperature. Next, the membrane (Cl^- form) was dried in vacuum at 60 °C for 48 h, weighed, then immersed in 30.0 mL 0.1 mol L^{-1} $NaNO_3$ solution for 48 h at room temperature. This solution was titrated with 0.05 mol L^{-1} $AgNO_3$ with K_2CrO_4 as the indicator. IEC was calculated according to the following equation:

$$\mathrm{IEC} = \frac{V_{AgNO_3} \times C_{AgNO_3}}{M}, \qquad \text{(Equation 3.1)}$$

where V_{AgNO_3} is the volume of $AgNO_3$ solution, C_{AgNO_3} is the concentration of $AgNO_3$ solution, and M is the mass of dried membrane in Cl^- form. For reinforced membranes, M is the total mass (including the ePTFE material) of the dried membrane in Cl^- form.

3.2.3.5 Water Uptake (WU) and Swelling Ratio (SR) of Membranes

WU and SR of membranes were determined by weight difference and linear expansion ratio, respectively. A membrane sample was immersed in DI water at room temperature for 24 h. After removing the excess water on the surface of the membrane with tissue paper, the weight of the wet membrane (W_{wet}) and length of the wet membrane (L_{wet}) were measured. Then the wet membrane was dried at 60 °C under vacuum for 48 h. Weight of the dry membrane (W_{dry}) and length of the dry membrane (L_{dry}) were measured afterward. WU and SR were calculated according to the following equations:

$$\mathrm{WU}\ (\%) = \frac{W_{wet} - W_{dry}}{W_{dry}} \times 100 \qquad \text{(Equation 3.2)}$$

$$\mathrm{SR}\ (\%) = \frac{L_{wet} - L_{dry}}{L_{dry}} \times 100 \qquad \text{(Equation 3.3)}$$

3.2.3.6 Anion (OH^- and ClO_4^-) Conductivity Measurement

Before measuring conductivity, the AEM was anion exchanged to either OH^- form or ClO_4^- form by immersing the membrane in exceeded 2 M NaOH or 1 M $NaClO_4$ solution, respectively, for 60 h with the exchange solution changed at 12 h intervals. The AEM was then washed with DI water 3 times to remove the residual base/salt in the membrane.

The in-plane conductivity of membrane sample (1 cm in width) was measured by electrochemical impedance spectroscopy with four-probe method (1 cm distance between adjacent probes) by Solartron SI 1287. The intercept at axis Z_{re} was recorded as the impedance. During the measurement, the membrane was fully immersed in DI water bath with a temperature control unit.

3.2.3.7 Oxidative Stability Test in Cerium (IV) Aqueous Solution

Accelerated chemical stability tests of membranes were conducted in 0.5 M cerium (IV) and 1.3 M $HClO_4$ at 60 °C. Nafion 212, F_6PBI membrane, FAS-30 (purchased from fumasep®), and FAB-PK-130 (purchased from fumasep®) were also tested and compared with prepared TTMPP-PBI-3/PTFE membrane.

3.3 Results and Discussion

3.3.1 Polymer Backbone Stability in Cerium (IV) and $HClO_4$ Solution

As discussed in Chapter 2, polystyrene (PS), poly(2,6-dimethyl-phenylene oxide) (PPO), polysulfone (PSF), and F_6PBI were prepared, and their degradations were investigated in 0.5 M Cerium (IV) and 1.3 M $HClO_4$ solution at 60 °C. The remaining weight results are shown in Figure 2.2. F_6PBI polymer showed the best stability.

3.3.2 Tris(2,4,6-trimethylphenyl)phosphonium Functionalized Polybenzimidazole (TTMePP-PBI) Membrane

Direct quaternization through center phosphorus atom was investigated, and we found that Cu played a critical role in the reaction as it could inhibit the decomposition of alkyl iodide during the reaction. Once we added an adequate amount of Cu into the reaction, the reaction mixture did not turn purple anymore, which indicate that I_2 did not form.

Figure 3.1 shows the model reactions we tried between TTMePP and iodohexane. At 25 °C, because of the high steric hindrance of TTMePP, large alkyl groups could not link to the central phosphorus. At 150 °C, the quaternization could occur, but the yield was trivial based on ^{31}P NMR spectroscopy analysis. After further investigation, we discovered that the major obstacle at high temperature was the decomposition of alkyl iodide to I_2 which could then react with TTMePP to form complex side products.[229-230] As Cu inhibits the decomposition of alkyl iodide, the addition of Cu to the reaction mixture resulted in a 70% crude yield out of this reaction at 150 °C.

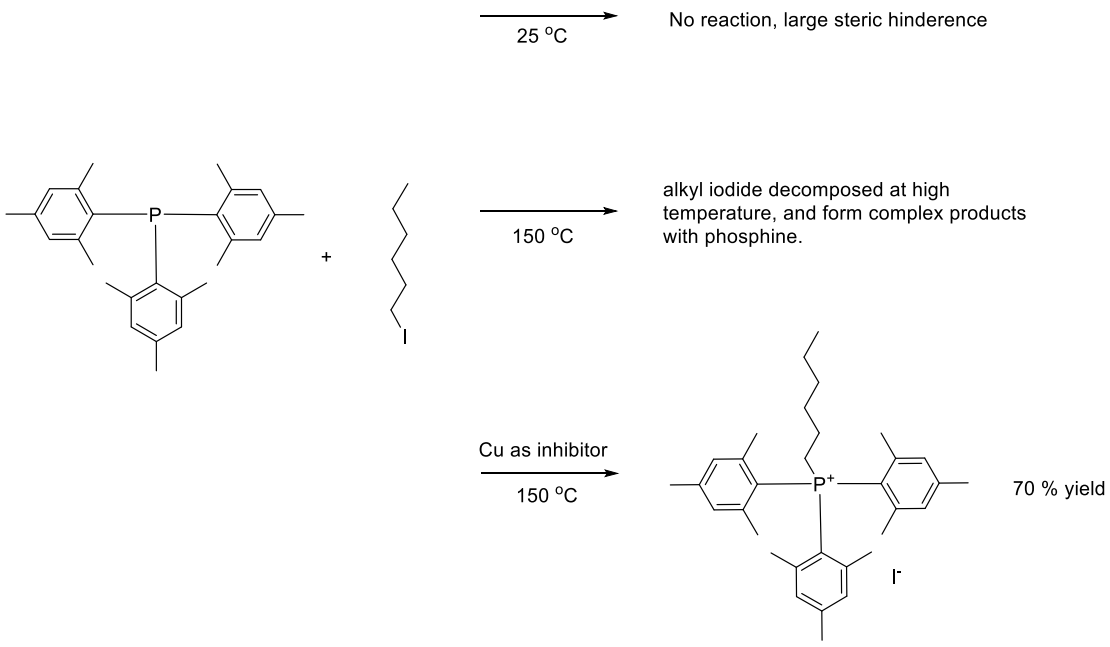

Figure 3.1: Model reactions between TTMePP and iodohexane, quaternization of TTMePP with alkyl iodide could only be achieved by adding copper as decomposition inhibitor and using high temperature to overcome the steric hindrance of TTMePP.

Based on the quaternization reaction condition we discovered in this Section, TTMePP was quaternized by diiodobutane with Cu added as an inhibitor at high temperature. An excess of diiodobutane was added to avoid double reaction on two ends of the diiodobutane. The reaction scheme and NMR spectroscopy of the obtained $IBTTMePP^+$ are shown in Figure 3.2 and Figure 3.3.

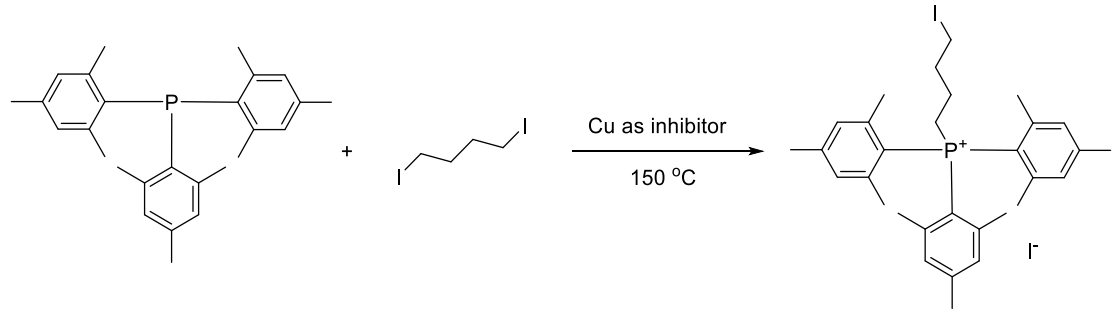

Figure 3.2: Synthesis of IBTTMePP$^+$ from TTMePP and diiodobutane. The mole ratio of TTMePP/1,4-diiodobutane was 1/29 to avoid couple linkage. Cu was added as an inhibitor to prevent alkyl iodide decomposition.

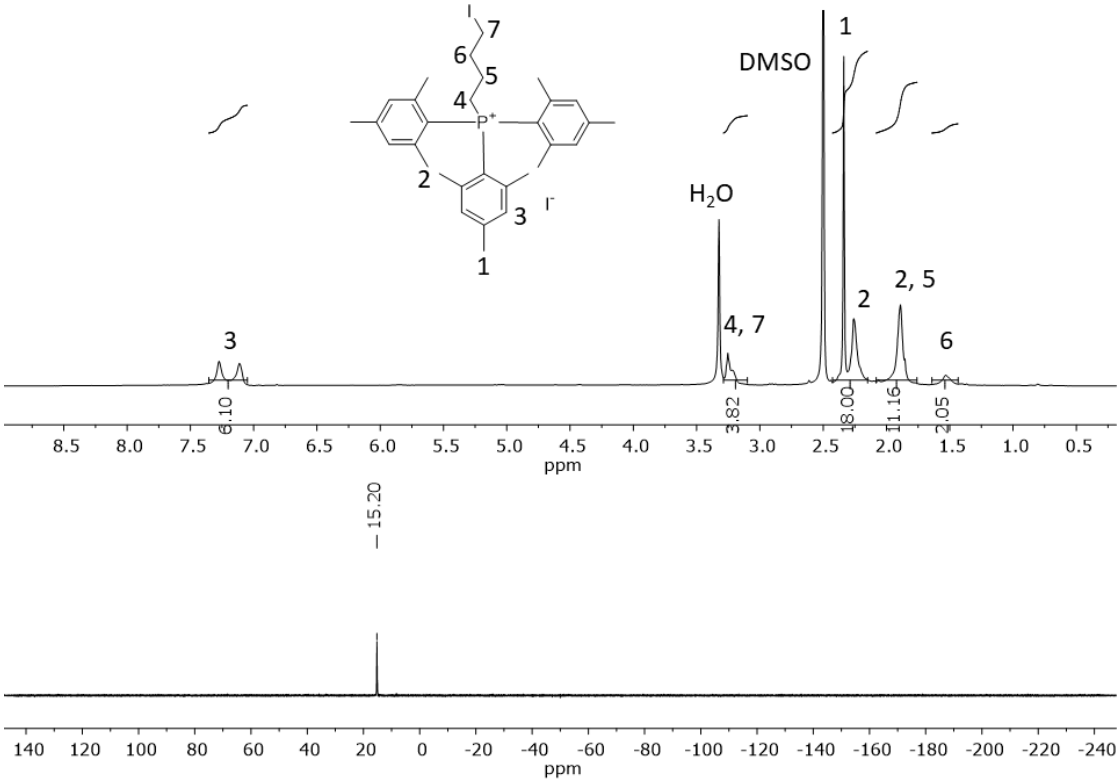

Figure 3.3: ^{1}H NMR spectroscopy and ^{31}P NMR spectroscopy of synthesized IBTTMePP$^+$ after purification. DMSO-d6 was used as the solvent. There is only one peak in ^{31}P NMR spectroscopy indicating that the purified IBTTMePP$^+$ was obtained.

IBTTMePP$^+$ was used to functionalize F_6PBI backbone to form the desired TTMePP-PBI membrane for cerium RFBs. The membrane was cast by solvent evaporation method. The overall synthesis route for TTMePP-PBI polymer is in Figure 3.4. The prepared TTMePP-PBI membrane is shown in Figure 3.5. However, the prepared TTMePP-PBI membrane is very hydrophobic and has no anion conductivity. The characterizations of the prepared TTMePP-PBI membrane are shown in Table 3.1 and Table 3.2.

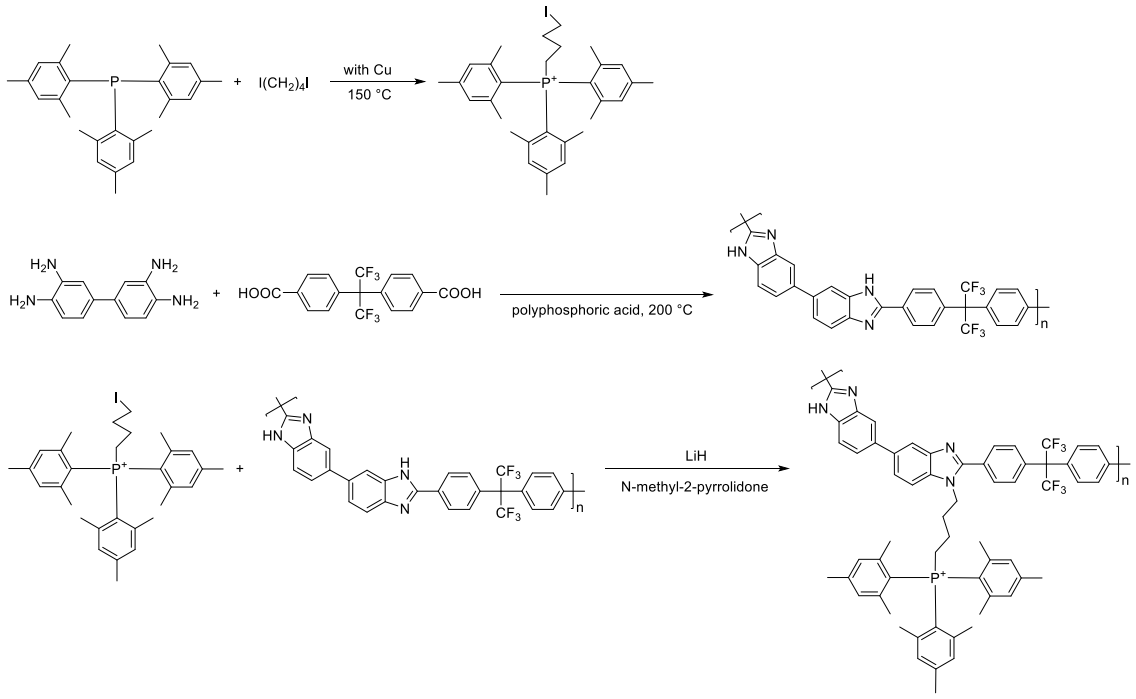

Figure 3.4: Synthetic route for TTMePP-PBI polymer. IBTTMePP$^+$ and F_6PBI were synthesized before final linkage. The synthetic details are reported in Section 3.2.2.1, Section 3.2.2.2, and Section 3.2.2.3.

Figure 3.5: Picture of prepared TTMePP-PBI membrane.

3.3.3 Tris(2,4,6-trimethoxyphenyl)phosphonium Functionalized Polybenzimidazole (TTMPP-PBI) Membrane

The prepared TTMePP-PBI membrane exhibited a WU of only 3.6 % (weight based), which is even less than the WU of a pure PBI membrane. This was mainly due to the hydrophobic TTMePP cation. Although the TTMePP cation has been proven to be more chemically stable than TTMPP cation by Yan et al.,[110] it is not suitable for application as an AEM functional group in an aqueous system due to its hydrophobicity.

Besides the chemically stable TTMePP, TTMPP functional group is also an excellent chemically stable cation. TTMPP cation was proposed by Yan et al.[157, 159, 231] before the TTMePP cation. Ramani et al. also proved that its functionalized polymers showed much better IEC stability than traditional ammonium-functionalized polymers in oxygen saturated alkaline environment.[232] TTMPP can be quaternized and linked to the desired polymer backbone by 1,4-bis(chloromethyl)benzene as a linker molecule. The synthetic route and NMR spectroscopy of polymer structures are shown in Figure 3.6, Figure 3.7, Figure 3.8, and Figure 3.9. The obtained TTMPP-PBI membranes showed reasonable WU and anion conductivity. TTMPP-PBI polymers with different degrees of substitution were also prepared. The mechanical strength of the TTMPP-PBI membrane was improved by reinforcing it with ePTFE, a common support material for ion-exchange members.[233-234] The prepared ePTFE reinforced TTMPP-PBI membrane is shown in Figure 3.10.

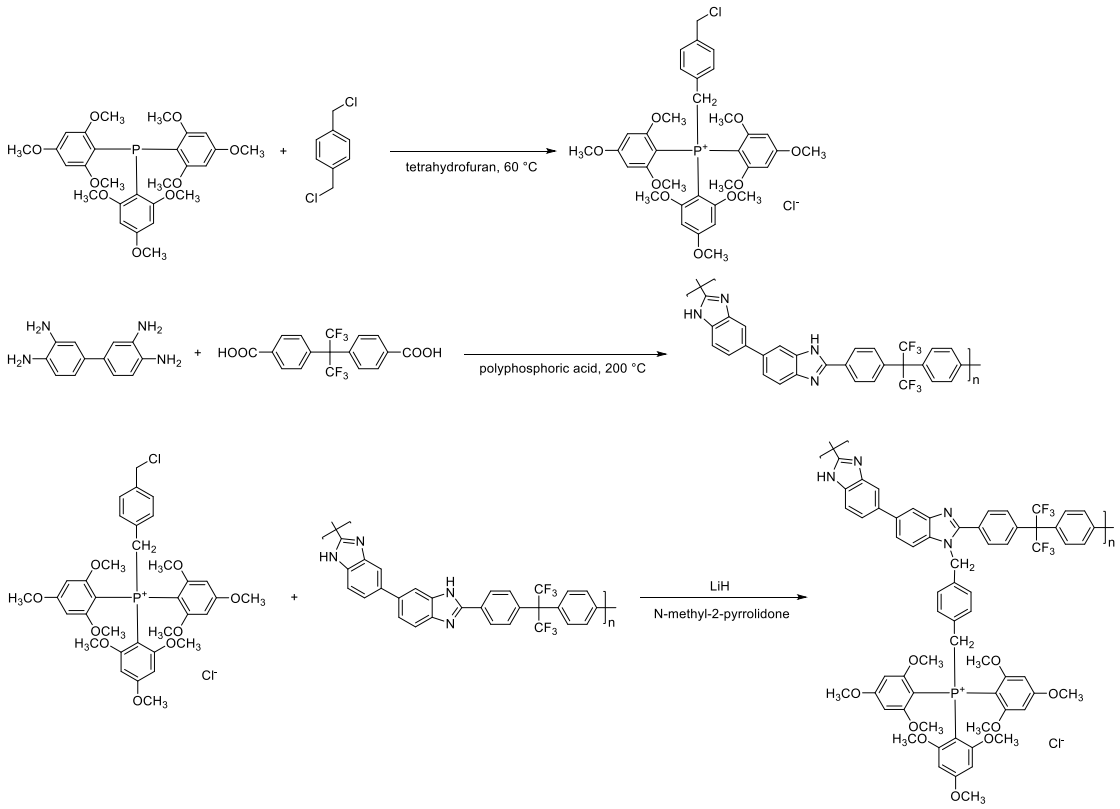

Figure 3.6: Synthetic route for TTMPP-PBI polymer. TTMPP can be quaternized by a linker molecule. The synthetic details are reported in Section 3.2.2.1, Section 3.2.2.4, and Section 3.2.2.5.

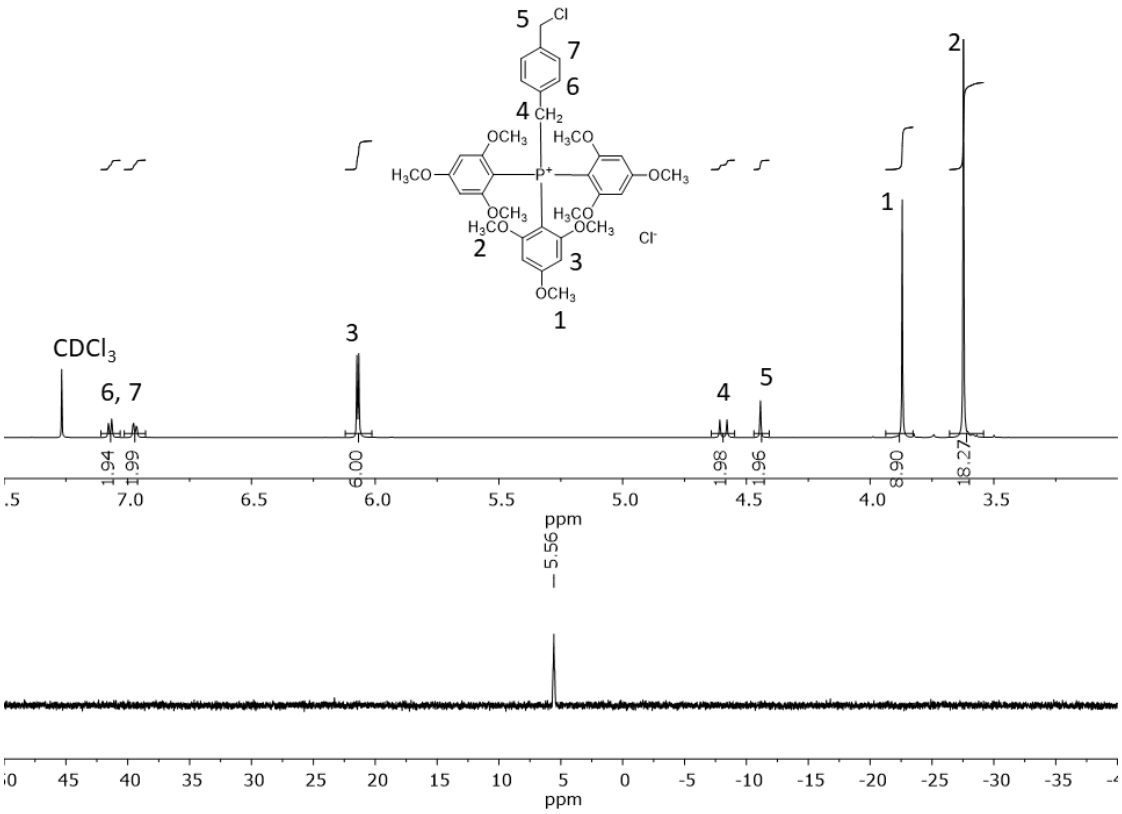

Figure 3.7: ^{1}H NMR spectroscopy and ^{31}P NMR spectroscopy of purified $CBTTMPP^{+}Cl^{-}$, DMSO-d6 as the solvent. There is only one peak in ^{31}P NMR spectroscopy indicating that the purified $CBTTMPP^{+}Cl^{-}$ was obtained.

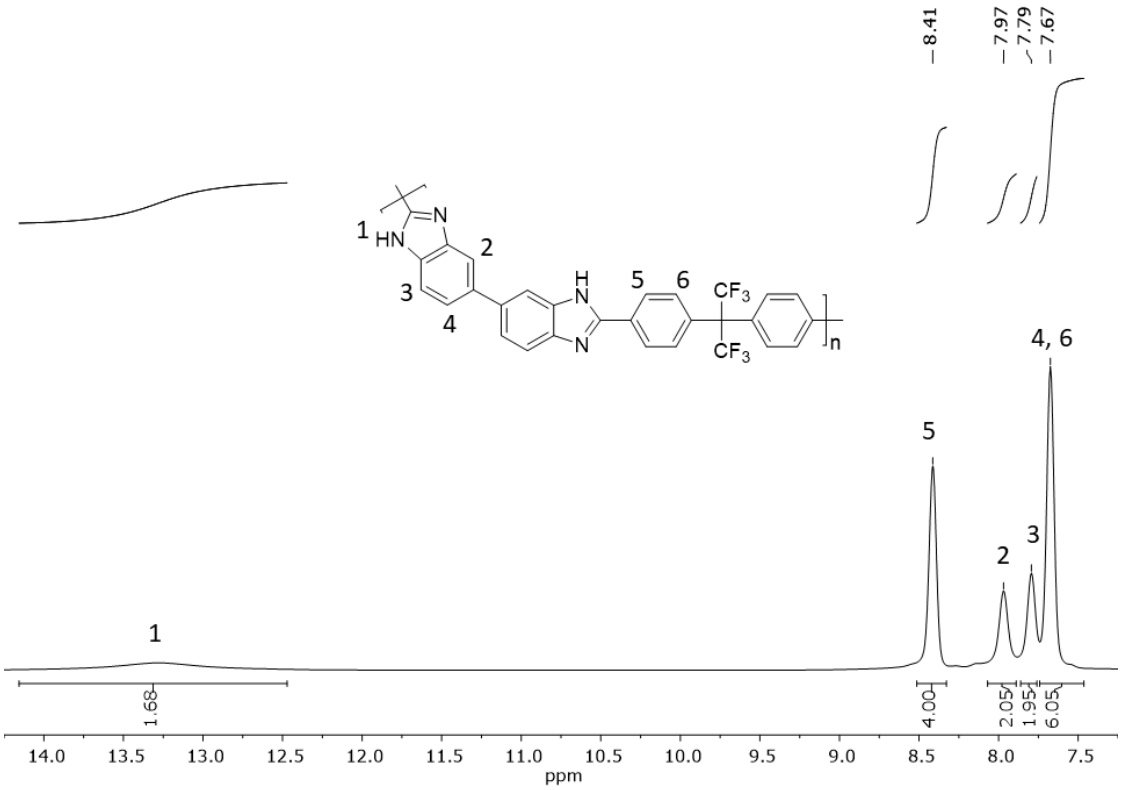

Figure 3.8: ^{1}H NMR spectroscopy of purified F_6PBI, DMSO-d6 as the solvent.

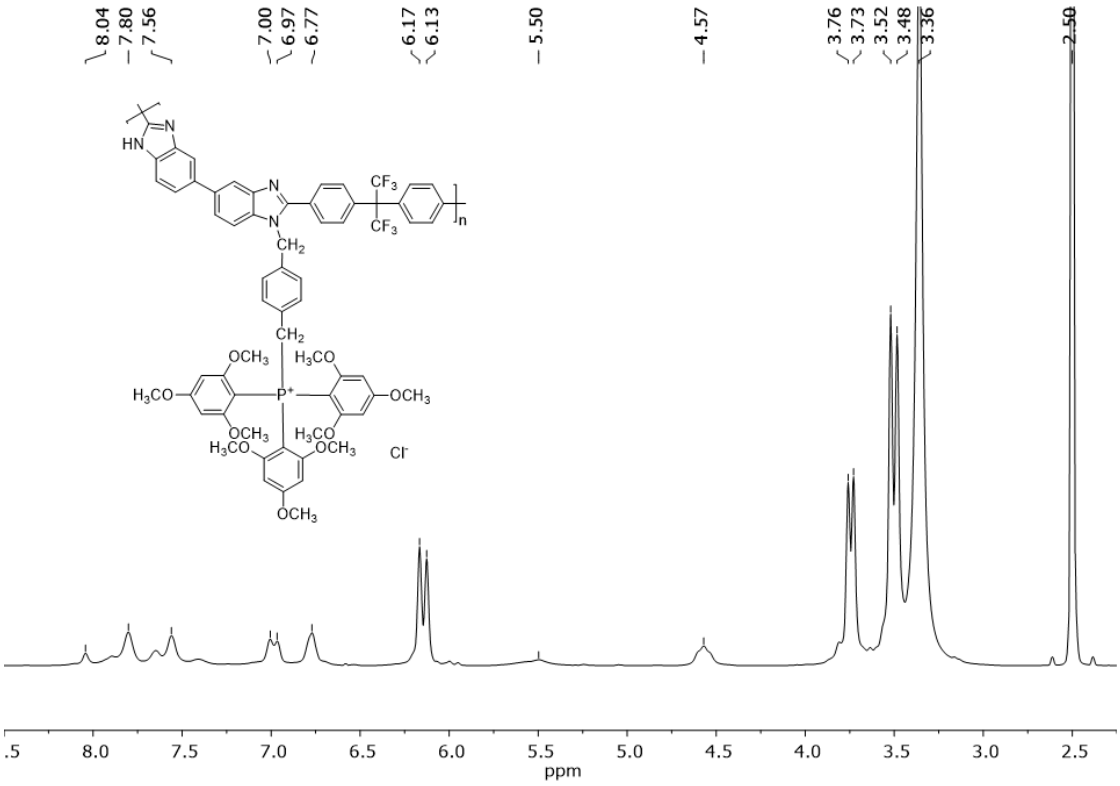

Figure 3.9: ^{1}H NMR spectroscopy of purified TTMPP-200-F_6PBI, DMSO-d6 as the solvent.

;

Figure 3.10: Prepared TTMPP-PBI-3/PTFE reinforced membrane. ePTFE was used as reinforcement support.

3.3.4 Characterization of Phosphonium Functionalized Polybenzimidazole Membranes

The degree of substitution, theoretical IEC, titration measured IEC, WU, mechanical properties, and OH^- and ClO_4^- conductivity of prepared TTMePP-PBI membrane and TTMPP-PBI membrane are shown in Table 3.1 and Table 3.2. Due to

the hydrophobic nature of TTMePP, the prepared TTMePP-PBI membrane showed insufficient WU and trivial anion conductivity. The average measured IEC of the TTMePP-PBI membrane was lower than theoretical IEC due to the hydrophobicity. For TTMPP-PBI membranes with different degree of substitution, the membranes tended to become weak and brittle with the increasing substitution of TTMPP cations. A higher degree of substitution with the large function groups blocked entanglement of the polymer chains resulting in lower mechanical strength. In order to improve the mechanical strength of TTMPP-PBI membrane, ePTFE reinforcement technology was used, and the data of TTMPP-PBI-3/PTFE membrane characterization are also shown in Table 3.1 and Table 3.2. As expected, the ClO_4^- conductivities of prepared membranes were much lower than OH^- conductivities, because the ionic mobility of ClO_4^- is only 34 % of OH^- in water.

Due to the good balance of anion conductivity and mechanical strength, TTMPP-PBI-3/PTFE membrane was chosen for further analysis in the cerium electrolyte of the RFB.

Table 3.1: Degree of substitution (DS), theoretical ion exchange capacity (IEC^t), titration measured ion exchange capacity (IEC^{md}), tensile strength, and elongation at break of pure F_6PBI membrane, TTMePP and TTMPP functionalized polybenzimidazole membranes. Error bars are standard errors of the measurements (n = 3).

Membrane	**DS (%)**	**IEC^t (mmol g^{-1})**	**IEC^{md} (mmol g^{-1})**	**Tensile strength (MPa)**	**Elongation at break (%)**
TTMePP-PBI	90	0.94	0.52 ± 0.02	26.2 ± 1.2	1.7 ± 0.3
TTMPP-PBI-1	70	0.71	0.68 ± 0.04	7.9 ± 0.7	17.4 ± 0.9
TTMPP-PBI-2	110	0.89	0.88 ± 0.02	4.0 ± 0.6	12.5 ± 0.9
TTMPP-PBI-3	200	1.11	1.13 ± 0.03	- [a]	- [a]
TTMPP-PBI-3/PTFE	200	- [b]	0.97 ± 0.02	17.3 ± 0.7	17.1 ± 1.1
F_6PBI	0	- [c]	- [c]	72.0 ± 3.6	10.9 ± 1.1

[a]: TTMPP-PBI-3 membrane is too brittle to test mechanical properties.
[b]: TTMPP-PBI-3/PTFE reinforced membrane has no theoretical IEC.
[c]: F_6PBI membrane has no IEC and no anion conductivity.

Table 3.2: WU, OH^- conductivity, and ClO_4^- conductivity of pure F_6PBI membrane, TTMePP and TTMPP functionalized polybenzimidazole membranes. Error bars are standard errors of the measurements (n = 3).

Membrane	**WU (%)**	**OH^- conductivity (mS cm^{-1})**	**ClO_4^- conductivity (mS cm^{-1})**
TTMePP-PBI	3.6 ± 0.5	1.0 ± 0.6	0.3 ± 0.2
TTMPP-PBI-1	18 ± 2	4.5 ± 0.2	1.3 ± 0.1
TTMPP-PBI-2	58 ± 8	5.9 ± 0.4	1.6 ± 0.2
TTMPP-PBI-3	81 ± 5	12.0 ± 1.0	3.2 ± 0.1
TTMPP-PBI-3/PTFE	26 ± 3	9.8 ± 0.2	2.7 ± 0.1
F_6PBI	9.2 ± 0.8	-[c]	-[c]

[c]: F_6PBI membrane has no IEC and no anion conductivities.

3.3.5 Membrane Chemical Stability in Cerium (IV) Electrolyte

One major goal of this work is to develop a cationic membrane that could survive the super oxidative cerium (IV) and acid environment. 0.5 M cerium (IV) in 1.3 M

$HClO_4$ solution was used to simulate the environment of cerium RFBs. The accelerated degradation test of membranes is conducted at 60 °C with TTMPP-PBI-3/PTFE, F_6PBI, Nafion 212, FAB-PK-130, and FAS-30 membranes. Among these five membranes, the FAB-PK-130 membrane was PEEK reinforced and claimed to be stable in the acidic environment. The commercially available FAS-30 and FAB-PK-130 both failed in the first 100 h. While TTMPP-PBI-3/PTFE membrane had no appreciable morphological change even after 200 h in 0.5 M cerium (IV) in 1.3 M $HClO_4$ at 60 °C. The results are shown in Table 3.3, and the optical images of FAB-PK-130 and TTMPP-PBI-3/PTFE membranes before and after the accelerated stability test are shown in Figure 3.11. For our prepared TTMPP-PBI-3/PTFE membrane, SEM images were collected before and after the accelerated stability test shown in Figure 3.12. No noticeable change was observed in the SEM images. Freeze fracturing in liquid nitrogen did not work for the ePTFE reinforced membrane. Instead, the membrane samples were prepared by cut resulting in imperfections in the cross sections.

Table 3.3: Accelerated membrane stability test of prepared TTMPP-PBI-3/PTFE membrane, F_6PBI membrane, Nafion 212, FAB-PK-130, and FAS-30 at 60 °C in 0.5 M cerium (IV) and 1.3 M $HClO_4$.

	Thickness (μm)	**25 h**	**100 h**	**200 h**
TTMPP-PBI-3/PTFE	14			No appearance change
F_6PBI	14			No appearance change
Nafion 212	50			No appearance change
FAB-PK-130	130		Loss of polymer	
FAS-30	30	Broken		

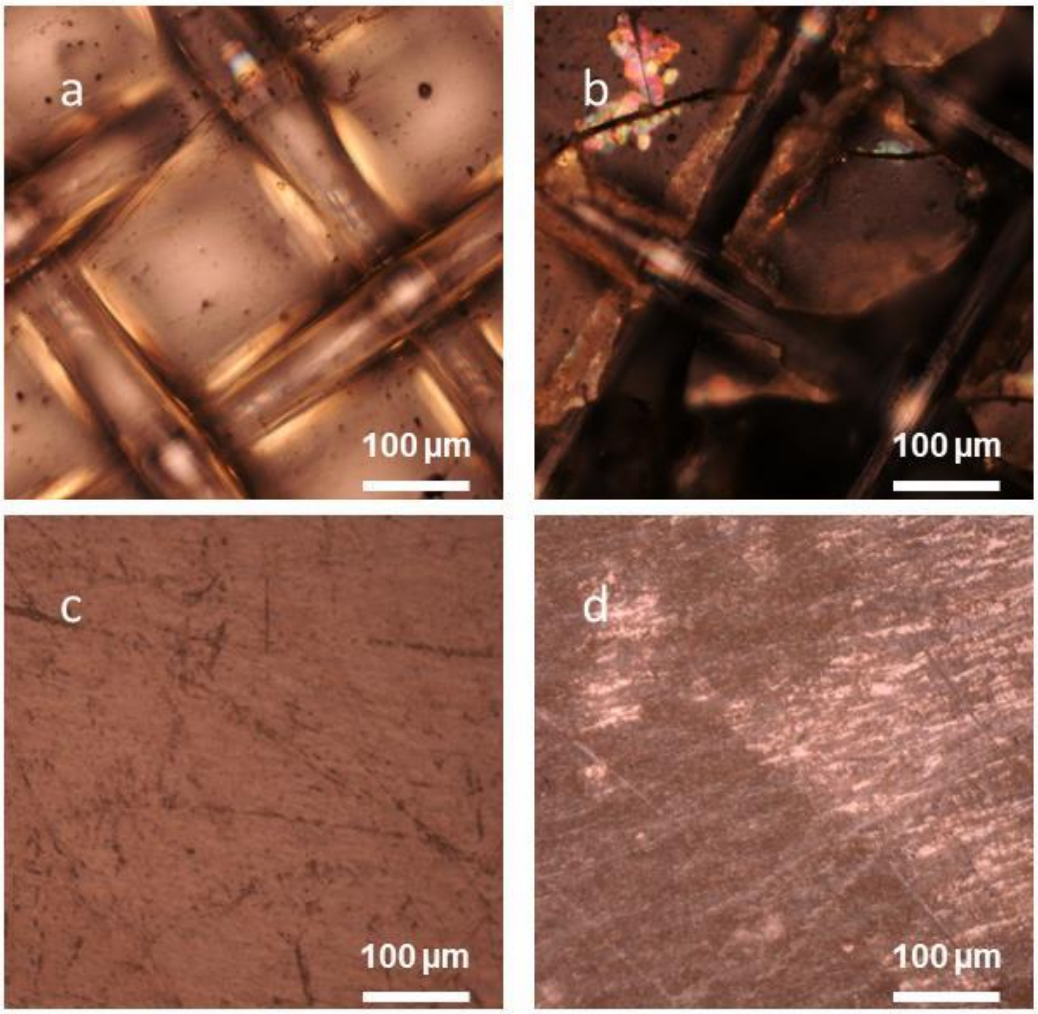

Figure 3.11: Optical microscopy images of FAB-PK-130 and TTMPP-PBI-3/PTFE reinforced membrane before and after accelerated oxidation stability test in 0.5 M cerium (IV) and 1.3 M $HClO_4$ at 60 °C for 100 h. (a and b: FAB-PK-130 before and after; c and d: TTMPP-PBI-3/PTFE reinforced membrane before and after).

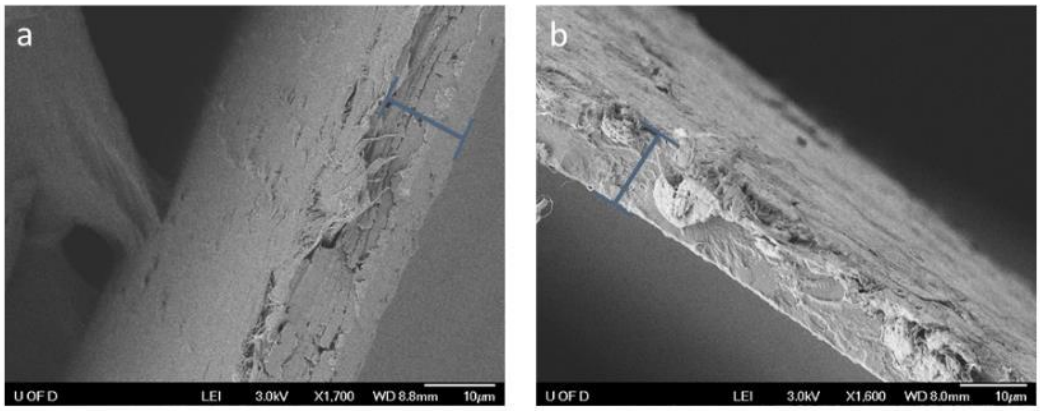

Figure 3.12: SEM images of TTMPP-PBI-3/PTFE membrane cross section and surface before (a) and after (b) 200 h accelerated chemical stability test (blue bar indicated the cross section; the ePTFE substrate is not suitable for freeze fracturing in liquid nitrogen, membrane samples are prepared by cut).

TTMPP-PBI-3/PTFE membrane showed superior chemical stability over the two commercial AEMs during accelerated chemical stability test. The ClO_4^- conductivity and infrared spectra of TTMPP-PBI-3/PTFE membranes are shown in Figure 3.13 and Figure 3.14, respectively. The ClO_4^- conductivity was measured from 20 °C to 70 °C to encompass the range of cerium RFB operating temperatures. As we can see from Figure 3.13, the conductivity suffered a 17 % to 19 % loss on average after the stability test across the range of temperatures. From the infrared spectra in Figure 3.14, no appreciable change was found for TTMPP-PBI-3/PTFE membrane after the accelerated stability test. Besides conductivity and infrared spectroscopy monitoring, we also noticed the thickness of the membrane decreased from 14 μm to 12 μm after the accelerated chemical stability test. Although no noticeable changes were observed from the infrared spectra, the conductivity loss and thickness decrease were likely due to some chemical degradation of the membrane. In this case, the degradation amount

was small. The decomposed products were likely dissolved in the cerium electrolyte, thus no significant change was found in the infrared spectra.

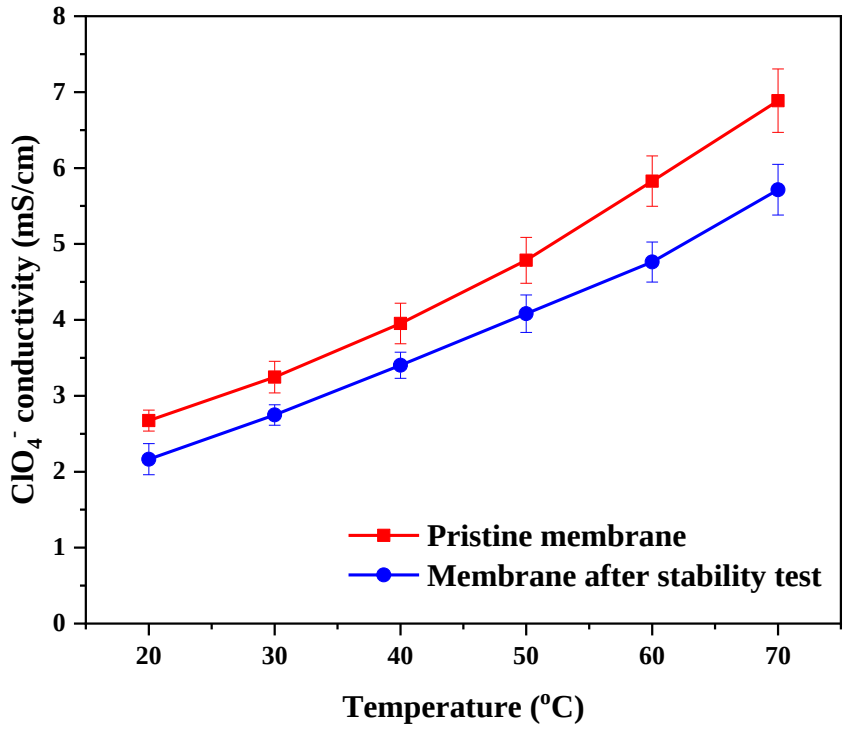

Figure 3.13: ClO_4^- conductivity of TTMPP-PBI-3/PTFE membranes before and after the accelerated stability test in 0.5 M cerium (IV) and 1.3 M $HClO_4$ at 60 °C. The conductivity of membrane samples was tested at different temperatures from 20 °C to 70 °C in DI water. Error bars are standard errors of the measurements (n = 3).

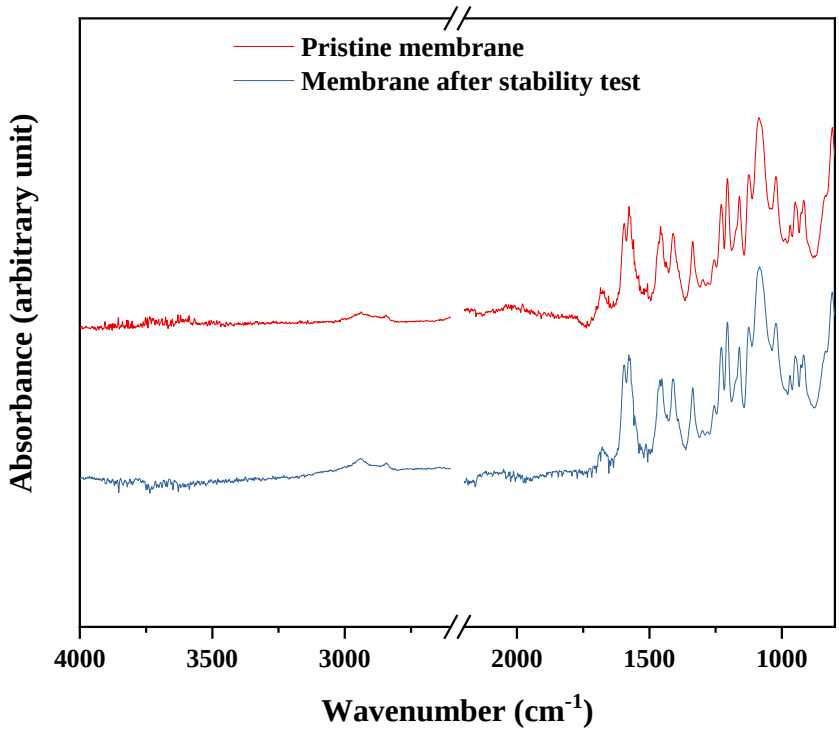

Figure 3.14: Infrared spectra of TTMPP-PBI-3/PTFE membranes before and after the accelerated stability test in 0.5 M cerium (IV) and 1.3 M $HClO_4$ at 60 °C. No noticeable change was observed.

3.4 Conclusion

To design an oxidative resistant AEM for double-membrane zinc-cerium RFB systems, TTMPP-PBI membranes were prepared and demonstrated superior oxidative resistance over commercial AEMs. To choose the best polymer backbone, PS, PPO, PSF, and F_6PBI were tested in the cerium electrolyte, and only the F_6PBI membrane showed no significant weight loss after the screening. TTMePP functionalized F_6PBI was first designed and synthesized, however, the obtained TTMePP-PBI showed insufficient anion conductivity due to the hydrophobic nature of TTMePP cation.

TTMPP was then considered, and its TTMPP-PBI membrane showed excellent oxidative resistance and satisfied anion conductivity.

Chapter 4

HIGHLY CONDUCTIVE AND STABLE PHOSPHONIUM POLYBENZIMIDAZOLE MEMBRANES FOR VANADIUM REDOX FLOW BATTERIES

The tris(2,4,6-trimethoxyphenyl)phosphonium functionalized polybenzimidazole (TTMPP-PBI) membrane obtained in Chapter 3 exhibited excellent oxidative stability in cerium electrolyte and sufficient anion conductivity. We also envisioned that the cation functionalized membrane is able to dope acid in polyprotic acid (H_2SO_4 and H_3PO_4) environment and become a proton-exchange membrane (PEM) in polyprotic acids.[117] In this chapter, we studied TTMPP-PBI's potential as a PEM for vanadium redox flow batteries (VRFBs).

A high acid doping level (ADL) membrane for VRFB is achieved by using the Tris(2,4,6-trimethoxyphenyl)phosphonium (TTMPP) functional group, which has large size and nine methoxy hydrophilic groups for sulfuric acid doping. Hexafluoropropylidene polybenzimidazole (F_6PBI) polymer, which has superior chemical stability and decent acid doping ability due to the hydrogen bond formation, is used as the backbone. The prepared membrane exhibited 3.4-fold ADL of F_6PBI membrane, lower area specific resistance (ASR) than Nafion 115 in 3 M sulfuric acid solution, and only 3.1 % of vanadium permeability of Nafion 115 in the vanadium electrolyte. The prepared membrane showed excellent coulombic efficiency, voltage efficiency, and energy efficiency in VRFB single cell test.

4.1 Introduction

Renewable energy sources, such as wind and solar, can help mitigate the issues of air pollution, climate change, and fossil-fuel shortage, but they are intermittent, and thus their integration to the grid must be managed.[221, 223-224] It has been suggested that if non-dispatchable renewable energy exceeds 20% of the energy-generation capacity without energy storage, an electric grid could become destabilized.[228, 235-237] Thus, the key to the deployment of large scale renewable energy is an energy storage system.[18]

VRFBs are considered as the most appealing technology for large scale energy storage.[116, 238] The power and energy ratings of VRFBs can be independently scaled due to its decoupled design of the energy storage section (electrolyte tanks) and power section (cell stacks).[116, 118] VRFB is also safe for large-scale energy storage because the energy is stored in aqueous electrolytes. The capacity of VRFB can be regenerated after vanadium permeation or accidentally mixed with no permanent damage.

The key component of VRFB is the ion-exchange membrane (IEM) in the cell stack which seperates the negative electrolyte of V^{2+} / V^{3+} acidic solution from the positive electrolyte of VO^{2+} / VO_2^{+} acidic solution.[122] Supporting ions must transfer through the IEM to balance the charges on both sides, while active vanadium species must be separated to avoid cross-over. The supporting ion resistance and ion selectivity of the IEM greatly affect the performance of VRFBs. Perfluorosulfonic acid polymers like Nafion series have been traditionally used as the IEMs for VRFBs.[106] Although featuring high proton conductivity and high chemical stability, the high cost and low ion selectivity of the perfluorosulfonic acid polymers hamper the further commercialization of VRFBs.[104, 106]

Significant effort has been made towards seeking alternative polymer materials for VRFBs. One of the exciting achievements is introducing porous polybenzimidazole

(PBI) membranes into the VRFB. Zhang et al.[104] achieved high VRFB performance of 13,000 cycles with PBI. However, due to the insufficient ADL and high ASR of PBI membranes in VRFB electrolytes, sponge-like membranes had to be used.

TTMPP functional group was proposed by Yan et al.[157, 159, 231] Its functionalized polymers showed much better ion-exchange capacity (IEC) stability than traditionally ammonium functionalized polymers in oxygen saturated alkaline environment in the published work by Ramani et al.[232] Besides its oxidative and alkaline stability,[110, 232, 239] we envisioned that the TTMPP functionalized polymer will have a high conductivity in a polyprotic acid environment due to its high ADL. The high ADL is attributed to the large size and the nine hydrophilic methoxy groups of the phosphoniums, which are able to form hydrogen bond with acids.

In this work, a combination of chemical stable PBI backbones and high acid doping phosphonium functional groups was achieved. In order to further increase the mechanical strength of the final membrane, the expanded polytetrafluoroethylene (ePTFE) support is also used in the membrane fabrication. The ASR and vanadium permeability of the TTMPP-PBI reinforced membranes with ePTFE support (TTMPP-PBI/PTFE) were evaluated. The VRFB single cell test exhibited excellent coulombic efficiency, voltage efficiency, and energy efficiency compared with commercial Nafion 115 and dense F_6PBI membranes.

4.2 Materials and Methods

4.2.1 Materials

All chemicals were obtained from Sigma-Aldrich and used as received unless otherwise stated. Vanadium (IV) sulfate oxide hydrate was purchased from Alfa Aesar,

and thermogravimetric analysis (TGA) was used to determine the water content of the purchased $VOSO_4$ powder before preparing the solution. Nafion 115 was purchased from FuelCellStore. ePTFE was obtained from Xergy Inc. Carbon electrode felts were purchased from FuelCellStore. Gaskets were made of FKM rubber purchased from McMaster-Carr.

4.2.2 Synthesis

4.2.2.1 Synthesis of Hexafluoropropylidene Polybenzimidazole (F_6PBI)

F_6PBI was synthesized using a literature procedure.[133]

4.2.2.2 Synthesis of (4-(chloromethyl)benzyl)tris(2,4,6-trimethoxyphenyl)phosphonium Chloride

The synthetic procedure is reported in Section 3.2.2.4.

4.2.2.3 Synthesis of Tris(2,4,6-trimethoxyphenyl)phosphonium Functionalized Polybenzimidazole

The synthetic procedure is reported in Section 3.2.2.5.

4.2.3 Experimental Methods

4.2.3.1 Membrane Fabrication

The procedure of membrane fabrication is the same as the fabrication procedure reported in Section 3.2.3.2.

4.2.3.2 Composite Membrane Fabrication

The procedure of composite membrane fabrication is reported in Section 3.2.3.3.

4.2.3.3 Ion-Exchange Capacity (IEC) of Membranes

The procedure of titration of IEC is reported in Section 3.2.3.4.

4.2.3.4 Water Uptake (WU) and Swelling Ratio (SR) of Membranes

The procedure of WU and SR measurements is reported in Section 3.2.3.5.

4.2.3.5 Acid Doping Level (ADL) of Membranes

The ADLs of membranes were determined by acid-base titration through the following procedure: Sulfuric acid doped membrane samples measuring 1.0 cm × 6.0 cm were weighed and then titrated with 0.1 M NaOH solution using methyl orange as indicator. The samples were then washed with water and dried in a vacuum at 100 °C for 48 h and weighed again. ADL of F_6PBI samples was calculated from the following equation:

$$ADL_{F6PBI} = \frac{V_{NaOH} \times C_{NaOH}}{2 \times \frac{W_{dry}}{M_w}}, \qquad \text{(Equation 4.1)}$$

where V_{NaOH} (L) and C_{NaOH} (mol L^{-1}) are the volume and the concentration of NaOH solution; W_{dry} (g) and M_w (g mol^{-1}) are the dry weight and the molecule weight of F_6PBI polymer repeating unit.

For TTMPP-PBI-3/PTFE samples, the TTMPP-200-F_6PBI polymer content (r) and anion acids according to the degree of substitution (DS) are considered:

$$ADL_{\text{TTMPP-PBI-3/PTFE}} = \frac{V_{NaOH} \times C_{NaOH}}{2 \times \frac{W_{dry} \times r}{M_w}} + \frac{DS}{2}, \qquad \text{(Equation 4.2)}$$

where r is 85.8 % in this case (determined from the ratio of measured IEC of TTMPP-PBI-3/PTFE membrane to measured IEC of TTMPP-PBI-3 membrane), DS is 200 % in this case; M_w (g mol^{-1}) is the molecule weight of TTMPP-F_6PBI-3 polymer (in SO_4^{2-} form) repeating unit.

4.2.3.6 Area Specific Resistance of Membranes

The ASR of membranes in sulfuric acid solution were measured by two-probe electrochemical impedance spectroscopy (EIS). The detailed procedure was as follows: 1 M H_2SO_4 aqueous solution and 3 M H_2SO_4 aqueous solution were both used for test solutions. Membrane sample was first soaked in test solution at room temperature for 24 h. Then the membrane was fixed between two PTFE half-cells containing a 0.500 cm2 (A) hole. Each half cell was filled with the test solution. The resistance with membrane (r_1) and without membrane (r_2) were measured at 20 °C via Solartron SI 1287. The frequency range was 2 MHz to 1000 Hz, and the intercept at x-axis was used as the impedance. The ASR of the membrane was calculated by the following equation:

$$ASR = (r_1 - r_2) \times A \qquad \text{(Equation 4.3)}$$

4.2.3.7 Vanadium Permeability

In a VRFB, the permeability of different vanadium ions, including self-discharge and capacity decay, has a great influence on battery performance. Diffusion coefficients of four kinds of vanadium ions were found to be in the order of $V^{2+} > VO^{2+} > VO_2^{+} > V^{3+}$.[104] Due to the fact that V^{2+} can be easily oxidized by oxygen in the air, VO^{2+} is usually detected to characterize the vanadium permeability of the membranes. In a diffusion cell separated by a membrane, the right cell was filled with 1.5 M $VOSO_4$ (Thermogravimetric analysis (TGA) was used to determine the water content of purchased $VOSO_4$ powder before preparing the solution) in 3 M H_2SO_4 (30 mL), while the left was filled with 1.5 M $MgSO_4$ in 3 M H_2SO_4 (30 mL) to equalize the ionic strengths and minimize the osmotic pressure effects. Solutions in both half cells were vigorously stirred to avoid concentration polarization. The effective area of the membrane was 1.00 cm^2. VO^{2+} has a significant peak at around 750 nm wavelength in

UV-VIS spectra. Samples of a 1 mL solution from the left cell were collected at regular time intervals for UV-vis spectrometer detection of vanadium (IV) concentration with 1 mL 1.5 M $MgSO_4$ in 3 M H_2SO_4 put back afterward. The vanadium (IV) permeability was calculated according to Fick's diffusion law using the following equation:

$$V_B \frac{\mathrm{d}C_B(t)}{\mathrm{dt}} = \mathrm{A}\frac{\mathrm{P}}{\mathrm{L}}(C_A - 2C_B(t)) \qquad \text{(Equation 4.4)}$$

where V_B and C_B are the solution volume and the vanadium (IV) concentration in the left reservoir, C_A is the vanadium (IV) concentration in the right reservoir, A and L are the effective area and the thickness of the membrane, P is the permeability of vanadium (IV).

4.2.3.8 Vanadium Redox Flow Battery Performance

VRFBs were assembled by sandwiching a membrane between two carbon felt electrodes with an active area of 10 cm^2, clamped by two graphite plates with no flow channels. The target compression rate of carbon felts was 50 %. All components were fixed between two PTFE blocks. 15 mL 1.5 M V^{2+}/V^{3+} in 3 M H_2SO_4 solution and 15 mL 1.5 M VO^{2+}/VO_2^{+} in 3 M H_2SO_4 solution were used as negative and positive electrolytes (Fresh electrolytes were used), respectively. The electrolytes were cyclically pumped through the corresponding electrodes at 30 mL/min in airtight pipelines. Electrolyte tanks and the cell were nitrogen pumped before cycling. Charge-discharge cycling tests were conducted using an Arbin BT-I at constant current density ranging from 80 to 200 mA cm^{-2} with 5 cycles at each current density. The cut-off voltages for discharge and charge were set at 1.0 V and 1.7 V respectively, to avoid the corrosion of carbon felts and graphite polar plates.

4.3 Results and Discussion

4.3.1 Polymer Synthesis and Reinforced Membrane Casting

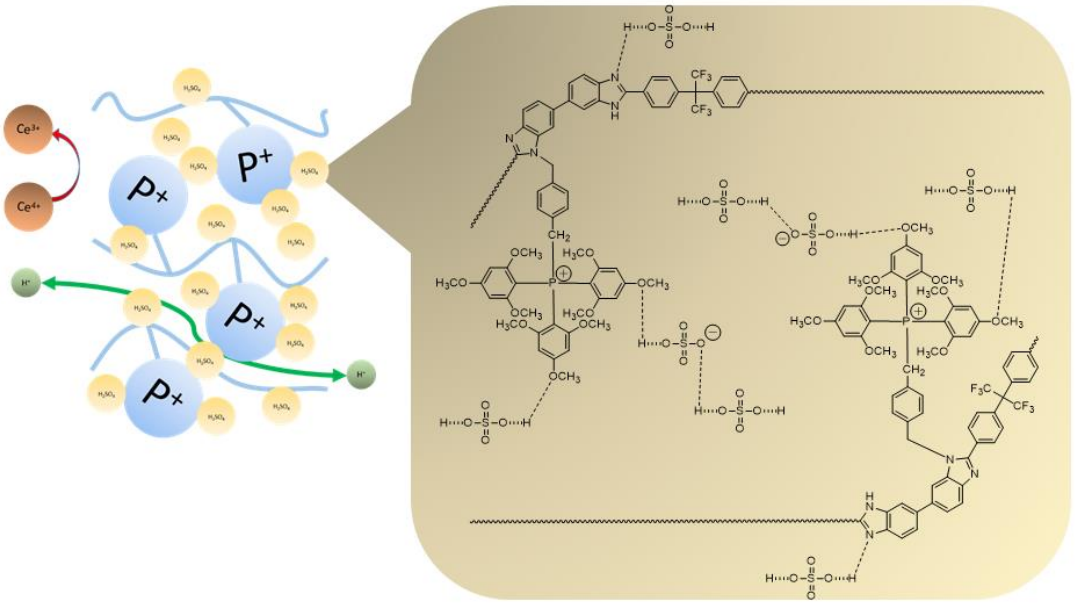

Figure 4.1: (left) a schematic principle of the designed membrane with large phosphonium TTMPP-sulfuric acid conducting channel; (right) acid doping and proton conducting mechanism of TTMPP-PBI membranes.

PBI was chosen as the polymer backbone in this work because of its super thermo-oxidative stability which has been proved in high-temperature fuel cells and VRFBs.[128, 132-133] In particular, F_6PBI has increased stability and flexibility compared to traditional m-PBI due to its amorphous structure caused by the hexafluoropropylidene

group.[133] F_6PBI's high thermo-oxidative stability and ease of further processing and modification make it the perfect choice for a stable polymer backbone used in VRFB. F_6PBI polymers were prepared via a typical aromatic nucleophilic substitution condensation of 4,4′-(hexafluoroisopropylidene)bis(benzoic acid) and 3,3′-diaminobenzidine.

TTMPP functionalized polymers show a much higher λ value (the number of water molecules per cationic head-group) than general ammonium functionalized polymers.[151, 158] This is attributed by the large size of TTMPP and nine hydrophilic methoxy groups on the phosphonium. Thus, a high ADL of TTMPP functionalized polymer is achieved by absorbing a large number of acid molecules through hydrogen bonds. TTMPP is connected to the chosen F_6PBI by 1,4-bis(chloromethyl)benzene as a linker molecule. (4-(chloromethyl)benzyl)tris(2,4,6-trimethoxyphenyl)phosphonium chloride ($CBTTMPP^+Cl^-$) is synthesized by a typical quaternization reaction.

TTMPP-PBI polymer with a different degree of substitution was then synthesized by tethering $CBTTMPP^+Cl^-$ to deprotonated F_6PBI. To the best of our knowledge, this is the first work which utilizes phosphonium functionalized polymer membrane in an aqueous redox flow battery (RFB) system. ePTFE is a common support material to increase the mechanical strength of ion-exchange members.[233-234] In order to improve the mechanical strength and durability of the membrane, ePTFE reinforced membranes were also prepared.

The synthetic route and NMR spectroscopy proven of synthesis of TTMPP-PBI is shown in Section 3.3.3.

Table 4.1: Degree of substitution (DS), theoretical ion exchange capacity (IEC^t), titration measured ion exchange capacity (IEC^{md}), WU, tensile strength, and elongation at break of TTMPP-PBI membranes. Error bars are standard errors of the measurements (n = 3). (For reading convenience, partial data from Table 3.1 and Table 3.2 is re-used to construct this table.)

Membrane	**DS (%)**	**IEC^t (mmol g^{-1})**	**IEC^{md} (mmol g^{-1})**	**WU (%)**	**Tensile strength (MPa)**	**Elongation at break (%)**
TTMPP-PBI-1	70	0.71	0.68 ± 0.04	18 ± 2	7.9 ± 0.7	17.4 ± 0.9
TTMPP-PBI-2	110	0.89	0.88 ± 0.02	58 ± 8	4.0 ± 0.6	12.5 ± 0.9
TTMPP-PBI-3	200	1.11	1.13 ± 0.03	81 ± 5	- [a]	- [a]
TTMPP-PBI-3/PTFE	200	- [b]	0.97 ± 0.02	26 ± 3	17.3 ± 0.7	17.1 ± 1.1
F6PBI	0	- [c]	- [c]	9.2 ± 0.8	72.0 ± 3.6	10.9 ± 1.1

[a]: TTMPP-PBI-3 membrane is too brittle to test mechanical properties
[b]: TTMPP-PBI-3/PTFE reinforced membrane has no theoretical IEC
[c]: F_6PBI membrane has no IEC

4.3.2 Membrane Acid Doping Behavior, Area Specific Resistance and Vanadium Permeability

It is well known that PBI membranes can absorb acid molecules.[240-242] The nitrogen atoms of the benzimidazole units in PBI are protonated by acids, forming up to two chemically bound acids (referred as 'bound acids'). In more concentrated acid solutions, PBI will absorb additional acid molecules (referred as 'free acids') by osmosis and the formation of hydrogen bonds between the acid molecules (especially in polyprotic acids like phosphoric acid and sulfuric acid). Recently, Kim et al. published that ammonium functionalized anion-exchange membrane (AEM) could absorb a higher amount of phosphoric acids than phosphoric acid doped PBI from the sol-gel method.[134] For cationic membranes, the cationic head-group will absorb acids (referred to as 'anion acids') to form ion-pair complexes. In a more concentrated acid solution, due to the affiliation between fixed positive charged cationic head-groups and negative

charged deprotonated acids, a cationic polymer will usually absorb more ‘free acids’ than traditional PBI.

Unlike traditional ammonia cations, TTMPP is attractive for acid doping because its large cationic group size which induces enough space for extra ‘free acids’ as well as its nine protruding methoxy groups which are capable of forming hydrogen bonds with acids, especially in a concentrated acid solution. As listed in Table 4.2, the average ADL of TTMPP-PBI-3/PTFE membrane was 3.4-fold of the average ADL of F_6PBI membrane in 3 M sulfuric acid solution.

Table 4.2: ADL, acid weight percentage (W_A), water weight percentage (W_W), and water acid mole ratio (W/A) of F_6PBI and TTMPP-PBI-3/PTFE membranes in 1 M and 3 M sulfuric acid solution. Error bars are standard errors of the measurements (n = 3).

		H_2SO_4 concentration	
		1 M	3 M
F_6PBI	ADL	1.0 ± 0.2	1.5 ± 0.2
	W_A (wt%)	12.2 ± 1.6	17.2 ± 1.0
	W_W (wt%)	21.3 ± 0.9	21.2 ± 2.1
	W/A	9.5 ± 0.8	6.7 ± 0.3
TTMPP-PBI-3/PTFE	ADL	3.0 ± 0.3	5.1 ± 0.5
	W_A (wt%)	6.9 ± 0.6	14.6 ± 1.2
	W_W (wt%)	26.9 ± 1.8	16.4 ± 2.0
	W/A	14.2 ± 0.2	4.9 ± 0.3

Nafion 115 was suggested to be the most suitable commercial membrane for VRFB applications due to the good balance between low specific area resistance and low permeability of active vanadium cations.[106] Therefore, Nafion 115 was used as a benchmark in this work to compare with the TTMPP-PBI-3/PTFE membrane and the F_6PBI membrane. We first compared the ASR of the three membranes. The result is shown in Figure 4.2. Because of the high ADL of TTMPP-PBI-3/PTFE membrane, the average ASR of prepared TTMPP-PBI-3/PTFE membrane was much lower than the average value of F_6PBI membrane in both 1 M and 3 M sulfuric acid solutions. Moreover, in the 3 M sulfuric acid solution, the average values and calculated standard errors of the TTMPP-PBI-3/PTFE and Nafion 115 indicated that there is no significant difference between the two samples.

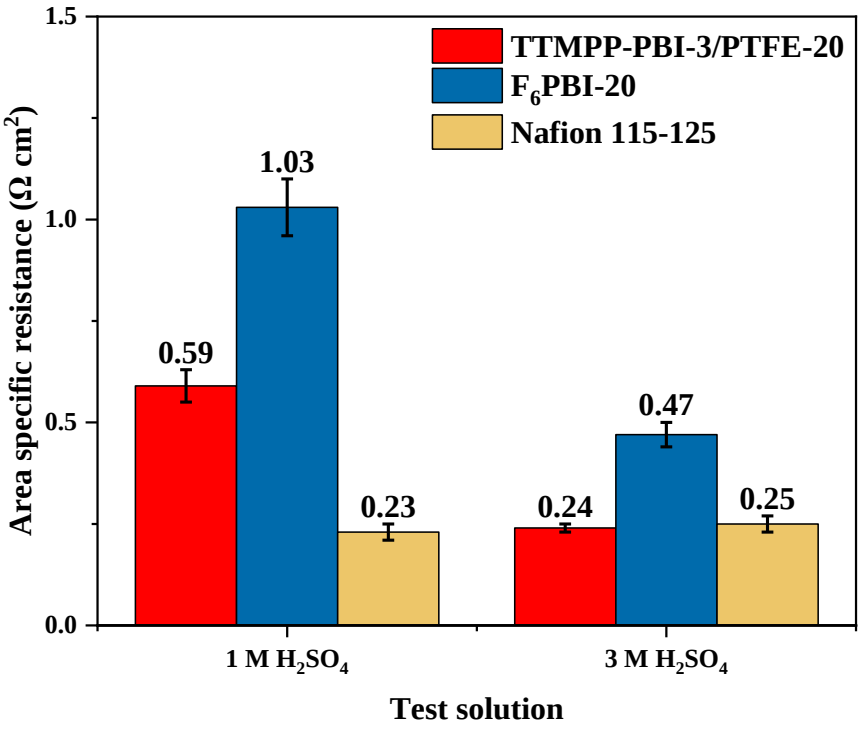

Figure 4.2: ASR of TTMPP-PBI-3/PTFE (20 µm), F_6PBI (20 µm), and Nafion 115 (125 µm) in 1 M and 3 M sulfuric acid solutions respectively. Error bars are standard errors of the measurements (n = 3).

The next important characterization of VRFB membranes is their vanadium permeability. VRFB contains V^{2+} / V^{3+} on the negative side and VO^{2+} / VO_2^+ on the positive side. The stability of VRFB relies on the low vanadium permeability of the middle membrane. As mentioned in the experimental section, the permeability of VO_2^+ was used to characterize the ion selectivity of the membrane. Due to the strongly acidic environment of the VRFB electrolytes, the F_6PBI backbone of TTMPP-PBI-3/PTFE membrane was also positively charged with the formation of hydrogen bonds between

sulfuric acid and nitrogen groups. The repulsion between TTMPP cations along with the positively charged basic heterocyclic groups and the vanadium ions created a high selectivity based on the Donnan exclusion. The permeability results of TTMPP-PBI-3/PTFE, F_6PBI, and Nafion 115 are shown in Figure 4.3. Calculated average permeabilities for TTMPP-PBI-3/PTFE (20 μm), F_6PBI (20 μm), and Nafion 115 (125 μm) were 3.35×10^{-8} cm^2min^{-1}, 3.00×10^{-9} cm^2min^{-1}, and 1.07×10^{-6} cm^2min^{-1}, respectively. In short, the average vanadium (IV) permeability of prepared TTMPP-PBI-3/PTFE membrane was only 3.1 % of the average value of the commercial Nafion 115 membrane. The relatively low permeability of the TTMPP-PBI-3/PTFE membrane would lead to a high coulombic efficiency in the VRFB application. Because the vanadium (IV) concentration of the permeability test with F_6PBI sample was very low, systematic errors of the UV-VIS measurements likely caused a large relative standard error. The calculated error bar was 51 % of the average permeability value for F_6PBI. Nafion 115 showed a larger absolute standard error in permeability than the others. This phenomenon was likely due to the random errors in the process of Nafion pretreatment (i.e., H_2O_2 and acid treatment) and random errors in the $VOSO_4$ solution preparation (since there is water content in purchased $VOSO_4$ powder, nonuniform hydration could introduce extra errors).

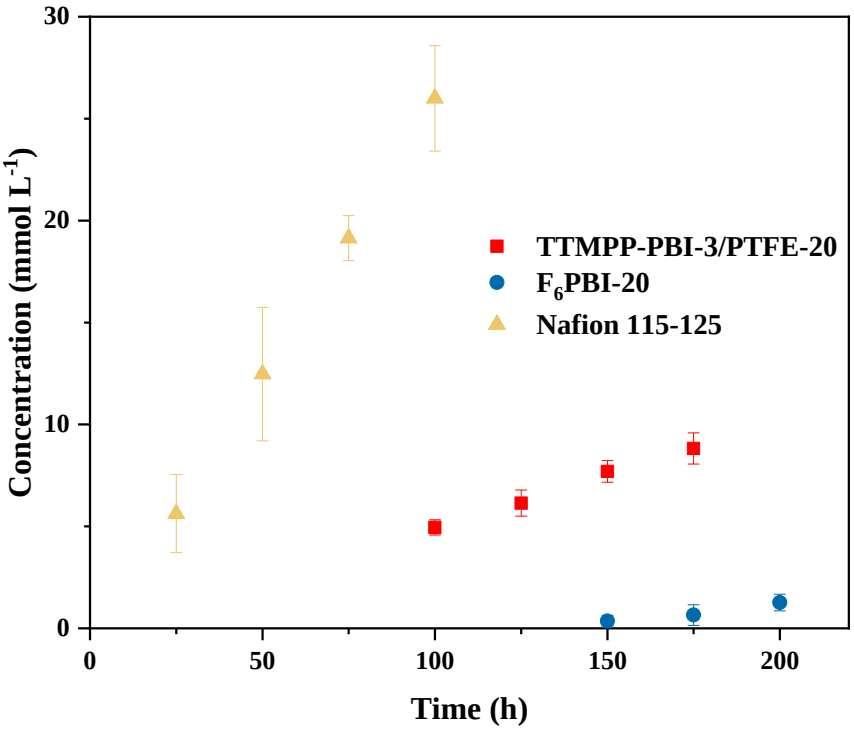

Figure 4.3: Concentration versus time at the deficiency side with TTMPP-PBI-3/PTFE (20 μm), F_6PBI (20 μm), and Nafion 115 (125 μm) membranes. Calculated permeabilities for TTMPP-PBI-3/PTFE (20 μm), F_6PBI (20 μm), and Nafion 115 (125 μm) were $(3.37 \pm 0.28)\times10^{-8}$ cm^2min^{-1}, $(3.00 \pm 1.53)\times10^{-9}$ cm^2min^{-1}, and $(1.09 \pm 0.13)\times10^{-6}$ cm^2min^{-1}, respectively. Error bars are standard errors of the measurements or calculation results (n = 3).

The thickness of a membrane is also an important factor for the membrane performance. Thicker membranes usually have lower overall permeance of active species but suffer resistance increasement. In this work, although the thickness of Nafion 115 (125 μm) is 6.25-fold of the values of TTMPP-PBI-3/PTFE (20 μm) and F_6PBI (20 μm) membranes, its overall permeance was still lower than the others. Thus,

relative thin TTMPP-PBI-3/PTFE and F_6PBI membranes (20 μm) were fabricated to gain the benefits of low ASR and low material cost.

In order to compare our TTMPP-PBI-3/PTFE membrane with reported membranes in VRFB, in Figure 4.4, the vanadium permeance (permeability/thickness) versus the ASR of TTMPP-PBI-3/PTFE was plotted with selected reported membranes (literature details in Appendix C). TTMPP-PBI-3/PTFE membrane presented lower vanadium permeance than Nafion series membranes and decent ASR in 3 M H_2SO_4.

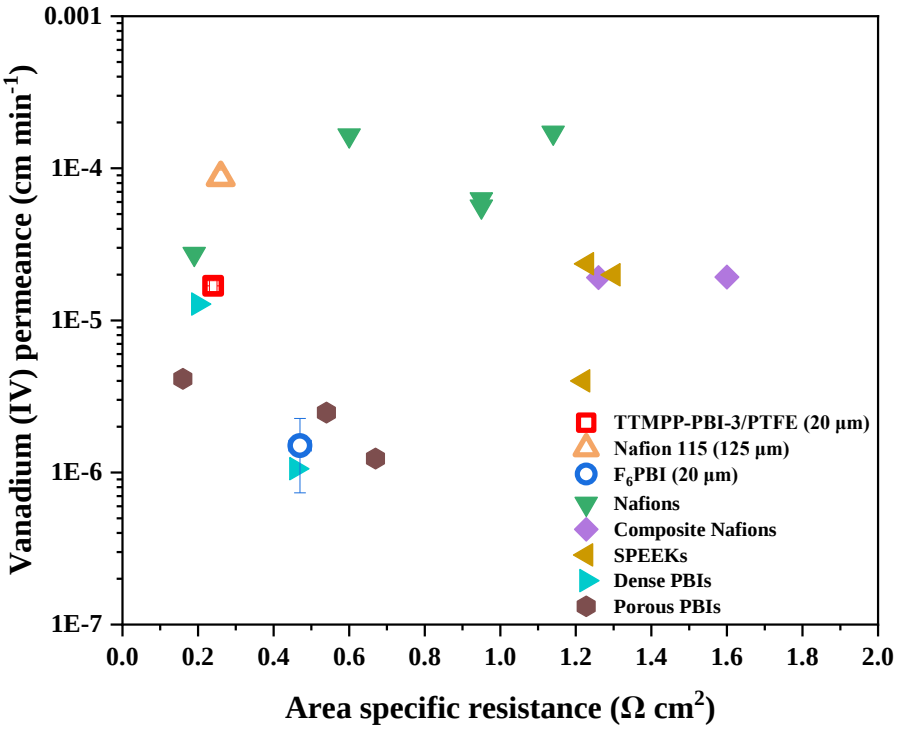

Figure 4.4: Plots of vanadium (IV) permeance (permeability/thickness) to ASR based on data obtained in this work and published literature (Details are shown in Appendix C). The red square is the prepared TTMPP-PBI-3/PTFE membrane in this work. For data collected in this work (hollow points), error bars are standard errors of the measurements or calculation results (n = 3). Some error bars are not visible, because they are very short.

4.3.3 Vanadium Redox Flow Battery (VRFB) Single Cell Test

VRFB single cell performance with TTMPP-PBI-3/PTFE (20 µm), F_6PBI (20 µm), and Nafion 115 (125 µm) are shown in Figure 4.5. Each membrane was operated under various current densities (80, 100, 120, 140, 160, 180, and 200 mA cm^{-2}) with the same cut-off voltage (1.0 V – 1.7 V). The experimental details are in the experimental section.

The ratio of a cell's discharge capacity divided by its charge capacity is the coulombic efficiency. Thus, the coulombic efficiency of the cell is decreased with the increase of vanadium ion permeability of the membranes. Because of the high vanadium permeability, the average coulombic efficiency of Nafion 115, which gradually increased from 96.8 % to 98.0 % with increasing current density from 80 to 200 mA cm^{-2}, was the lowest among the three membranes tested. In contrast, the average coulombic efficiencies of the TTMPP-PBI-3/PTFE and the F_6PBI membranes were much better than Nafion 115. Over the entire range of current densities from 80 to 200 mA cm^{-2}, TTMPP-PBI-3/PTFE exhibited an increased average coulombic efficiency from 98.9 % to 99.5 %, and F_6PBI exhibited an increased average coulombic efficiency from 99.5 % to almost 100.0 %. The excellent coulombic efficiencies of TTMPP-PBI-3/PTFE and F_6PBI were attributed to the substantially lower vanadium permeability.

The ratio of the battery's discharge voltage to its charge voltage is defined as voltage efficiency. Due to the increased ohmic polarization, the voltage efficiency of VRFB decreases with increasing the current density from 80 to 200 mA cm^{-2}. Over the entire range of current densities, VRFB with the TTMPP-PBI-3/PTFE membrane exhibited a slightly higher average voltage efficiency, from 87.7 % to 71.7 %, than Nafion 115, from 86.3 % to 70.9 %, while the average voltage efficiency of F_6PBI membrane was from 83.2 % to 64.5 %. Voltage efficiencies of the three tested membranes were consistent with the ASR of the membranes in 3 M sulfuric acid (Figure 4.2). The exceptionally low ASR of prepared TTMPP-PBI-3/PTFE membrane was benefited from the high ADL caused by the large hydrophilic phosphonium cation.

The product of coulombic efficiency and voltage efficiency is defined as energy efficiency. This is an essential indicator of energy loss during the charge-discharge

process. VRFB with TTMPP-PBI-3/PTFE membrane exhibited the highest average energy efficiency among the three membranes, from 86.8 % to 71.4 % with current density increased from 80 to 200 mA cm^{-2}. For the reference membrane Nafion 115, due to relatively low coulombic efficiency, the average energy efficiency was 83.6 % to 69.5 % with current density from 80 to 200 mA cm^{-2}. Moreover, because of the low voltage efficiency of F_6PBI, it had a lower average energy efficiency (82.7 % to 64.5 %), especially at high current densities.

With the lowest ASR and relatively good vanadium permeability, TTMPP-PBI-3/PTFE membrane (20 μm) exhibited an outstanding efficiency performance at various current densities (80, 100, 120, 140, 160, 180, and 200 mA cm^{-2}).

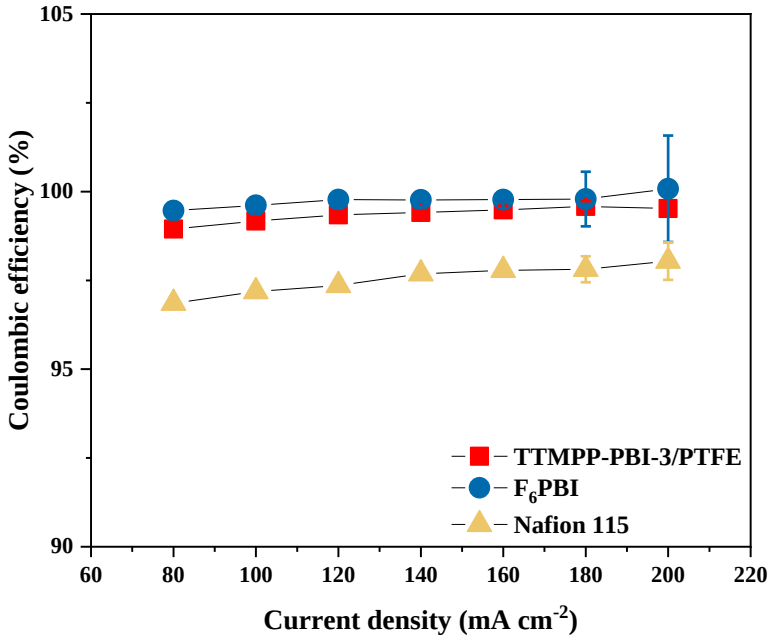
Coulombic efficiency (%)
105
100
95
90
60
80
100
120
140
160
180
200
220
Current density (mA cm-2)
TTMPP-PBI-3/PTFE
F6PBI
Nafion 115

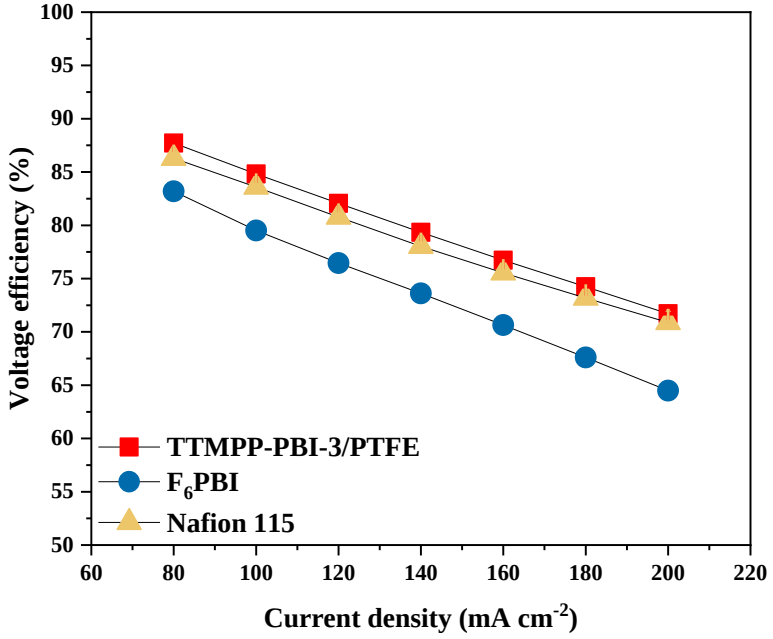
Voltage efficiency (%)
100
95
90
85
80
75
70
65
60
55
50
60
80
100
120
140
160
180
200
220
Current density (mA cm-2)
TTMPP-PBI-3/PTFE
F6PBI
Nafion 115

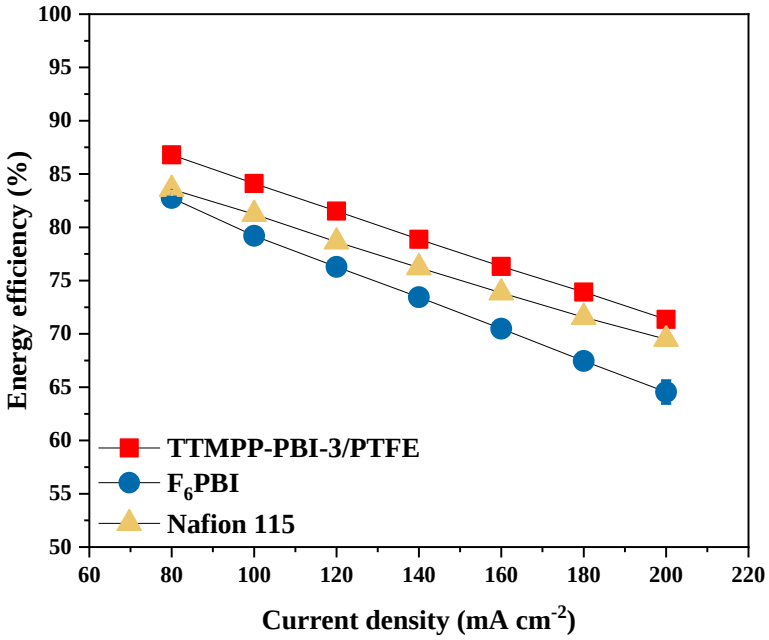

Figure 4.5: VRFB single cell performance of TTMPP-PBI-3/PTFE (20 µm), F_6PBI (20 µm), and Nafion 115 (125 µm) membranes at various current densities (80-200 mA/cm^2): (up) coulombic efficiency, (middle) voltage efficiency, and (down) energy efficiency. Test conditions: 1.5 vanadium and 3 M sulfuric acid electrolyte 15 mL on both sides. 30 mL/min flow rate, 20 ℃ operating temperature, and cut off voltage 1.0 V – 1.7 V. At each current density, data of the last 4 cycles of the same sample was used, and 95 % confident intervals of t-distributions were calculated as error bars (n = 4). Some error bars are not visible, because they are very short.

4.4 Conclusion

A new ePTFE reinforced phosphonium functionalized F_6PBI membrane (TTMPP-PBI-3/PTFE) was prepared. The realization of high ADL, which is resulted from the combination of large TTMPP with methoxy groups and benzimidazole structure on the polymer backbone, creates the opportunities to prepare new highly conductive cationic membranes in polyprotic acid flow battery solutions. In addition to

the high ADL and low ASR, the prepared TTMPP-PBI-3/PTFE membrane (20 um) exhibited much lower vanadium permeability than commercial Nafion 115 membrane. With the good balance of ASR and vanadium permeability, the VRFB single cell with TTMPP-PBI-3/PTFE membrane showed the highest energy efficiency compared with Nafion 115 and F_6PBI.

Chapter 5

STUDY OF HIGHLY CONDUCTIVE METHYLATED POLY(BENZIMIDAZOLIUM) MEMBRANES FOR VANADIUM REDOX FLOW BATTERIES

As reported in Chapter 4, a polybenzimidazole (PBI) membrane functionalized by phosphonium group exhibited increased proton conductivity in polyprotic acids. In this chapter, we will investigate another method of modifying PBI to increase its proton conductivity.

Positively charged methylated poly(benzimidazolium) membranes are studied for the first time in vanadium redox flow batteries (VRFBs). The membrane shows low area specific resistance (ASR) and excellent efficiencies, but it degrades severely in VRFB. The degradation mechanism is examined to provide knowledge for future robust membrane material designs.

5.1 Introduction

The key to the deployment of large scale renewable energy is an energy storage system.[18, 243] Currently, the aqueous vanadium redox flow battery (VRFB) technology is considered as one of the best energy storage systems for renewable energy integration[227-228] due to its flexible design, excellent scalability, and long cycle life. Aqueous redox flow battery (RFB) systems are also safer compared to flammable lithium-ion batteries and more stable as the redox pairs are separated in different tanks during non-operation.[18, 227-228]

At present, the commercialization of VRFBs is hampered by their high cost (500-700 $ m^{-2}) and low selectivity of the applied perfluorinated membranes (e.g., Nafion series).[151, 238, 244-245] Therefore, numerous efforts have been devoted to the investigation of alternative separators with low ASR, high chemical and mechanical stability, and low cost.[116, 238, 246-248] Among these requirements, ASR plays an important role as lower ASR can lead to higher voltage efficiency, higher energy efficiency, and eventually lower levelized cost of the VRFB.

PBI as an alternative membrane material has been reported with high performance over 13,000 cycles by Zhang et al.[104] However, in order to achieve sufficiently low ASR, sponge-like membranes had to be fabricated. The sponge structure weakens the mechanical strength of the membrane. The conductivity of PBI material in an acid operation environment is ascribed to the 'bond acid' (i.e., acid protonating the nitrogen atoms of benzimidazole units) and the 'free acid' (i.e., acid due to osmosis or hydrogen bond formation between acid molecules).[132] The conductivity of PBI in VRFBs is generally low due to the insufficient acid doping level (ADL, number of acids per polymer repeating unit) in 3-4 M sulfuric acid environment (the reported ADL is usually lower than 2).[128] In high-temperature fuel cells, Kim et al. reported that quaternary ammonium functionalized membranes with a much higher ADL and phosphoric acid retention than PBIs from the sol-gel process.[134] This indicated that higher ADL could be achieved with cationic functional groups, such as cationic benzimidazolium, instead of nucleophilic benzimidazole.

A wealth of literature has been published on positively charged poly(benzimidazolium),[148, 249-251] and its alkaline stability has been widely studied and improved for hydroxide exchange membrane fuel cell (HEMFC) applications.[252-253]

Despite a recent publication employing crosslinked methylated poly(benzimidazolium) in a neutral zinc-TEMPO aqueous flow battery by Chen et al.,[254] the performance and stability of poly(benzimidazolium) in acidic VRFB has not been investigated. Herein, we report our efforts to use methylated hexafluoropropylidene polybenzimidazole (DMF_6PBI) in VRFBs. We demonstrated that DMF_6PBI membranes have higher ADL and lower ASR than traditional PBI membranes. As a result, DMF_6PBI membranes (40 μm) achieved the highest voltage efficiency (VE) and energy efficiency (EE) compared to Nafion 115 and F_6PBI (40 μm), and higher coulombic efficiency (CE) than Nafion 115 in single-cell VRFB tests. However, DMF_6PBI membranes degrade severely during the tests. Detailed characterizations of the DMF_6PBI membranes after the in-situ and ex-situ degradation tests are performed. Specific degradation products and pathways are proposed, which may be valuable for the future optimization of the material stability.

5.2 Materials and Methods

5.2.1 Materials

All chemicals were obtained from Sigma-Aldrich and used as received unless otherwise stated. Vanadium (IV) sulfate oxide hydrate was purchased from Alfa Aesar. Nafion 115 was purchased from FuelCellStore. Carbon electrode felts were purchased from FuelCellStore. Gaskets were made of FKM rubber purchased from McMaster-Carr.

5.2.2 Synthesis

5.2.2.1 Synthesis of Hexafluoropropylidene Polybenzimidazole (F_6PBI)

F_6PBI was synthesized using a literature procedure.[133]

5.2.2.2 Synthesis of Methylated Hexafluoropropylidene Polybenzimidazole (DMF_6PBI)

Synthesis of DMF_6PBI was carried out according to a published procedure with slight modification.[252] In a 250 mL round bottom flask equipped with a mechanical overhead stirrer and nitrogen purge, F_6PBI (2.00 g, 3.7 mmol) was vigorously stirred in dry N-methyl-2-pyrrolidone (NMP) (150 mL) at 80 °C overnight until the solid was completely dissolved. The solution was cooled to room temperature, and then LiH (0.176 g, 22.2 mmol) was slowly added. The solution was heated to 50 °C and stirred for another 15 h. Iodomethane (5 mL, 80 mmol) was added drop-wise over 15 min to the stirred solution and the solution was heated to 80 °C and stirred for 24 h. The light brown precipitate from the reaction was collected by centrifuge and then re-dissolved in dimethyl sulfoxide (DMSO) (60 mL). Additional iodomethane (5 mL, 80 mmol) was dropwise added, and the solution was heated to 80 °C and stirred for 24 h. After cooling, the polymer was precipitated in acetone, and residual DMSO was removed via Soxhlet extraction (acetone as extraction solvent) for 48 h.

5.2.3 Experimental Methods

5.2.3.1 Membrane Fabrication and Acid Doping

The polymer was completely dissolved in dimethylacetamide (DMAc) to make a 2.5 w/v% solution. The solution was cast on a glass plate and dried in air at 80 °C for 24 h. After the solvent was completely evaporated, the glass plate was immersed in DI water, and the membrane was gently peeled from the glass.

F_6PBI membranes were directly doped in 3 M sulfuric acid for 24 h at 20 °C. While DMF_6PBI membranes were firstly anion exchanged in 0.3 M Na_2SO_4 solution

for 2 days at 20 °C followed by thoroughly washing in DI water for 2 days at 20 °C before acid doping in 3 M sulfuric acid for 24 h at 20 °C.

5.2.3.2 Area Specific Resistance (ASR) of Membranes

The ASR measurement is reported in Section 4.2.3.6.

5.2.3.3 Mechanical Properties of Membranes

The mechanical properties of the membranes (size: 30 mm × 6 mm) were measured using TA instruments Q800 DMA. For each membrane, three samples were tested, and the average value was reported.

5.2.3.4 Viscosity Measurements of Polymer Solutions

The inherent viscosity was measured on a Cannon ubbelohde viscometer with membranes dissolved in 96 % sulfuric acid at a concentration of 0.2 g/dL.

5.2.3.5 Characterization of Chemical Structures

Attenuated total reflection-Fourier transformed infrared spectroscopy (ATR-FTIR) spectra were recorded on Bruker Tensor 27.

^{1}H nuclear magnetic resonance (NMR) spectroscopy were recorded on Bruker AVIII 600 with polymers or membranes dissolved in deuterated dimethyl sulfoxide.

5.2.3.6 Sulfuric Acid Doping Level (ADL) of Membranes

The ADLs of membranes were determined by acid-base titration through the following procedure: sulfuric acid doped membrane samples measuring 1.0 cm × 6.0 cm were weighted and then titrated with 0.1 M NaOH solution using methyl orange as indicator. The samples were then washed with water, dried in a vacuum at 100 °C for 48 h and weighed again.

The ADL measurement of F_6PBI samples is reported in Section 4.2.3.5 and Equation 4.1.

For DMF_6PBI (SO_4^{2-} form) samples, $DMF_6PBI^{2+}SO_4^{2-}$ became $DMF_6PBI^{2+}(HSO_4^-)_2$ after acid doping and then changed back to $DMF_6PBI^{2+}SO_4^{2-}$ after titration. Thus, anion acids according to the methylated benzimidazolium (N) are considered:

$$ADL_{DMF6PBI} = \frac{V_{NaOH} \times C_{NaOH}}{2 \times \frac{W_{dry}}{M_w}} + 1 , \qquad \text{(Equation 5.1)}$$

where M_w (g mol^{-1}) is the molecule weight of DMF_6PBI polymer (in SO_4^{2-} form) repeating unit, the residual SO_4^{2-} anion in the cationic polymer after titration is also counted by adding 1.

5.2.3.7 VRFB Single Cell Test

The VRFB single cell test procedure was the same as the procedure reported in Section 4.2.3.8.

5.2.3.8 Ex-situ Degradation Test

Ex-situ degradation test of DMF_6PBI membranes was conducted by putting 5 cm × 5 cm membrane samples in 50 mL 1.5 M vanadium (V) in sulfuric acid solution (produced from electro-oxidation of 1.5 M $VOSO_4$ and 3 M H_2SO_4 solution) at 80 °C for 500 h.

5.3 Results and Discussion

5.3.1 Preparation and Characterization of F_6PBI and DMF_6PBI Membranes

F_6PBI polymers with hexafluoropropylidene groups were prepared via a typical aromatic nucleophilic substitution condensation of 4,4′-(hexafluoroisopropylidene)bis(benzoic acid) and 3,3′-diaminobenzidine (Figure 5.1). After that, DMF_6PBI polymers were prepared by deprotonation of F_6PBI with NaH, and then methylation with methyl iodide twice in NMP and DMSO, respectively. The obtained DMF_6PBI showed 100 % double methylation on benzimidazole groups (Figure 5.1).[252] The successful synthesis of F_6PBI and DMF_6PBI were verified by ^{1}H NMR spectroscopy (Figure 5.2 and Figure 5.3).

F_6BPI membranes were directly doped in 3 M sulfuric acid at 20 °C for 24 h before VRFB single-cell test. DMF_6BPI membranes (I^- form after synthesis and membrane casting) were anion exchanged into SO_4^{2-} before acid doping to remove I^-. In addition to acting as an anion contaminant, I^- could be oxidized to I_2, which resulted in red-colored membranes.

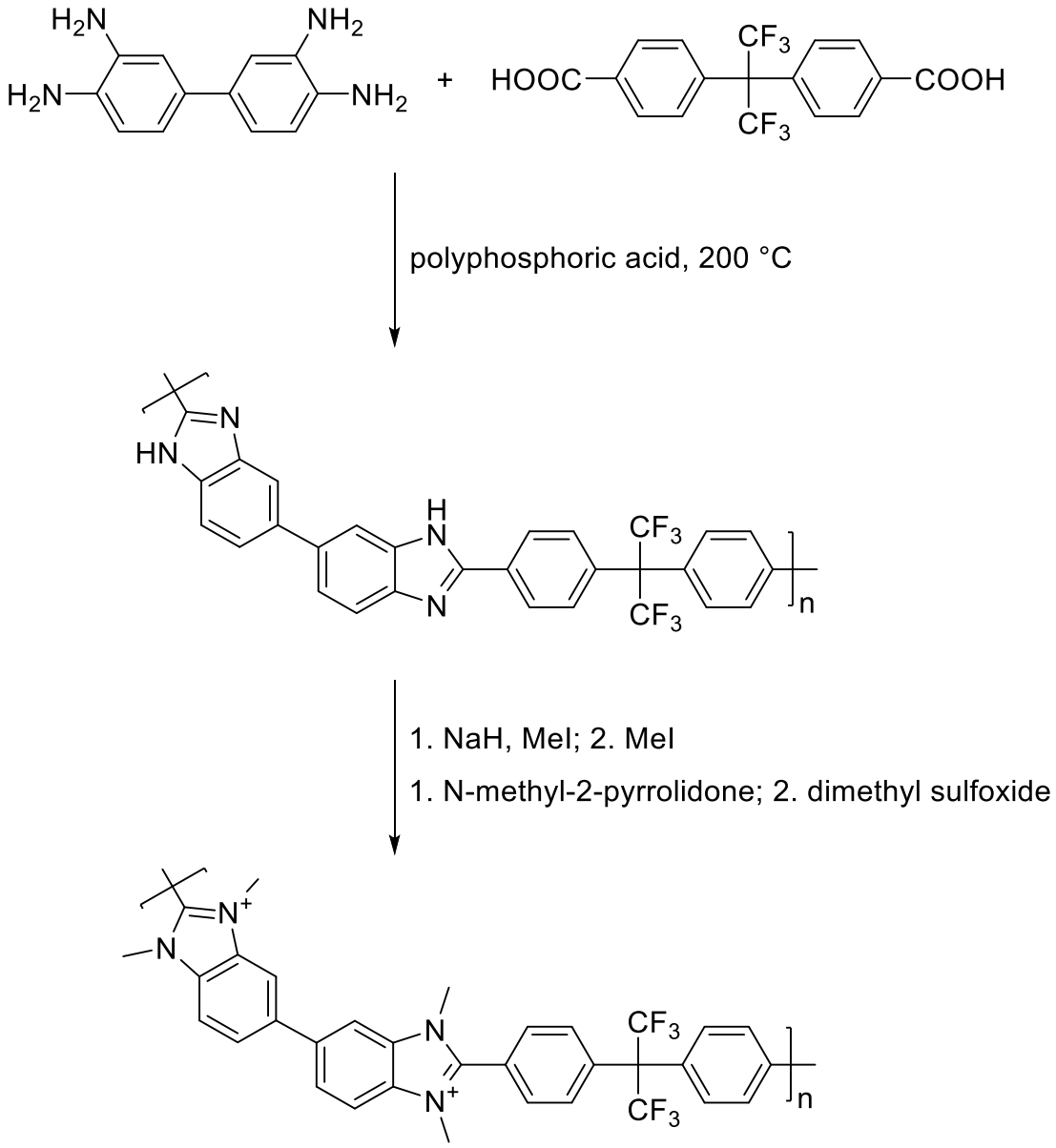

Figure 5.1: Synthetic route of F_6PBI and DMF_6PBI polymer.

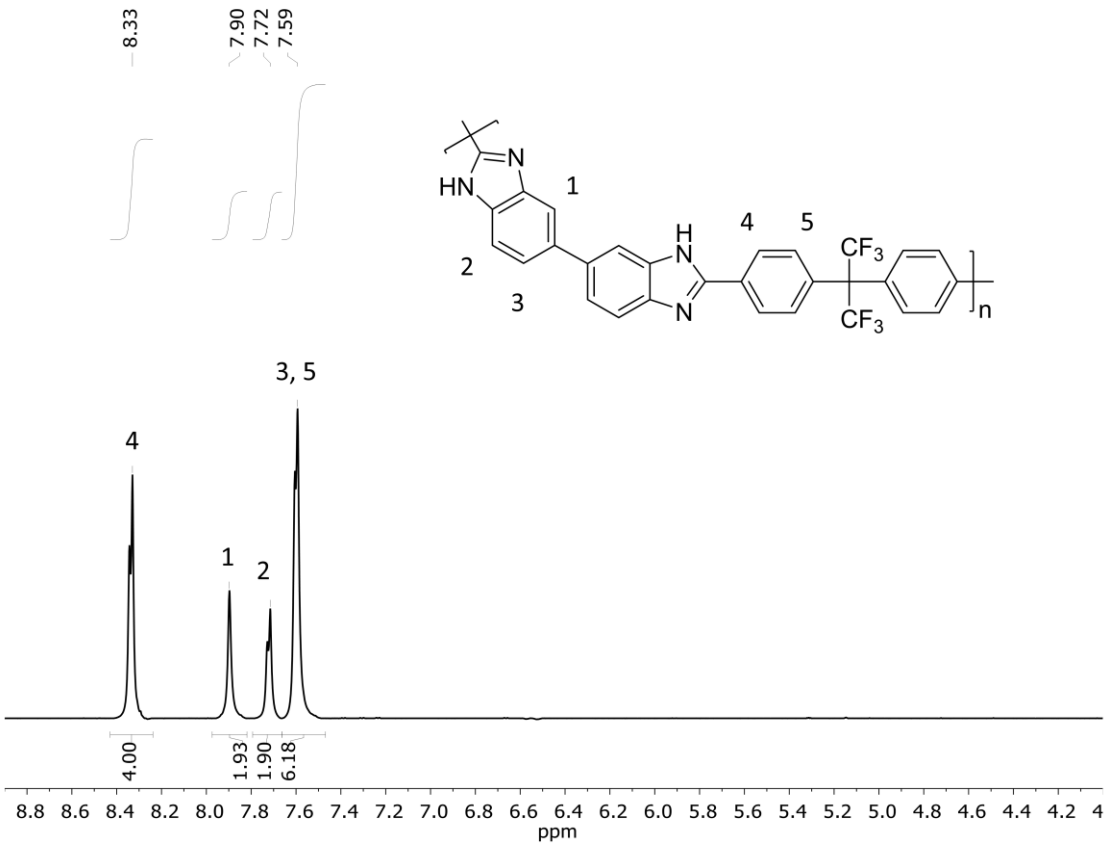

Figure 5.2: ^{1}H NMR spectroscopy of F_6PBI polymer, DMSO-d6 as the solvent.

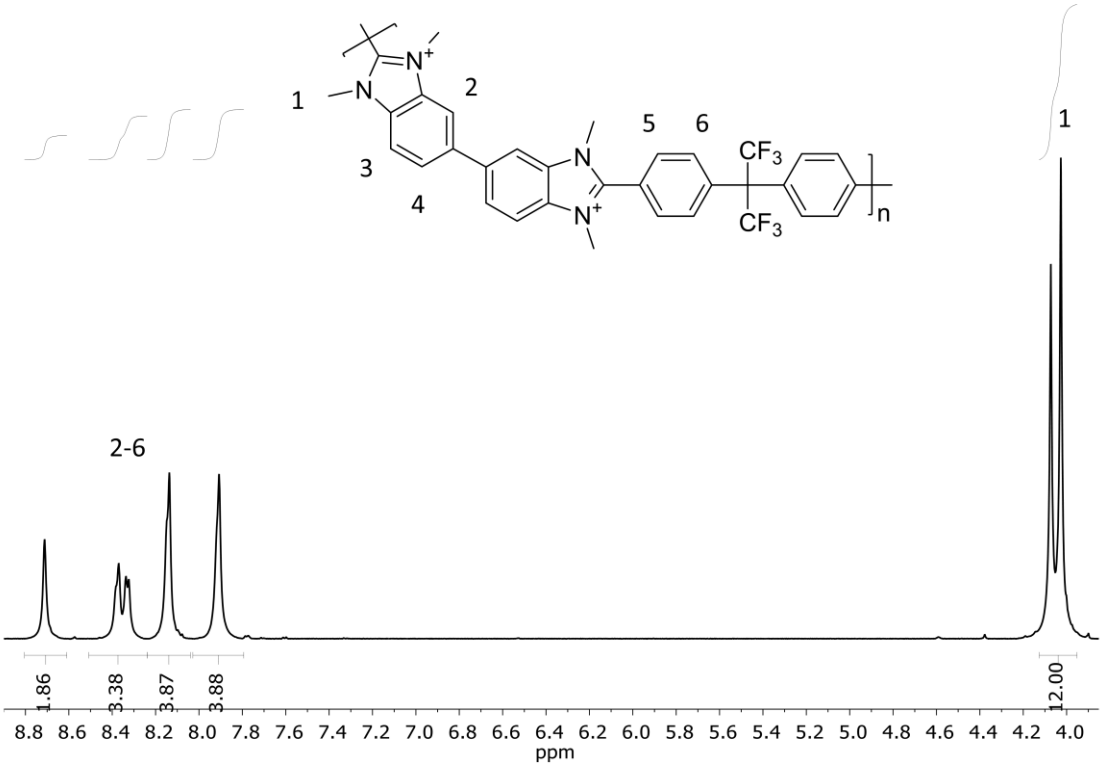

Figure 5.3: ^{1}H NMR spectroscopy of DMF_6PBI polymer, DMSO-d6 as the solvent.

It is known that PBI membranes can absorb acid molecules. The nitrogen atoms of the benzimidazole units in PBI are protonated by acids, forming up to two chemically bound acids (referred to as 'bound acids'). In more concentrated acid solutions, PBI will absorb additional acid molecules (referred to as 'free acids') by osmosis and formation of hydrogen bonds between the acid molecules (especially in multi protic acids like phosphoric acid and sulfuric acid). Recently, Kim et al. published that ammonium functionalized anion-exchange membrane (AEM) could absorb a higher amount of phosphoric acids than phosphoric acid doped neutral PBI from the sol-gel method.[134] For cationic membranes, the cationic head-group will absorb acids (referred to as 'anion

acids') to form ion-pair complexes. In a more concentrated acid solution, due to the electrostatic interaction between fixed positive charged cationic head-groups and negative charged deprotonated acids, a cationic polymer could usually absorb more acids than traditional PBI.

ADLs of DMF_6PBI in 3M sulfuric acid were measured by titration. Besides the 2 units of anion acids (HSO_4^-), 0.9 units of free acids were also observed on average. While F_6PBI with benzimidazole functional group only absorbed 1.5 sulfuric acids per repeating unit in 3 M sulfuric acid on average (Table 5.1). Figure 5.4 shows the ASR results of DMF_6PBI, F_6PBI, and Nafion 115 membranes in 3 M sulfuric acid solution. There was no significant difference between the ASR of DMF_6PBI membrane (0.24 Ω cm^2 on average) and the ASR of Nafion 115 (0.25 Ω cm^2 on average) according to standard errors of the measurements, and it was only about one-third of the traditional F_6PBI membrane (0.69 Ω cm^2 on average) of the same thickness. These results indicated that compared to traditional benzimidazole functional group in F_6PBI, the dimethyl benzimidazolium functional group in DMF_6PBI leads to an almost doubled ADL and an exceptionally low ASR.

Table 5.1: ADL of DMF_6PBI (HSO_4^- form in acid) and F_6PBI in 3 M sulfuric acid. Error bars are standard errors of the measurements (n = 3).

	ADL	Acid content[a] (wt%)	Water content[a] (wt%)	Water per acid[b]
DMF_6PBI (HSO_4^-)	2.9 ± 0.2[c]	25.2 ± 0.8[d]	21.7 ± 1.6	4.7 ± 0.3
F_6PBI	1.5 ± 0.2	17.2 ± 1.0	21.2 ± 2.1	6.7 ± 0.3

[a]: The acid content and the water content was calculated from the ADL and the weight change in ADL measurement.
[b]: Water per acid is calculated from water content and acid content
[c]: ADL of DMF_6PBI (HSO_4^-) includes the two HSO_4^- anion acids.
[d]: Acid content of DMF_6PBI (HSO_4^-) includes the weight of HSO_4^- anions.

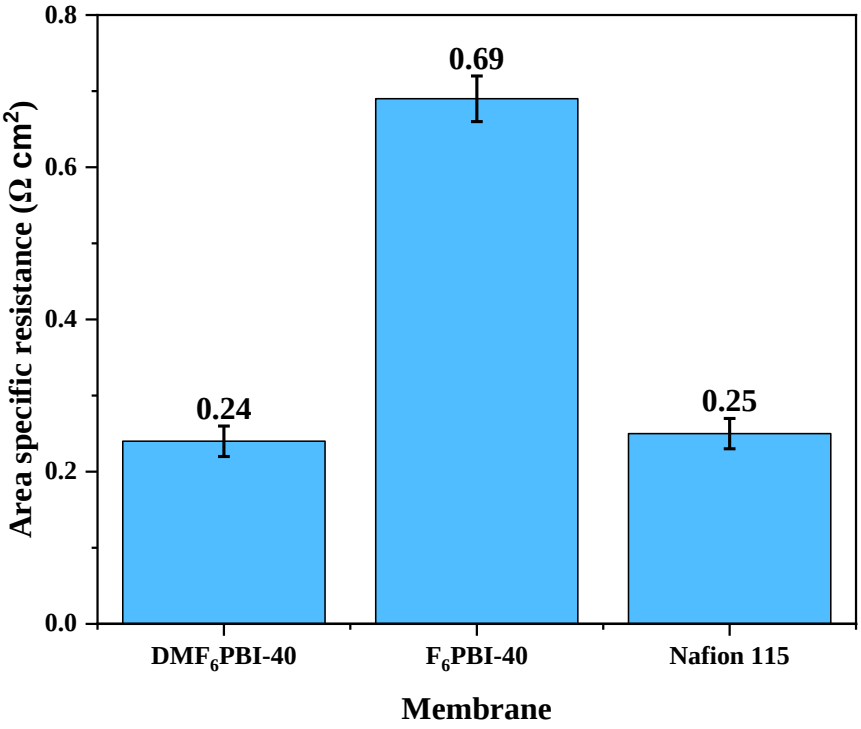

Figure 5.4: ASR of DMF_6PBI (40 µm), F_6PBI (40 µm), and Nafion 115 (125 µm) in 3 M sulfuric acid. Error bars are standard errors of the measurements (n = 3).

5.3.2 Vanadium Redox Flow Battery (VRFB) Single Cell Test

VRFB single cell performance with DMF_6PBI, F_6PBI, and Nafion 115 membranes, operating under various current densities (80, 100, 120, 140, 160, 180, and 200 mA cm^{-2}) are shown in Figure 5.5. The thickness of Nafion membranes affects the performance of VRFBs, and it was recently reported that owing to a good balance between vanadium ions permeability and membrane resistance, Nafion 115 with a thickness of 125 μm is the most suitable membrane for VRFB application.[106] Therefore, Nafion 115 was used as the reference membrane for VRFB performance testing in this work.

With the lowest ASR, DMF_6PBI membrane with a thickness of 40 μm exhibited an outstanding efficiency performance at various current densities (80, 100, 120, 140, 160, 180, and 200 mA cm^{-2}). CE is defined as the ratio of a cell's discharge capacity divided by its charge capacity, and therefore the diffusion of vanadium ions across the membrane will decrease the CE of the cell. Because of the large vanadium permeability, the average CE of Nafion 115, which gradually increased from 96.8 % to 98.0 % with increasing current density from 80 to 200 mA cm^{-2}, was the lowest among the three membranes tested. In contrast, the average CE performance of VRFB with DMF_6PBI and F_6PBI membranes were much better than the one with Nafion 115. Over the entire range of current densities from 80 to 200 mA cm^{-2}, DMF_6PBI exhibited an average CE increasing from 98.8 % to 99.4 %, and F_6PBI exhibited almost 100 % average CE. The excellent CEs of DMF_6PBI and F_6PBI VRFB were attributed to the substantially lower vanadium permeability.

VE is defined as the ratio of battery's discharge voltage to its charge voltage, and therefore the VE of VRFB decreases with the increasing of current density from 80 to 200 mA cm^{-2}, due to the increased ohmic polarization. Over the entire range of current

densities, VRFB with DMF_6PBI membrane exhibited a slightly higher average VE, from 86.6 % to 72.1 %, than Nafion 115, from 86.3 % to 70.9 %, while the average VEs of VRFB with F_6PBI membrane were much lower, from 82.3 % to 62.4 %. These VE results agreed well with the ASR measurement of the prepared membrane in 3 M sulfuric acid (Figure 5.5). The exceptionally low ASR of prepared DMF_6PBI membrane benefited from the high ADL caused by the methylated benzimidazolium functional group.

EE, defined as the product of CE and VE, is a key indicator of energy loss during the charge-discharge process. VRFB with DMF_6PBI membrane combined the excellent CE and VE, had the highest average EE among the three membranes, from 85.6 % to 71.6 % with current density increased from 80 to 200 mA cm^{-2}. For the reference membrane Nafion 115, due to relatively low CE, the average EE was 83.6 % to 69.5 % with current density from 80 to 200 mA cm^{-2}. Moreover, because of the low VE of F_6PBI, it also had a significantly lower average EE (81.4 % to 62.4%), especially at high current densities.

Although DMF_6PBI membrane showed excellent performance in the VRFB test, the membrane failed after 120 mA/cm^2 (i.e., 15 cycles, as the RFB operated 5 cycles at each current density). A new membrane was then used to continue the rest VRFB tests. Generally, because higher current density would lead to shorter cycle length at limited voltage range and then cause less crossover, higher coulombic efficiency should be observed at higher current density. In Figure 5.5, due to the changing of a new membrane before 140 mA/cm^2, fresh solution and nitrogen purge were also conducted. Since the charging at 140 mA/cm^2 was then started from 0 % state of charge (fresh V^{3+} on the negative side and fresh VO^{2+} on the positive side), the initial cycles of the new

membrane showed relatively low coulombic efficiency due to the state of charge adjustment.

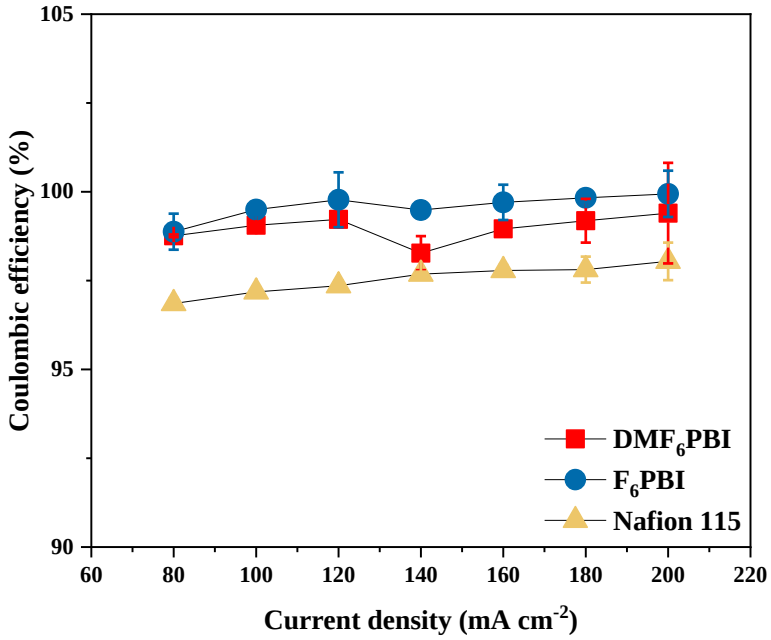
Coulombic efficiency (%)
105
100
95
90
60
80
100
120
140
160
180
200
220
Current density (mA cm-2)
DMF6PBI
F6PBI
Nafion 115

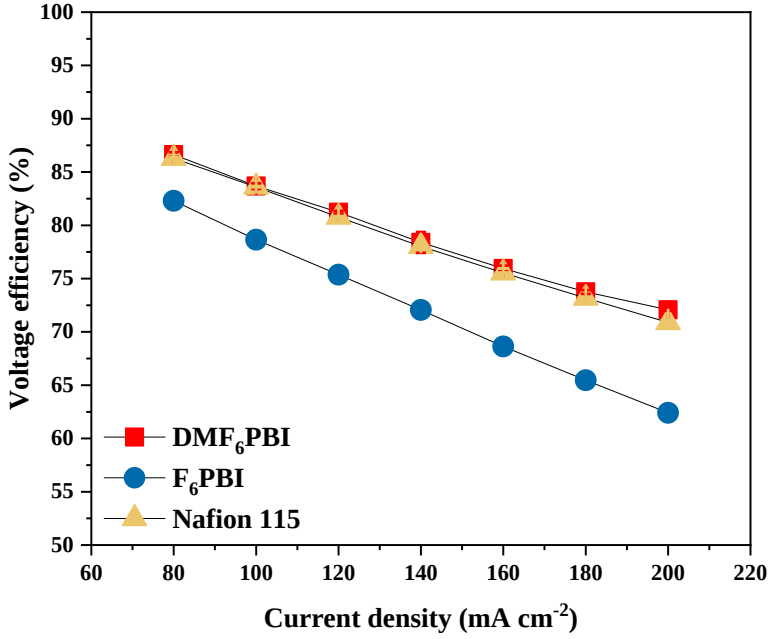
Voltage efficiency (%)
100
95
90
85
80
75
70
65
60
55
50
60
80
100
120
140
160
180
200
220
Current density (mA cm-2)
DMF6PBI
F6PBI
Nafion 115

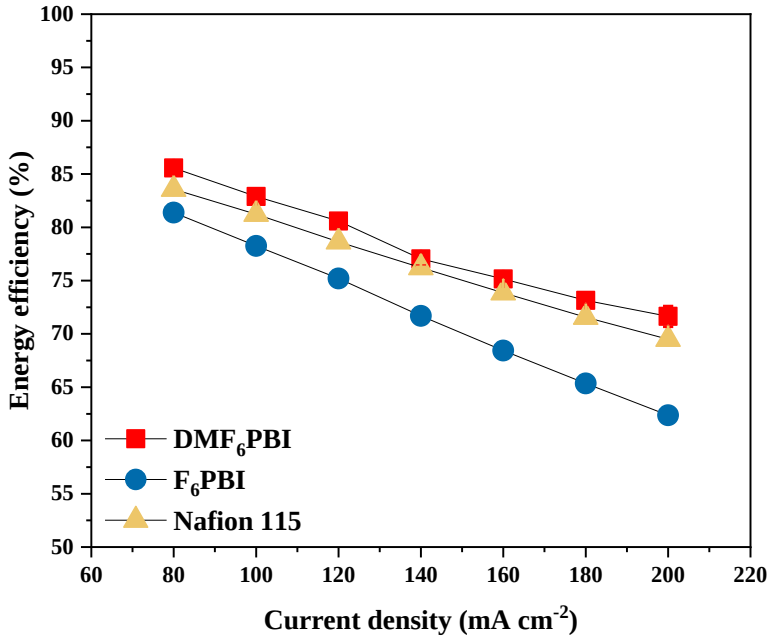

Figure 5.5: VRFB single cell performance of DMF_6PBI (two membranes used, first membrane broke after 120 mA cm^{-2} test), F_6PBI (single membrane), and Nafion 115 (single membrane) membranes at various current densities (80-200 mA/cm^2): (up) coulombic efficiency, (middle) voltage efficiency, and (down) energy efficiency. Test conditions: 1.5 M vanadium and 3 M sulfuric acid electrolyte 15 mL on both sides. 30 mL/min flow rate, 20 ℃ operating temperature, and cut off voltage 1.0 V – 1.7 V. At each current density, data of the last 4 cycles of the same sample was used, and 95 % confident intervals of t-distributions were calculated as error bars (n = 4). Some error bars are not visible, because they are very short.

5.3.3 Degradation of DMF_6PBI Membrane

Battery cycling tests were carried to verify the in-situ stability of DMF_6PBI membranes. However, the DMF_6PBI membrane only survived at 120 mA cm^{-2} for 46 cycles before they broke. Over the 46 cycles, VE of DMF_6PBI gradually decreased from 80.8 % to 77.4 %. Moreover, the capacity decreased 26.4 % (from 0.53 Ah to 0.39 Ah)

as shown in Figure 5.6. These results indicated that the DMF_6PBI membrane went through severe degradation during the test and was not stable during VRFB operation.

We examined the DMF_6PBI membrane after in-situ VRFB test. The membrane became discolored, and the membrane within the active area was fragile (Figure 5.7). In order to determine the specific degradation mechanism, the relative molecular weight (represented by inherent viscosity) and stress-strain curves were examined (Table 5.2). The average inherent viscosity decreased from 1.24 dL g^{-1} to 0.13 dL g^{-1}, while the active area of the DMF_6PBI membrane was too weak to be cut into strips for strain-stress tests. These results indicated that the DMF_6PBI polymer backbone went through harsh chain scission. While for F_6PBI membrane, there was no appreciable change in inherent viscosity and mechanical property after 100-cycle in-situ VRFB test. Compared with F_6PBI, DMF_6PBI has dimethyl benzimidazolium cation instead of partially protonated benzimidazole in an acid VRFB environment. Therefore, we suspected that the severe degradation of DMF_6PBI was caused by the oxidation of methylated benzimidazolium cation by vanadium (V) during VRFB cycling.

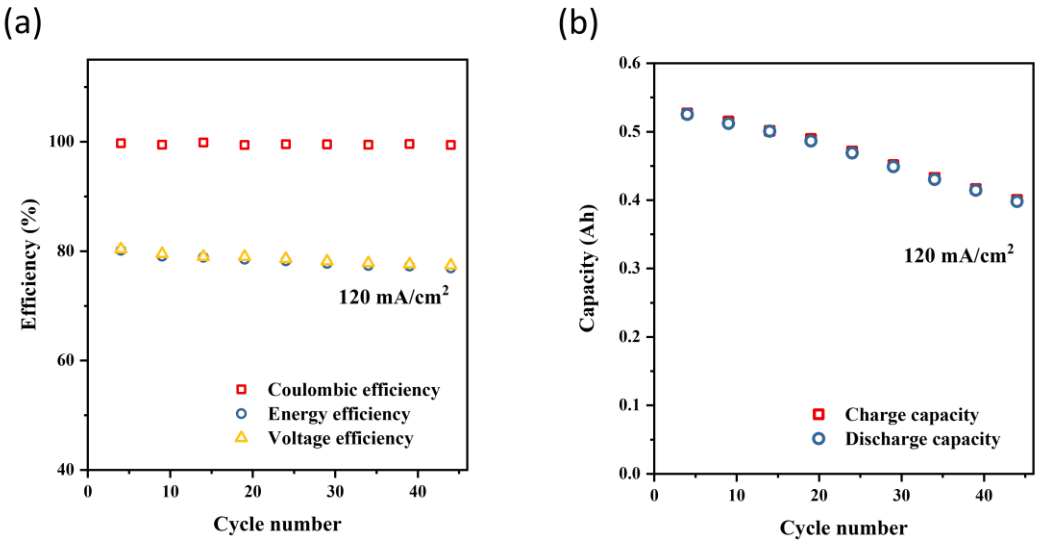

Figure 5.6: VRFB single cell performance of DMF_6PBI membrane at 120 mA/cm^2, with voltage limit from 1.0 V to 1.7 V, state of charge of the first cycle from 9 % to 74 %. The DMF_6PBI membrane broke after 46 cycles. (a) coulombic efficiency, voltage efficiency, and energy efficiency; (b) charge and discharge capacity decay.

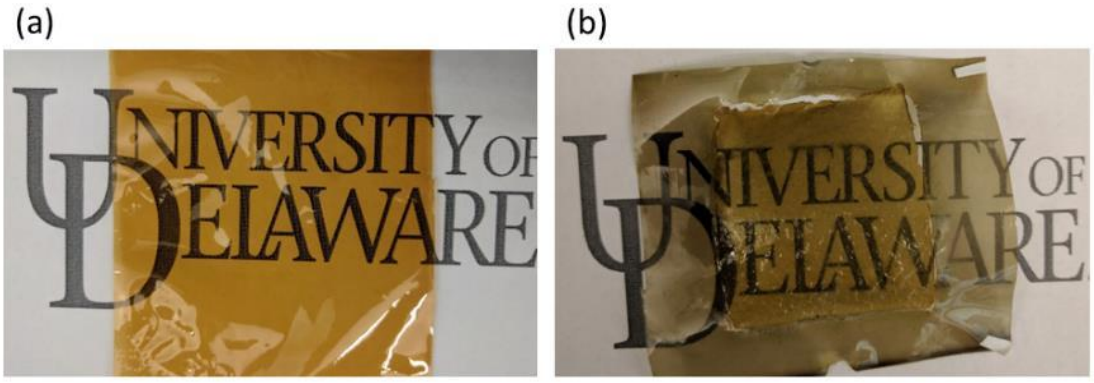

Figure 5.7: (a) acid doped pristine DMF_6PBI membrane and (b) DMF_6PBI membrane after 46-cycle VRFB degradation test, the active area became fragile.

Table 5.2: Properties of DMF_6PBI and F_6PBI membranes before and after VRFB cycling test. Error bars are standard errors of the measurements (n = 3).

Membrane		Inherent viscosity (dL g^{-1})	Stress at break (MPa)	Elongation at break (%)
DMF_6PBI	Pristine acid doped	1.24 ± 0.07	10.9 ± 0.8	17.4 ± 1.4
	After 46 cycles	0.13 ± 0.02	-[a]	-[a]
F_6PBI	Pristine acid doped	1.65 ± 0.09	60.5 ± 4.8	15.0 ± 1.5
	After 100 cycles	1.65 ± 0.10	60.5 ± 5.0	15.1 ± 1.4

[a]: DMF_6PBI membrane active area afterward was too fragile to cut strips for the stress-strain test.

In order to confirm the degradation of dimethyl benzimidazolium in VRFB and investigate the degradation products clearly, FTIR spectra of pristine DMF_6PBI membrane doped in 3 M sulfuric acid and degraded DMF_6PBI membrane (small pieces from the active area) after in-situ VRFB test were examined (Figure 5.8). For the degraded DMF_6PBI sample after in-situ VRFB degradation test, a significant new peak was found at 1713 cm^{-1}, which was attributed to the strong C=O stretching of carboxyl benzene.

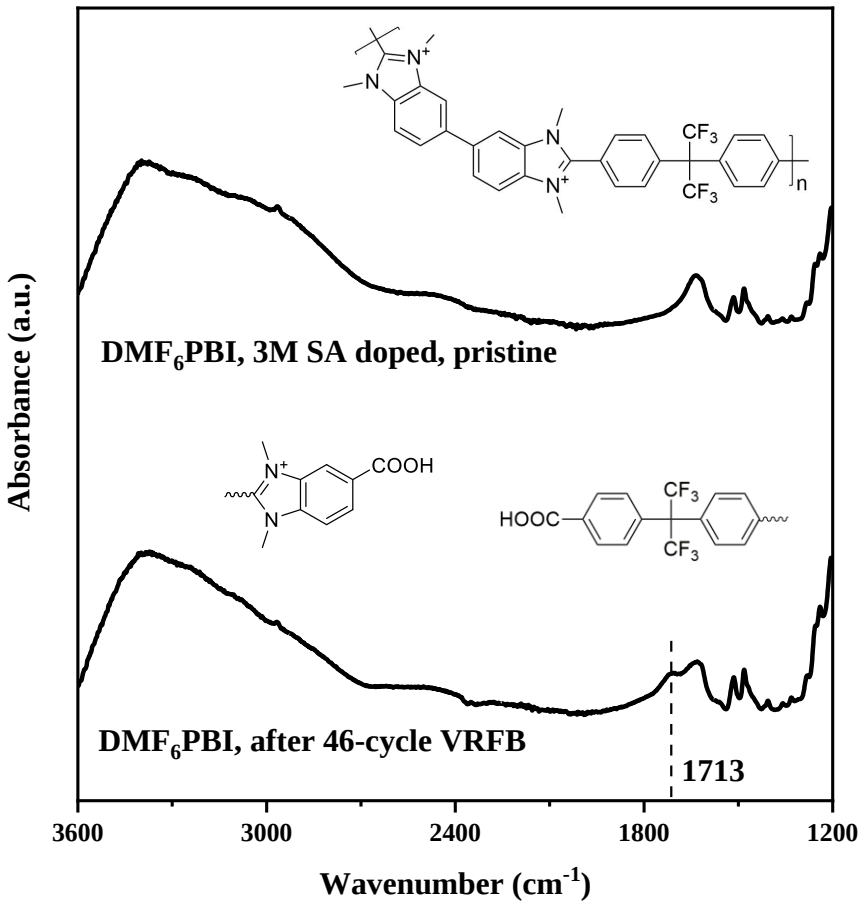

Figure 5.8: FTIR spectra of DMF_6PBI membrane before and after 46-cycle in-situ VRFB degradation test.

^1H NMR spectroscopy was employed to further investigate the degradation mechanism (Figure 5.9). The active area of the degraded DMF_6PBI membrane after in-situ degradation test was found to be more soluble in dimethyl sulfoxide (DMSO) than pristine DMF_6PBI. This increased solubility supported the molecular weight reduction

from inherent viscosity measurement and proved that there is no crosslinking during the in-situ VRFB degradation test. After the degradation, small new peaks appeared at around 3.9 ppm, 7.8 ppm, and 8.1 ppm. Since imidazolium cation is a stronger electron withdrawing substituent and therefore provides stronger deshielding effect compared to carboxyl groups,[255] the new small aromatic peaks at the higher field (7.8 ppm and 8.1 ppm) agreed with the formation of carboxyl benzene structures. However, these new peaks had relatively low intensity and were difficult to assign to the predicted degraded products.

Ex-situ degradation test of DMF_6PBI membrane in 1.5 M vanadium (V) at 80 °C for 500 h was employed to deteriorate the degradation condition and accelerate the degradation process. As shown in Figure 5.9, besides the original peaks, appreciable new peaks appeared at 3.9 ppm, 7.8 ppm, 7.9 ppm, 8.1 ppm, 8.3 ppm, and 8.4 ppm after ex-situ degradation test. Again, the new aromatic peaks at relatively higher field agreed with the formation of carboxyl benzene structures. The new set of methyl peaks at around 3.9 ppm will be assigned to the p1 of product P1 in the proposed degradation scheme (Figure 5.10).

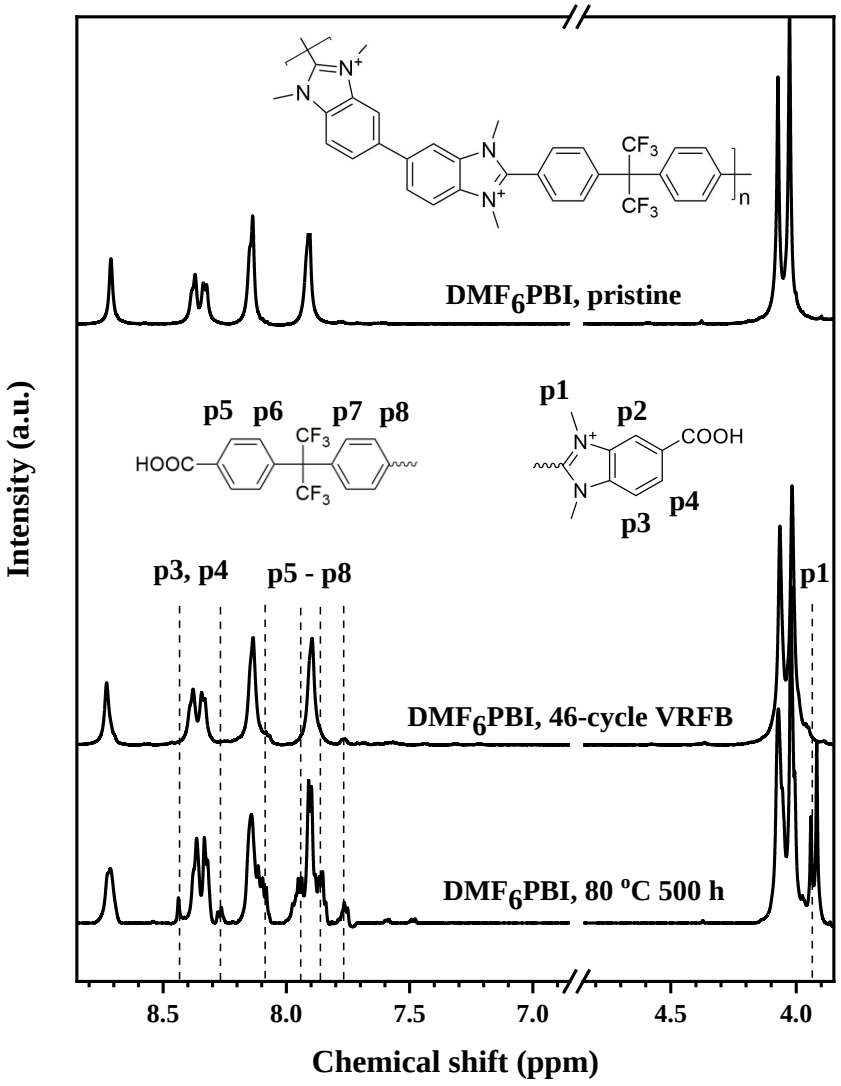

Figure 5.9: ^{1}H NMR spectroscopy of DMF_6PBI membrane pristine, after 46-cycle VRFB, and after 500 h degradation test in 1.5 M vanadium (V) at 80 °C.

Based on the above observations, we proposed the following degradation mechanism in Figure 5.10. Similar reactions have been proposed in the oxidation study of PBI polymers in the acid environment.[256] According to our evidence from FTIR and ^{1}H NMR spectroscopy characterization and published experimental evidence of similar degradations, this proposed degradation mechanism is the best assumption.

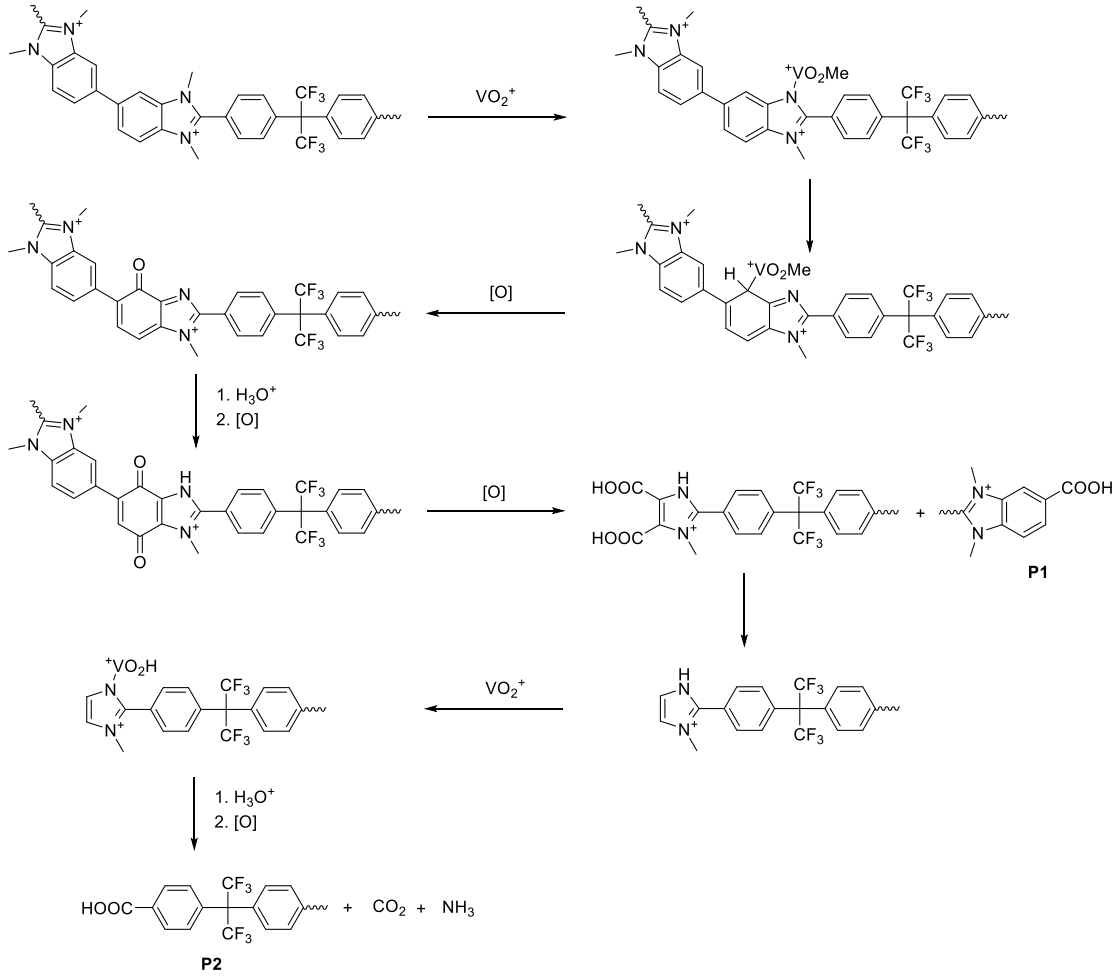

Figure 5.10: Proposed overall degradation of DMF_6PBI in VRFB application.

5.4 Conclusion

DMF_6PBI membrane was employed for the VRFB. Due to the superior ADL, attributed to the cationic dimethyl benzimidazolium units, DMF_6PBI membrane presented an impressive battery efficiency over a range of current densities. However, DMF_6PBI membrane failed during in-situ VRFB test within 46 cycles. The degradation products and pathway of in-situ VRFB test and ex-situ vanadium (V) solution test were investigated in detail, and the knowledge can be applied to improve future material design for VRFB applications.

Chapter 6

CONCLUSIONS AND FUTURE WORK

6.1 Conclusions

Polymeric ion-exchange membranes (IEMs) are the essential component of the redox flow battery (RFB) systems. The key requirements for an IEM in RFBs are: (1) good conductivity to efficiently transport supporting ions; (2) high chemical stability to resist the corrosive RFB electrolyte for long cycling life; and (3) low permeability of the active species to prevent crossover and capacity loss of the RFB cell.

Zinc-cerium double-membrane RFB has the highest cell voltage (3.08 V) in aqueous RFBs. This RFB requires a cation-exchange membrane (CEM) between the alkaline zinc electrolyte and the middle $NaClO_4$ electrolyte and an anion-exchange membrane (AEM) between the acidic cerium electrolyte and the middle $NaClO_4$ electrolyte. However, due to the limited chemical stability of commercial AEMs, this RFB could only demonstrate a few cycles of operation.[105] At the beginning of my Ph.D., I was focusing on the developing of chemically stable AEM for this zinc-cerium double membrane RFB.

Unlike the alkaline stability of AEMs in hydroxide-exchange membrane fuel cells (HEMFCs), the stability of AEMs in the cerium electrolyte is not well studied. The cerium electrolyte contains super oxidant cerium (IV) and acidic perchloric acid. Therefore, I focused on the polymeric backbones at the beginning. Weight loss tests of four different aromatic polymers were conducted, and only hexafluoropropylidene polybenzimidazole (F_6PBI) membrane showed no noticeable weight loss and no

appearance change. However, poly(2,6-dimethyl-phenylene oxide) (PPO) and polysulfone (PSF) membranes showed 41 % and 23 % weight loss respectively after the oxidation stability test. Without any cationic functionalization, these four membranes are all perfectly stable in an alkaline solution simulating HEMFCs. This phenomenon indicates that the cerium electrolytes pose more crucial challenges to the chemical stability of polymeric membranes, and the degradation of these membranes is worth investigating. Heteronuclear single quantum coherence (HSQC) spectroscopy was utilized to investigate the hydrogen-carbon correlation of degraded products, and the most likely degradation mechanisms of PPO and PSF were proposed based on obtained evidence.

With the chemical resistant F_6PBI as the polymeric backbone, a relative stable cation was required for the AEM. Tris(2,4,6-trimethylphenyl)phosphonium (TTMePP) was first considered due to its reported superior chemical stability.[110] The AEM synthesis with TTMePP as a functional group was not easy due to the high steric hindrance at the center phosphine. Initial quaternization trials failed due to this steric hindrance. A bromination strategy at the outside methyl group was proposed, and a series of bromination reactions were investigated (details in Appendix B). However, bromination reactions always led to multiple brominated products which could cause undesired crosslinking. Finally, the connection was successful with a novel quaternization approach with Cu added as an inhibitor to suppress the alkyl iodide decomposition. TTMePP functionalized membrane was finally synthesized and cast. However, the membrane exhibited insufficient conductivity due to the hydrophobic TTMePP cation. Another chemically stable cation (i.e., tris(2,4,6-trimethoxyphenyl)phosphonium (TTMPP)) was then chosen as the new functional

group. TTMPP cation has less steric hindrance at the center phosphine and can be directly quaternized by the traditional alkyl iodide treatment. The prepared TTMPP-PBI membrane with expanded polytetrafluoroethylene (ePTFE) reinforcement presented 26 % water uptake (WU), OH^- conductivity of 9.8 mS/cm, and ClO_4^- conductivity of 2.7 mS/cm at 20 °C. Besides the decent conductivity, the membrane also showed sufficient chemical stability in oxidative cerium electrolyte.

A further investigation of the TTMPP-PBI membrane revealed the acid doping ability of this membrane. In a concentrated sulfuric acid solution, TTMPP-PBI could dope acids in four ways: (1) acid-base doping on the nitrogen of the PBI backbone due to the hydrogen bond formation between benzimidazoles and acids, (2) acid-base doping on the oxygen of the TTMPP cation due to the hydrogen bond formation between methoxyl groups and acids, (3) cation-anion doping due to the bisulfate paired with TTMPP cation, and (4) free acids forming hydrogen bonds with doped acids. The measured acid doping level (ADL) of the prepared TTMPP-PBI/PTFE membrane is 3.4 fold of F_6PBI membrane in 3 M sulfuric acid solution. Vanadium redox flow battery (VRFB) with this TTMPP-PBI/PTFE membrane was assembled, and this VRFB showed the highest energy efficiency compared with Nafion 115 and F_6PBI membrane.

In terms of IEMs for VRFB applications, the state-of-art membrane was the porous polybenzimidazole (PBI) membrane reported in 2016.[104] To cope with the insufficient acid doping and low conductivity of pure PBI membranes, they employed a sponge-like porous structure. As we studied before, cation-anion acid doping could be more effective than the acid-base acid doping in polyprotic acids, a positively charged methylated polybenzimidazolium (DMF_6PBI) was synthesized and showed excellent ADL and area specific resistance (ASR) in 3 M sulfuric acid solution. However, a

further VRFB operation showed chemical decay of the DMF_6PBI membrane in vanadium electrolyte. A series of characterizations were taken to investigate this degradation of positively functionalized PBI, and a degradation mechanism is proposed based on the experimental evidence. DMF_6PBI was tested in VRFB for the first time, and this research could be useful guidance for future robust membrane design for VRFB system.

6.2 Future Work

6.2.1 Poly(2,5-benzimidazole) for Vanadium Redox Flow Batteries

In Chapter 4, the acid doping behavior of F_6PBI membrane is reported, including ADL, acid weight percentage of the doped membrane, water weight percentage of the doped membrane and water to acid mole ratio. In Chapter 5, we also reported that there were no noticeable changes of stress at break and elongation at break for F_6PBI membrane after 100 cycles in VRFB. However, for DMF_6PBI membrane, it degraded severely within 46 cycles of VRFB. The next generation membrane for VRFB requires a chemically stable structure with good ADL to meet the performance requirements of VRFB.

6.2.1.1 Chemical Stability Issue of Polybenzimidazoles

As investigated in Chapter 5, although cationic functionalization of PBI could improve its acid doping conductivity in the sulfuric acid electrolyte, the chemical stability is compromised (details in Section 5.3.3). For the F_6PBI membrane with no modification, no noticeable changes of polymer solution viscosity, stress at break, and elongation at break were observed. Besides the experiment results collected in Chapter 5, PBI materials are also proven to be chemically stable in VRFB by Zhang at el for

over 10,000 cycles of operation.[104] The core functional chemical structure of PBI material is the benzimidazole group which could be doped with sulfuric acid and make the material proton conductive.[128] Therefore, a reasonable approach to a chemically stable membrane for VRFB based on PBI related material is to keep the original structure of the benzimidazole.

6.2.1.2 Acid Doping Level of Polybenzimidazoles with Different Chemical Structures

The acid doping happens on the nitrogen site of the benzimidazole groups in PBIs, a valid method to improve the conductivity is increasing the density of benzimidazole groups in the PBI polymer. Compared to the F_6PBI used in previous chapters of this work. poly(2,5-benzimidazole) (ABPBI) only contains the benzimidazole groups without any other redundant structures and should have the highest ADL and lowest ASR in a sulfuric acid electrolyte. The chemical structures of F6PBI and ABPBI are shown in Figure 6.1.

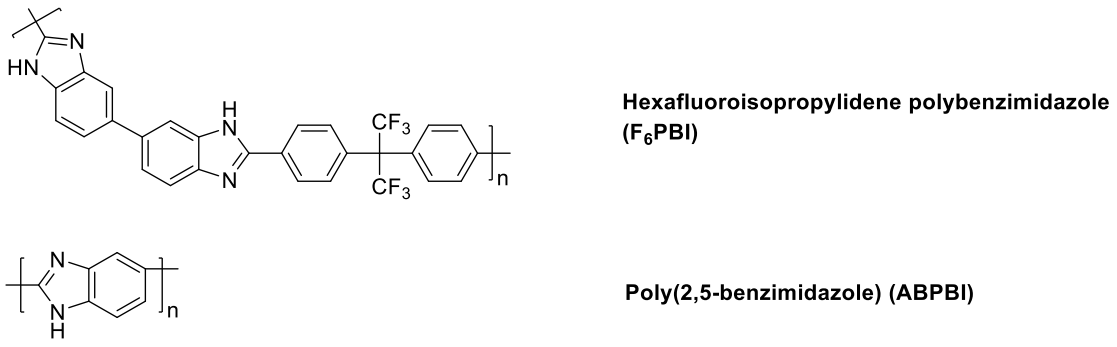

Figure 6.1: Chemical structure comparison between F_6PBI and ABPBI. ABPBI has the highest density of benzimidazole groups.

6.2.1.3 Implementation of Poly(2,5-benzimidazole) for Vanadium Redox Flow Batteries

From Table 5.2, DMF_6PBI was much less stable compared with F_6PBI, and the neutral benzimidazole group did not cause noticeable stability issue during VRFB cycling. Thus, the ABPBI polymer, which is only composed of benzimidazole groups (as shown in Figure 6.1), should be chemically stable in VRFB.

The synthesis of ABPBI was investigated, and a few batches of the polymer were synthesized before this dissertation. The synthesized polymer was found to be not soluble in organic solvents like chloroform, acetone, DMSO, NMP, etc. Thus, NMR spectroscopy was not available.

6.2.2 Investigation of the ePTFE reinforcement on ion-exchange membrane properties

Reinforcement is a technology that helps improve the mechanical strength of the membrane material. For IEMs, besides the mechanical properties, WU, ion-exchange capacity (IEC), and ion conductivity of the membrane are all affected by the reinforcement.

6.2.2.1 Mechanical Properties of Ion-Exchange Membranes with Reinforcement

As shown in Table 6.1, the TTMPP-PBI-3 polymer membrane synthesized in Chapter 3 was too brittle to test mechanical properties. After reinforcement with ePTFE, the membrane showed reasonable strength and was measured to have an average tensile strength of 17.3 MPa and an average elongation at break of 17.1 %. Besides the 10 μm ePTFE mesh used in Chapter 3, there are also ePTFE materials commercially available with other thickness. The amount of polymer solution used to make the reinforced membrane could also be changed to meet specific requirement of mechanical properties.

A higher weight ratio of the ePTFE to polymer material would provide better support, and the reinforced membrane would likely have better mechanical properties.

Table 6.1. Tensile strength and elongation at break of TTMPP-PBI membrane and TTMPP-PBI membrane with ePTFE reinforcement. Error bars are standard errors of the measurements (n = 3). (For reading convenience, partial data from Table 3.1 is re-used to construct this table.)

Membrane	Tensile strength (MPa)	Elongation at break (%)
TTMPP-PBI-3	- [a]	- [a]
TTMPP-PBI-3/PTFE	17.3 ± 0.7	17.1 ± 1.1

[a]: TTMPP-PBI-3 membrane is too brittle to test mechanical properties.

6.2.2.2 Water Uptake, Ion Exchange Capacity and Ion Conductivity of Ion-Exchange Membranes with Reinforcement

In Table 3.1, the average measured IEC of TTMPP-PBI-3/PTFE was about 86 % of the average value of TTMPP-PBI-3, which indicated that the weight ratio of TTMPP-PBI polymer to the ePTFE was approximately 6.1 : 1 (i.e., 86 % / 14 %) in the prepared reinforced membrane. After this reinforcement, the average WU dropped 68 % due to the hydrophobicity of the ePTFE material (Table 3.2). As discussed in Section 6.2.2.1, higher weight ratio of ePTFE should help the mechanical properties. However, it would inevitably harm the WU, IEC and ion conductivity of the membrane material due to the hydrophobicity nature of the ePTFE.

6.2.2.3 Tris(2,4,6-trimethoxyphenyl)phosphonium Functionalized Polybenzimidazole Membrane with Different Levels of ePTFE Reinforcement

By tuning the ratio of the ion exchange polymer to the supporting material, membranes with different IEC, conductivity, and mechanical property could be

obtained. A systematic examination of the reinforcement component ratio could potentially help us achieve better overall membrane properties and battery performance. Moreover, a detailed investigation of the reinforcement mechanism could provide useful guidance for the future reinforcement membrane casting.

REFERENCES

[1] Pelc, R.; M.Fujita, R., Renewable energy from the ocean. *Marine Policy* **2002,** *26*, 471-479.

[2] BULL, S. R., Renewable Energy Today and Tomorrow. *PROCEEDINGS OF THE IEEE* **2001,** *89*.

[3] REN21 *RENEWABLES 2010 GLOBAL STATUS REPORT*; 2010.

[4] Lund, H.; Mathiesen, B. V., Energy system analysis of 100% renewable energy systems—The case of Denmark in years 2030 and 2050. *Energy* **2009,** *34* (5), 524-531.

[5] Jacobsson, S.; Lauber, V., The politics and policy of energy system transformation—explaining the German diffusion of renewable energy technology. *Energy Policy* **2006,** *34* (3), 256-276.

[6] Ellabban, O.; Abu-Rub, H.; Blaabjerg, F., Renewable energy resources: Current status, future prospects and their enabling technology. *Renewable and Sustainable Energy Reviews* **2014,** *39*, 748-764.

[7] REN21 *Global Status Report 2016*; 2016.

[8] Birol, F. *Key world energy statistics*; International Energy Agency 2018.

[9] Merchant, E. *2017 Was Another Record-Busting Year for Renewable Energy, but Emissions Still Increased*; Green Tech Media, 2018.

[10] Johansson, T. B.; Kelly, H.; Reddy, A. K. N.; Williams, R. H., Renewable Fuels and Electricity for a Growing World Economy: Defining and Achieving the Potential. *Energy Studies Review* **1992,** *4* (3).

[11] Chakraborty, A., Advancements in power electronics and drives in interface with growing renewable energy resources. *Renewable and Sustainable Energy Reviews* **2011,** *15* (4), 1816-1827.

[12] Greenwood, C.; Hohler, A.; Hunt, G.; Liebreich, M.; Sonntag-O'Brien, V.; Usher, E. *GLOBAL TRENDS IN SUSTAINABLE ENERGY INVESTMENT 2007: Analysis of Trends and Issues in the Financing of Renewable Energy and Energy Efficiency in OECD and Developing Countries*; UNEP: 2007.

[13] Halamay, D. A.; Brekken, T. K. A.; Simmons, A.; McArthur, a. S., Reserve Requirement Impacts of Large-Scale Integration of Wind, Solar, and Ocean Wave Power Generation. *IEEE TRANSACTIONS ON SUSTAINABLE ENERGY* **2011,** *2*.

[14] Chedid, R.; Rahman, S., UNIT SIZING AND CONTROL OF HYBRID WIND-SOLAR POWER SYSTEMS. *IEEE Transactions on Energy Conversion* **1997,** *12*.

[15] Heide, D.; von Bremen, L.; Greiner, M.; Hoffmann, C.; Speckmann, M.; Bofinger, S., Seasonal optimal mix of wind and solar power in a future, highly renewable Europe. *Renewable Energy* **2010,** *35* (11), 2483-2489.

[16] Denholm, P.; Ela, E.; Kirby, B.; Milligan, M. *The Role of Energy Storage with Renewable Electricity Generation*; National Renewable Energy Laboratory: 2010.

[17] Evans, A.; Strezov, V.; Evans, T. J., Assessment of utility energy storage options for increased renewable energy penetration. *Renewable and Sustainable Energy Reviews* **2012,** *16* (6), 4141-4147.

[18] Dunn, B.; Kamath, H.; Tarascon, J. M., Electrical energy storage for the grid: a battery of choices. *Science* **2011,** *334* (6058), 928-35.

[19] Huggins, R. A., *Energy Storage*. 2010.

[20] Steffen, B., Prospects for pumped-hydro storage in Germany. *Energy Policy* **2012,** *45*, 420-429.

[21] Bueno, C.; Carta, J. A., Wind powered pumped hydro storage systems, a means of increasing the penetration of renewable energy in the Canary Islands. *Renewable and Sustainable Energy Reviews* **2006,** *10* (4), 312-340.

[22] Swider, D. J., Compressed Air Energy Storage in an Electricity System With Significant Wind Power Generation. *IEEE Transactions on Energy Conversion* **2007,** *22*, 95-102.

[23] Lund, H.; Salgi, G., The role of compressed air energy storage (CAES) in future sustainable energy systems. *Energy Conversion and Management* **2009,** *50* (5), 1172-1179.

[24] Liu, H.; Jiang, J., Flywheel energy storage—An upswing technology for energy sustainability. *Energy and Buildings* **2007,** *39* (5), 599-604.

[25] Bolund, B.; Bernhoff, H.; Leijon, M., Flywheel energy and power storage systems. *Renewable and Sustainable Energy Reviews* **2007,** *11* (2), 235-258.

[26] Miller, J. R.; Simon, P., Materials science. Electrochemical capacitors for energy management. *Science* **2008,** *321* (5889), 651-2.

[27] Banerjee, P.; Perez, I.; Henn-Lecordier, L.; Lee, S. B.; Rubloff, G. W., Nanotubular metal-insulator-metal capacitor arrays for energy storage. *Nat Nanotechnol* **2009,** *4* (5), 292-6.

[28] Dubal, D. P.; Ayyad, O.; Ruiz, V.; Gomez-Romero, P., Hybrid energy storage: the merging of battery and supercapacitor chemistries. *Chemical Society Reviews* **2015,** *44* (7), 1777-90.

[29] Bae, J.; Song, M. K.; Park, Y. J.; Kim, J. M.; Liu, M.; Wang, Z. L., Fiber supercapacitors made of nanowire-fiber hybrid structures for wearable/flexible energy storage. *Angew Chem Int Ed Engl* **2011,** *50* (7), 1683-7.

[30] Denholm, P., Improving the technical, environmental and social performance of wind energy systems using biomass-based energy storage. *Renewable Energy* **2006,** *31* (9), 1355-1370.

[31] Sevilla, M.; Mokaya, R., Energy storage applications of activated carbons: supercapacitors and hydrogen storage. *Energy Environ. Sci.* **2014,** *7* (4), 1250-1280.

[32] Zhang, F.; Zhao, P.; Niu, M.; Maddy, J., The survey of key technologies in hydrogen energy storage. *International Journal of Hydrogen Energy* **2016,** *41* (33), 14535-14552.

[33] Bai, F.; Xu, C., Performance analysis of a two-stage thermal energy storage system using concrete and steam accumulator. *Applied Thermal Engineering* **2011,** *31* (14-15), 2764-2771.

[34] Medrano, M.; Gil, A.; Martorell, I.; Potau, X.; Cabeza, L. F., State of the art on high-temperature thermal energy storage for power generation. Part 2—Case studies. *Renewable and Sustainable Energy Reviews* **2010,** *14* (1), 56-72.

[35] Morgan, R.; Nelmes, S.; Gibson, E.; Brett, G., Liquid air energy storage – Analysis and first results from a pilot scale demonstration plant. *Applied Energy* **2015,** *137*, 845-853.

[36] Guizzi, G. L.; Manno, M.; Tolomei, L. M.; Vitali, R. M., Thermodynamic analysis of a liquid air energy storage system. *Energy* **2015,** *93*, 1639-1647.

[37] Perry, M. L.; Darling, R. M.; Zaffou, R., High Power Density Redox Flow Battery Cells. In *223rd ECS Meeting*, United Technologies Research Center (UTRC): 2013.

[38] Brushett, F. R.; Vaughey, J. T.; Jansen, A. N., An All-Organic Non-aqueous Lithium-Ion Redox Flow Battery. *Advanced Energy Materials* **2012,** *2* (11), 1390-1396.

[39] Wang, W.; Luo, Q.; Li, B.; Wei, X.; Li, L.; Yang, Z., Recent Progress in Redox Flow Battery Research and Development. *Advanced Functional Materials* **2013,** *23* (8), 970-986.

[40] Wei, X.; Xu, W.; Huang, J.; Zhang, L.; Walter, E.; Lawrence, C.; Vijayakumar, M.; Henderson, W. A.; Liu, T.; Cosimbescu, L.; Li, B.; Sprenkle, V.; Wang, W., Radical Compatibility with Nonaqueous Electrolytes and Its Impact on an All-Organic Redox Flow Battery. *Angew Chem Int Ed Engl* **2015,** *54* (30), 8684-7.

[41] Yue, L.; Li, W.; Sun, F.; Zhao, L.; Xing, L., Highly hydroxylated carbon fibres as electrode materials of all-vanadium redox flow battery. *Carbon* **2010,** *48* (11), 3079-3090.

[42] Yun, S.; Parrondo, J.; Ramani, V., A Vanadium-Cerium Redox Flow Battery with an Anion-Exchange Membrane Separator. *Chempluschem* **2015,** *80* (2), 412-421.

[43] Bruce, P. G.; Scrosati, B.; Tarascon, J. M., Nanomaterials for rechargeable lithium batteries. *Angew Chem Int Ed Engl* **2008,** *47* (16), 2930-46.

[44] Goodenough, J. B.; Park, K. S., The Li-ion rechargeable battery: a perspective. *J Am Chem Soc* **2013,** *135* (4), 1167-76.

[45] Bruce, P. G.; Freunberger, S. A.; Hardwick, L. J.; Tarascon, J. M., Li-O2 and Li-S batteries with high energy storage. *Nat Mater* **2011,** *11* (1), 19-29.

[46] Bruce, P. G., Energy storage beyond the horizon: Rechargeable lithium batteries. *Solid State Ionics* **2008,** *179* (21-26), 752-760.

[47] Rastler, D. *Electricity energy storage technology options*; Electric Power Research Institute: 2010.

[48] Service, R. F., Tanks for the Batteries. *Science* **2014,** *344* (6182), 352-354.

[49] Doerffel, D.; Sharkh, S. A., A critical review of using the Peukert equation for determining the remaining capacity of lead-acid and lithium-ion batteries. *Journal of Power Sources* **2006,** *155* (2), 395-400.

[50] Sabatier, J.; Aoun, M.; Oustaloup, A.; Grégoire, G.; Ragot, F.; Roy, P., Fractional system identification for lead acid battery state of charge estimation. *Signal Processing* **2006,** *86* (10), 2645-2657.

[51] Sakai, T.; Hazama, T.; Miyamura, H.; N. Kuriyama; Kato, A.; Ishikawa, H., Rare-earth-based alloy electrodes for a nickel-metal hydride battery. *Journal of the Less-Common Metals* **1991,** *172*, 1175-1184.

[52] Majeau-Bettez, G.; Hawkins, T. R.; Stromman, A. H., Life cycle environmental assessment of lithium-ion and nickel metal hydride batteries for plug-in hybrid and battery electric vehicles. *Environ Sci Technol* **2011,** *45* (10), 4548-54.

[53] Nam, K. T.; Kim, D. W.; Yoo, P. J.; Chiang, C. Y.; Meethong, N.; Hammond, P. T.; Chiang, Y. M.; Belcher, A. M., Virus-enabled synthesis and assembly of nanowires for lithium ion battery electrodes. *Science* **2006,** *312* (5775), 885-8.

[54] Vetter, J.; Novák, P.; Wagner, M. R.; Veit, C.; Möller, K. C.; Besenhard, J. O.; Winter, M.; Wohlfahrt-Mehrens, M.; Vogler, C.; Hammouche, A., Ageing mechanisms in lithium-ion batteries. *Journal of Power Sources* **2005,** *147* (1-2), 269-281.

[55] Lu, L.; Han, X.; Li, J.; Hua, J.; Ouyang, M., A review on the key issues for lithium-ion battery management in electric vehicles. *Journal of Power Sources* **2013,** *226*, 272-288.

[56] Daniel, C., Materials and Processing for Lithium-Ion Batteries. *JOM* **2008,** *60*.

[57] Yunjian, L.; Xinhai, L.; Huajun, G.; Zhixing, W.; Qiyang, H.; Wenjie, P.; Yong, Y., Electrochemical performance and capacity fading reason of LiMn2O4/graphite batteries stored at room temperature. *Journal of Power Sources* **2009,** *189* (1), 721-725.

[58] Lin, D.; Liu, Y.; Cui, Y., Reviving the lithium metal anode for high-energy batteries. *Nat Nanotechnol* **2017,** *12* (3), 194-206.

[59] Ponce de León, C.; Frías-Ferrer, A.; González-García, J.; Szánto, D. A.; Walsh, F. C., Redox flow cells for energy conversion. *Journal of Power Sources* **2006,** *160* (1), 716-732.

[60] Alotto, P.; Guarnieri, M.; Moro, F., Redox flow batteries for the storage of renewable energy: A review. *Renewable and Sustainable Energy Reviews* **2014,** *29*, 325-335.

[61] Zhou, X. L.; Zhao, T. S.; An, L.; Zeng, Y. K.; Wei, L., Critical transport issues for improving the performance of aqueous redox flow batteries. *Journal of Power Sources* **2017,** *339*, 1-12.

[62] Sanz, L.; Lloyd, D.; Magdalena, E.; Palma, J.; Kontturi, K., Description and performance of a novel aqueous all-copper redox flow battery. *Journal of Power Sources* **2014,** *268*, 121-128.

[63] Winsberg, J.; Stolze, C.; Muench, S.; Liedl, F.; Hager, M. D.; Schubert, U. S., TEMPO/Phenazine Combi-Molecule: A Redox-Active Material for Symmetric Aqueous Redox-Flow Batteries. *ACS Energy Letters* **2016,** *1* (5), 976-980.

[64] Hwang, B.; Park, M. S.; Kim, K., Ferrocene and cobaltocene derivatives for non-aqueous redox flow batteries. *ChemSusChem* **2015,** *8* (2), 310-4.

[65] Wei, X.; Duan, W.; Huang, J.; Zhang, L.; Li, B.; Reed, D.; Xu, W.; Sprenkle, V.; Wang, W., A High-Current, Stable Nonaqueous Organic Redox Flow Battery. *ACS Energy Letters* **2016,** *1* (4), 705-711.

[66] Escalante-García, I. L.; Wainright, J. S.; Thompson, L. T.; Savinell, R. F., Performance of a Non-Aqueous Vanadium Acetylacetonate Prototype Redox Flow Battery: Examination of Separators and Capacity Decay. *Journal of the Electrochemical Society* **2014,** *162* (3), A363-A372.

[67] Gong, K.; Fang, Q.; Gu, S.; Li, S. F. Y.; Yan, Y., Nonaqueous redox-flow batteries: organic solvents, supporting electrolytes, and redox pairs. *Energy & Environmental Science* **2015,** *8* (12), 3515-3530.

[68] Leung, P. K.; Ponce-de-León, C.; Low, C. T. J.; Walsh, F. C., Zinc deposition and dissolution in methanesulfonic acid onto a carbon composite electrode as the negative electrode reactions in a hybrid redox flow battery. *Electrochimica Acta* **2011,** *56* (18), 6536-6546.

[69] Wu, M. C.; Zhao, T. S.; Jiang, H. R.; Zeng, Y. K.; Ren, Y. X., High-performance zinc bromine flow battery via improved design of electrolyte and electrode. *Journal of Power Sources* **2017,** *355*, 62-68.

[70] Al-Fetlawi, H.; Shah, A. A.; Walsh, F. C., Non-isothermal modelling of the all-vanadium redox flow battery. *Electrochimica Acta* **2009,** *55* (1), 78-89.

[71] Tang, A.; Bao, J.; Skyllas-Kazacos, M., Studies on pressure losses and flow rate optimization in vanadium redox flow battery. *Journal of Power Sources* **2014,** *248*, 154-162.

[72] Gong, K., Study of novel redox flow batteries based on double-membrane, single-membrane, and membrane-less cell configurations. University of Delaware: 2016.

[73] Adams, G. B.; Hollandsworth, R. P.; Littauer, E. L., *Proceedings of the 16th Intersociety Energy Conversion Engineering Conference* **1981**, 812-816.

[74] Dirkse, T. P., The Nature of the Zinc-Containing Ion in Strongly Alkaline Solutions. *Journal of the Electrochemical Society* **1954,** *101* (6), 328-331.

[75] Bae, C. H.; Roberts, E. P. L.; Dryfe, R. A. W., Chromium redox couples for application to redox flow batteries. *Electrochimica Acta* **2002,** *48* (3), 279-287.

[76] Lim, H. S.; Lackner, A. M.; Knechtli, R. C., Zinc-Bromine Secondary Battery. *Journal of the Electrochemical Society* **1977,** *124* (8), 1154-1157.

[77] Zhang, L. Q.; Lai, Q. Z.; Zhang, J. L.; Zhang, H. M., A High-Energy-Density Redox Flow Battery based on Zinc/Polyhalide Chemistry. *Chemsuschem* **2012,** *5* (5), 867-869.

[78] Clarke, R. L.; Dougherty, B. J.; Harrison, S.; Millington, J. P.; Mohanta, S. Battery with bifunctional electrolyte. 6986966, 2006.

[79] Clarke, R. L.; Dougherty, B.; Harrison, S.; Millington, P. J.; Mohanta, S. Cerium batteries. 7625663, 2004.

[80] Tang, C.; Zhou, D. B., Methanesulfonic acid solution as supporting electrolyte for zinc-vanadium redox battery. *Electrochimica Acta* **2012,** *65*, 179-184.

[81] Remick, R. J.; Ang, P. G. P. Electrically rechargeable anionically active reduction-oxidation electrical storage-supply system. 4485154, 1984.

[82] Hruska, L. W.; Savinell, R. F., Investigation of Factors Affecting Performance of the Iron-Redox Battery. *Journal of the Electrochemical Society* **1981,** *128* (1), 18-25.

[83] Thaller, L. H., Electrically rechargeable redox flow cells. *The 9th Intersociety Energy Conversion Engineering Conference Proceedings* **1974**, 924-928.

[84] Hiroko, K.; Takeshi, N. Redox Battery. 57009072, 1982.

[85] Doria, J.; Andres, M. C. D.; Armenta, C., *NTERSOL 85: Proceedings of the Ninth Biennial Congress of the International Solar Energy Society* **1985,** (3), 1500.

[86] Skyllas-Kazacos, M., Novel vanadium chloride/polyhalide redox flow battery. *Journal of Power Sources* **2003,** *124* (1), 299-302.

[87] Wang, W.; Kim, S.; Chen, B.; Nie, Z.; Zhang, J.; Xia, G.-G.; Li, L.; Yang, Z., A new redox flow battery using Fe/V redox couples in chloride supporting electrolyte. *Energy & Environmental Science* **2011,** *4* (10), 4068-4073.

[88] Skyllas-Kazacos, M.; Rychcik, M.; Robins, R. G.; Fane, A. G.; Green, M. A., New All-Vanadium Redox Flow Cell. *Journal of the Electrochemical Society* **1986,** *133* (5), 1057-1058.

[89] Wen, Y. H.; Zhang, H. M.; Qian, P.; Zhou, H. T.; Zhao, P.; Yi, B. L.; Yang, Y. S., Studies on iron (Fe3+/Fe2+)-complex/bromine (Br-2/Br-) redox flow cell in sodium acetate solution. *Journal of the Electrochemical Society* **2006,** *153* (5), A929-A934.

[90] Wadsworth, E.; Duke, F. R.; Goetz, C. A., Present Status of Cerium(Iv)-Cerium(Iii) Potentials. *Analytical Chemistry* **1957,** *29* (12), 1824-1825.

[91] Fang, B.; Iwasa, S.; Wei, Y.; Arai, T.; Kumagai, M., Study of the Ce(III)/Ce(IV) redox couple for redox flow battery application. *Electrochimica Acta* **2002,** *47* (24), 3971-3976.

[92] Xue, F. Q.; Wang, Y. L.; Wang, W. H.; Wang, X. D., Investigation on the electrode process of the Mn(II)/Mn(III) couple in redox flow battery. *Electrochimica Acta* **2008,** *53* (22), 6636-6642.

[93] Yamamura, T.; Watanabe, N.; Yano, T.; Shiokawa, Y., Electron-transfer kinetics of Np3+/Np4+, NpO2+/NpO22+, V2+/V3+, and VO2+/VO2+ at carbon electrodes. *Journal of the Electrochemical Society* **2005,** *152* (4), A830-A836.

[94] Oei, D. G., Chemically Regenerative Redox Fuel-Cells. *Journal of Applied Electrochemistry* **1982,** *12* (1), 41-51.

[95] Lide, D. R., *CRC Handbook of Chemistry and Physics*. 87th ed.; CRC Press: Bora Raton, FL, 2007.

[96] Mironov, V. E.; Lastovkina, N. P., Thermodynamics of trihalide ions. *Russian Journal of Physical Chemistry* **1967,** *41* (8), 991.

[97] Dean, J. A., *Lange's Handbook of Chemistry*. McGraw: 1998.

[98] Pierre, J. L.; Gautier-Luneau, I., Iron and citric acid: A fuzzy chemistry of ubiquitous biological relevance. *Biometals* **2000,** *13* (1), 91-96.

[99] RYCHCIK, M.; SKYLLAS-KAZACOS, M., CHARACTERISTICS OF A NEW ALL-VANADIUM REDOX FLOW BATTERY. *Journal of Power Sources* **1988,** *22*, 59 - 67.

[100] Roznyatovskaya, N.; Herr, T.; Küttinger, M.; Fühl, M.; Noack, J.; Pinkwart, K.; Tübke, J., Detection of capacity imbalance in vanadium electrolyte and its electrochemical regeneration for all-vanadium redox-flow batteries. *Journal of Power Sources* **2016,** *302*, 79-83.

[101] Li, L.; Kim, S.; Wang, W.; Vijayakumar, M.; Nie, Z.; Chen, B.; Zhang, J.; Xia, G.; Hu, J.; Graff, G.; Liu, J.; Yang, Z., A Stable Vanadium Redox-Flow Battery with High Energy Density for Large-Scale Energy Storage. *Advanced Energy Materials* **2011,** *1* (3), 394-400.

[102] Aaron, D. S.; Liu, Q.; Tang, Z.; Grim, G. M.; Papandrew, A. B.; Turhan, A.; Zawodzinski, T. A.; Mench, M. M., Dramatic performance gains in vanadium redox flow batteries through modified cell architecture. *Journal of Power Sources* **2012,** *206*, 450-453.

[103] Liu, Q. H.; Grim, G. M.; Papandrew, A. B.; Turhan, A.; Zawodzinski, T. A.; Mench, M. M., High Performance Vanadium Redox Flow Batteries with Optimized Electrode Configuration and Membrane Selection. *Journal of the Electrochemical Society* **2012,** *159* (8), A1246-A1252.

[104] Yuan, Z.; Duan, Y.; Zhang, H.; Li, X.; Zhang, H.; Vankelecom, I., Advanced porous membranes with ultra-high selectivity and stability for vanadium flow batteries. *Energy Environ. Sci.* **2016,** *9* (2), 441-447.

[105] Gu, S.; Gong, K.; Yan, E. Z.; Yan, Y., A multiple ion-exchange membrane design for redox flow batteries. *Energy Environ. Sci.* **2014,** *7* (9), 2986-2998.

[106] Jiang, B.; Wu, L.; Yu, L.; Qiu, X.; Xi, J., A comparative study of Nafion series membranes for vanadium redox flow batteries. *Journal of Membrane Science* **2016,** *510*, 18-26.

[107] Mai, Z.; Zhang, H.; Li, X.; Xiao, S.; Zhang, H., Nafion/polyvinylidene fluoride blend membranes with improved ion selectivity for vanadium redox flow battery application. *Journal of Power Sources* **2011,** *196* (13), 5737-5741.

[108] Zhang, B. Exploring alkaline stable organic cations for polymer hydroxide exchange membranes. University of Delaware, 2015.

[109] Hugar, K. M.; Kostalik, H. A. t.; Coates, G. W., Imidazolium Cations with Exceptional Alkaline Stability: A Systematic Study of Structure-Stability Relationships. *J Am Chem Soc* **2015,** *137* (27), 8730-7.

[110] Zhang, B.; Kaspar, R. B.; Gu, S.; Wang, J.; Zhuang, Z.; Yan, Y., A New Alkali-Stable Phosphonium Cation Based on Fundamental Understanding of Degradation Mechanisms. *ChemSusChem* **2016,** *9* (17), 2374-9.

[111] P, Z.; QUELLMALZ, D., NOVEL ION EXCHANGE MEMBRANES BASED ON AN AROMATIC POLYETHERSULFONE. *Journal of Membrane Science* **1985,** *22*, 325-332.

[112] Choe, Y.-K.; Fujimoto, C.; Lee, K.-S.; Dalton, L. T.; Ayers, K.; Henson, N. J.; Kim, Y. S., Alkaline Stability of Benzyl Trimethyl Ammonium Functionalized Polyaromatics: A Computational and Experimental Study. *Chemistry of Materials* **2014,** *26* (19), 5675-5682.

[113] Han, J.; Liu, Q.; Li, X.; Pan, J.; Wei, L.; Wu, Y.; Peng, H.; Wang, Y.; Li, G.; Chen, C.; Xiao, L.; Lu, J.; Zhuang, L., An effective approach for alleviating cation-induced backbone degradation in aromatic ether-based alkaline polymer electrolytes. *ACS Appl Mater Interfaces* **2015,** *7* (4), 2809-16.

[114] Arges, C. G.; Ramani, V., Two-dimensional NMR spectroscopy reveals cation-triggered backbone degradation in polysulfone-based anion exchange membranes. *PNAS* **2013,** *110*, 2490–2495.

[115] Dlugolecki, P.; Nymeijer, K.; Metz, S.; Wessling, M., Current status of ion exchange membranes for power generation from salinity gradients. *Journal of Membrane Science* **2008,** *319* (1-2), 214-222.

[116] Li, X.; Zhang, H.; Mai, Z.; Zhang, H.; Vankelecom, I., Ion exchange membranes for vanadium redox flow battery (VRB) applications. *Energy & Environmental Science* **2011,** *4* (4), 1147.

[117] Jörissen, J.; Breiter, S. M.; Funk, C., Ion transport in anion exchange membranes in presence of multivalent anions like sulfate or phosphate. *Journal of Membrane Science* **2003,** *213*, 247–261.

[118] Parasuraman, A.; Lim, T. M.; Menictas, C.; Skyllas-Kazacos, M., Review of material research and development for vanadium redox flow battery applications. *Electrochimica Acta* **2013,** *101*, 27-40.

[119] Yee, R. S. L.; Rozendal, R. A.; Zhang, K.; Ladewig, B. P., Cost effective cation exchange membranes: A review. *Chemical Engineering Research and Design* **2012,** *90* (7), 950-959.

[120] O'Hagan, D., Understanding organofluorine chemistry. An introduction to the C-F bond. *Chemical Society Reviews* **2008,** *37* (2), 308-19.

[121] Grot, W. G. Solution of fluorinated polymer containing sulfonic acid side chains. 1972.

[122] Minke, C.; Turek, T., Economics of vanadium redox flow battery membranes. *Journal of Power Sources* **2015,** *286*, 247-257.

[123] Chen, D.; Kim, S.; Li, L.; Yang, G.; Hickner, M. A., Stable fluorinated sulfonated poly(arylene ether) membranes for vanadium redox flow batteries. *Rsc Advances* **2012,** *2* (21), 8087.

[124] Qiu, J.; Zhao, L.; Zhai, M.; Ni, J.; Zhou, H.; Peng, J.; Li, J.; Wei, G., Pre-irradiation grafting of styrene and maleic anhydride onto PVDF membrane and subsequent sulfonation for application in vanadium redox batteries. *Journal of Power Sources* **2008,** *177* (2), 617-623.

[125] Qiu, J.; Zhai, M.; Chen, J.; Wang, Y.; Peng, J.; Xu, L.; Li, J.; Wei, G., Performance of vanadium redox flow battery with a novel amphoteric ion exchange membrane synthesized by two-step grafting method. *Journal of Membrane Science* **2009,** *342* (1-2), 215-220.

[126] Mai, Z.; Zhang, H.; Li, X.; Bi, C.; Dai, H., Sulfonated poly(tetramethydiphenyl ether ether ketone) membranes for vanadium redox flow battery application. *Journal of Power Sources* **2011,** *196* (1), 482-487.

[127] Maurya, S.; Shin, S.-H.; Lee, J.-Y.; Kim, Y.; Moon, S.-H., Amphoteric nanoporous polybenzimidazole membrane with extremely low crossover for a vanadium redox flow battery. *Rsc Advances* **2016,** *6* (7), 5198-5204.

[128] Jang, J.-K.; Kim, T.-H.; Yoon, S. J.; Lee, J. Y.; Lee, J.-C.; Hong, Y. T., Highly proton conductive, dense polybenzimidazole membranes with low permeability to vanadium and enhanced H2SO4absorption capability for use in vanadium redox flow batteries. *J. Mater. Chem. A* **2016,** *4* (37), 14342-14355.

[129] Zhou, X. L.; Zhao, T. S.; An, L.; Wei, L.; Zhang, C., The use of polybenzimidazole membranes in vanadium redox flow batteries leading to increased coulombic efficiency and cycling performance. *Electrochimica Acta* **2015,** *153*, 492-498.

[130] Xia, Z.; Ying, L.; Fang, J.; Du, Y.-Y.; Zhang, W.-M.; Guo, X.; Yin, J., Preparation of covalently cross-linked sulfonated polybenzimidazole membranes for vanadium redox flow battery applications. *Journal of Membrane Science* **2017,** *525*, 229-239.

[131] Luo, T.; David, O.; Gendel, Y.; Wessling, M., Porous poly(benzimidazole) membrane for all vanadium redox flow battery. *Journal of Power Sources* **2016,** *312*, 45-54.

[132] Li, Q., Water uptake and acid doping of polybenzimidazoles as electrolyte membranes for fuel cells. *Solid State Ionics* **2004,** *168* (1-2), 177-185.

[133] Li, Q. F.; Rudbeck, H. C.; Chromik, A.; Jensen, J. O.; Pan, C.; Steenberg, T.; Calverley, M.; Bjerrum, N. J.; Kerres, J., Properties, degradation and high temperature fuel cell test of different types of PBI and PBI blend membranes. *Journal of Membrane Science* **2010,** *347* (1-2), 260-270.

[134] Lee, K.-S.; Spendelow, J. S.; Choe, Y.-K.; Fujimoto, C.; Kim, Y. S., An operationally flexible fuel cell based on quaternary ammonium-biphosphate ion pairs. *Nature Energy* **2016,** *1* (9), 16120.

[135] Einsla, B. R.; Chempath, S.; Pratt, L.; Boncella, J.; Rau, J.; Macomber, C.; Pivovar, B., Stability of Cations for Anion Exchange Membrane Fuel Cells. **2007,** *11*, 1173-1180.

[136] Vandiver, M. A.; Horan, J. L.; Yang, Y.; Tansey, E. T.; Seifert, S.; Liberatore, M. W.; Herring, A. M., Synthesis and characterization of perfluoro quaternary ammonium anion exchange membranes. *Journal of Polymer Science Part B: Polymer Physics* **2013,** *51* (24), 1761-1769.

[137] Xu, H.; Fang, J.; Guo, M.; Lu, X.; Wei, X.; Tu, S., Novel anion exchange membrane based on copolymer of methyl methacrylate, vinylbenzyl chloride and ethyl acrylate for alkaline fuel cells. *Journal of Membrane Science* **2010,** *354* (1-2), 206-211.

[138] Qiu, B.; Lin, B.; Qiu, L.; Yan, F., Alkaline imidazolium- and quaternary ammonium-functionalized anion exchange membranes for alkaline fuel cell applications. *J. Mater. Chem.* **2012,** *22* (3), 1040-1045.

[139] Varcoe, J.; Slade, R., An electron-beam-grafted ETFE alkaline anion-exchange membrane in metal-cation-free solid-state alkaline fuel cells. *Electrochemistry Communications* **2006,** *8* (5), 839-843.

[140] Merle, G.; Wessling, M.; Nijmeijer, K., Anion exchange membranes for alkaline fuel cells: A review. *Journal of Membrane Science* **2011,** *377* (1-2), 1-35.

[141] Cheng, J.; He, G.; Zhang, F., A mini-review on anion exchange membranes for fuel cell applications: Stability issue and addressing strategies. *International Journal of Hydrogen Energy* **2015,** *40* (23), 7348-7360.

[142] Dang, H.-S.; Jannasch, P., Alkali-stable and highly anion conducting poly(phenylene oxide)s carrying quaternary piperidinium cations. *Journal of Materials Chemistry A* **2016,** *4* (30), 11924-11938.

[143] Strasser, D. J.; Graziano, B. J.; Knauss, D. M., Base stable poly(diallylpiperidinium hydroxide) multiblock copolymers for anion exchange membranes. *Journal of Materials Chemistry A* **2017,** *5* (20), 9627-9640.

[144] Salerno, H. L. S.; Elabd, Y. A., Anion exchange membranes derived from nafion precursor for the alkaline fuel cell: Effect of cation type on properties. *Journal of Applied Polymer Science* **2013,** *127* (1), 298-307.

[145] Guo, M.; Fang, J.; Xu, H.; Li, W.; Lu, X.; Lan, C.; Li, K., Synthesis and characterization of novel anion exchange membranes based on imidazolium-type ionic liquid for alkaline fuel cells. *Journal of Membrane Science* **2010,** *362* (1-2), 97-104.

[146] Chen, D.; Hickner, M. A., Degradation of imidazolium- and quaternary ammonium-functionalized poly(fluorenyl ether ketone sulfone) anion exchange membranes. *ACS Appl Mater Interfaces* **2012,** *4* (11), 5775-81.

[147] Lin, B.; Dong, H.; Li, Y.; Si, Z.; Gu, F.; Yan, F., Alkaline Stable C2-Substituted Imidazolium-Based Anion-Exchange Membranes. *Chemistry of Materials* **2013,** *25* (9), 1858-1867.

[148] Katzfuß, A.; Poynton, S.; Varcoe, J.; Gogel, V.; Storr, U.; Kerres, J., Methylated polybenzimidazole and its application as a blend component in covalently cross-linked anion-exchange membranes for DMFC. *Journal of Membrane Science* **2014,** *465*, 129-137.

[149] Jheng, L.-c.; Hsu, S. L.-c.; Lin, B.-y.; Hsu, Y.-l., Quaternized polybenzimidazoles with imidazolium cation moieties for anion exchange membrane fuel cells. *Journal of Membrane Science* **2014,** *460*, 160-170.

[150] Thomas, O. D.; Soo, K. J. W. Y.; Peckham, T. J.; Kulkarni, M. P.; Holdcroft, S., Anion conducting poly(dialkyl benzimidazolium) salts. *Polymer Chemistry* **2011,** *2* (8), 1641.

[151] Varcoe, J. R.; Atanassov, P.; Dekel, D. R.; Herring, A. M.; Hickner, M. A.; Kohl, P. A.; Kucernak, A. R.; Mustain, W. E.; Nijmeijer, K.; Scott, K.; Xu, T.; Zhuang, L., Anion-exchange membranes in electrochemical energy systems. *Energy Environ. Sci.* **2014,** *7* (10), 3135-3191.

[152] Schug, K. A.; Lindner, W., Noncovalent binding between guanidinium and anionic groups: focus on biological- and synthetic-based arginine/guanidinium interactions with phosph[on]ate and sulf[on]ate residues. *Chem Rev* **2005,** *105* (1), 67-114.

[153] Bowie, D.; Parvizi, P.; Duncan, D.; Nelson, C. J.; Fyles, T. M., Chemical-genetic identification of the biochemical targets of polyalkyl guanidinium biocides. *Org Biomol Chem* **2013,** *11* (26), 4359-66.

[154] Fyles, T. M.; Lee, J.; Rowe, R. D.; Robertson, G. D., Supramolecular membrane transport: From biomimics to membrane sensors. *Journal of Membrane Science* **2008,** *321* (1), 31-36.

[155] Hossain, M. A.; Jang, H.; Sutradhar, S. C.; Ha, J.; Yoo, J.; Lee, C.; Lee, S.; Kim, W., Novel hydroxide conducting sulfonium-based anion exchange membrane for alkaline fuel cell applications. *International Journal of Hydrogen Energy* **2016,** *41* (24), 10458-10465.

[156] Zhang, B. Z.; Gu, S.; Wang, J. H.; Liu, Y.; Herring, A. M.; Yan, Y. S., Tertiary sulfonium as a cationic functional group for hydroxide exchange membranes. *Rsc Advances* **2012,** *2* (33), 12683-12685.

[157] Gu, S.; Cai, R.; Luo, T.; Chen, Z.; Sun, M.; Liu, Y.; He, G.; Yan, Y., A Soluble and Highly Conductive Ionomer for High-Performance Hydroxide Exchange Membrane Fuel Cells. *Angew Chem Int Ed Engl* **2009,** *121* (35), 6621-6624.

[158] Gu, S.; Cai, R.; Luo, T.; Jensen, K.; Contreras, C.; Yan, Y., Quaternary Phosphonium-Based Polymers as Hydroxide Exchange Membranes. *ChemSusChem* **2010,** *3* (5), 555-558.

[159] Gu, S.; Cai, R.; Yan, Y., Self-crosslinking for dimensionally stable and solvent-resistant quaternary phosphonium based hydroxide exchange membranes. *Chem Commun (Camb)* **2011,** *47* (10), 2856-8.

[160] Zeng, Q. H.; Liu, Q. L.; Broadwell, I.; Zhu, A. M.; Xiong, Y.; Tu, X. P., Anion exchange membranes based on quaternized polystyrene-block-poly(ethylene-ran-butylene)-block-polystyrene for direct methanol alkaline fuel cells. *Journal of Membrane Science* **2010,** *349* (1-2), 237-243.

[161] Tsai, T.-H.; Maes, A. M.; Vandiver, M. A.; Versek, C.; Seifert, S.; Tuominen, M.; Liberatore, M. W.; Herring, A. M.; Coughlin, E. B., Synthesis and structure-conductivity relationship of polystyrene-block-poly(vinyl benzyl trimethylammonium) for alkaline anion exchange membrane fuel cells. *Journal of Polymer Science Part B: Polymer Physics* **2013,** *51* (24), 1751-1760.

[162] Vinodh, R.; Ilakkiya, A.; Elamathi, S.; Sangeetha, D., A novel anion exchange membrane from polystyrene (ethylene butylene) polystyrene: Synthesis and characterization. *Materials Science and Engineering: B* **2010,** *167* (1), 43-50.

[163] Noonan, K. J.; Hugar, K. M.; Kostalik, H. A. t.; Lobkovsky, E. B.; Abruna, H. D.; Coates, G. W., Phosphonium-functionalized polyethylene: a new class of base-stable alkaline anion exchange membranes. *J Am Chem Soc* **2012,** *134* (44), 18161-4.

[164] Kostalik, H. A.; Clark, T. J.; Robertson, N. J.; Mutolo, P. F.; Longo, J. M.; Abruña, H. c. D.; Coates, G. W., Solvent Processable Tetraalkylammonium-Functionalized Polyethylene for Use as an Alkaline Anion Exchange Membrane. *Macromolecules* **2010,** *43* (17), 7147-7150.

[165] Zhang, M.; Kim, H. K.; Chalkova, E.; Mark, F.; Lvov, S. N.; Chung, T. C. M., New Polyethylene Based Anion Exchange Membranes (PE–AEMs) with High Ionic Conductivity. *Macromolecules* **2011,** *44* (15), 5937-5946.

[166] Zhang, F.; Zhang, H.; Qu, C., Imidazolium functionalized polysulfone anion exchange membrane for fuel cell application. *Journal of Materials Chemistry* **2011,** *21* (34), 12744.

[167] Wang, G.; Weng, Y.; Chu, D.; Chen, R.; Xie, D., Developing a polysulfone-based alkaline anion exchange membrane for improved ionic conductivity. *Journal of Membrane Science* **2009,** *332* (1-2), 63-68.

[168] Li, N.; Zhang, Q.; Wang, C.; Lee, Y. M.; Guiver, M. D., Phenyltrimethylammonium Functionalized Polysulfone Anion Exchange Membranes. *Macromolecules* **2012,** *45* (5), 2411-2419.

[169] Janarthanan, R.; Horan, J. L.; Caire, B. R.; Ziegler, Z. C.; Yang, Y.; Zuo, X.; Liberatore, M. W.; Hibbs, M. R.; Herring, A. M., Understanding anion transport in an aminated trimethyl polyphenylene with high anionic conductivity. *Journal of Polymer Science Part B: Polymer Physics* **2013,** *51* (24), 1743-1750.

[170] Small, L. J.; Pratt, H. D.; Fujimoto, C. H.; Anderson, T. M., Diels Alder Polyphenylene Anion Exchange Membrane for Nonaqueous Redox Flow Batteries. *Journal of the Electrochemical Society* **2015,** *163* (1), A5106-A5111.

[171] Xia, Z.; Yuan, S.; Jiang, G.; Guo, X.; Fang, J.; Liu, L.; Qiao, J.; Yin, J., Polybenzimidazoles with pendant quaternary ammonium groups as potential anion exchange membranes for fuel cells. *Journal of Membrane Science* **2012,** *390-391*, 152-159.

[172] Lu, W.; Zhang, G.; Li, J.; Hao, J.; Wei, F.; Li, W.; Zhang, J.; Shao, Z.-G.; Yi, B., Polybenzimidazole-crosslinked poly(vinylbenzyl chloride) with quaternary 1,4-diazabicyclo (2.2.2) octane groups as high-performance anion exchange membrane for fuel cells. *Journal of Power Sources* **2015,** *296*, 204-214.

[173] Jung, M.-s. J.; Arges, C. G.; Ramani, V., A perfluorinated anion exchange membrane with a 1,4-dimethylpiperazinium cation. *Journal of Materials Chemistry* **2011,** *21* (17), 6158.

[174] Couture, G.; Alaaeddine, A.; Boschet, F.; Ameduri, B., Polymeric materials as anion-exchange membranes for alkaline fuel cells. *Progress in Polymer Science* **2011,** *36* (11), 1521-1557.

[175] Cao, Y.-C.; Wang, X.; Mamlouk, M.; Scott, K., Preparation of alkaline anion exchange polymer membrane from methylated melamine grafted poly(vinylbenzyl chloride) and its fuel cell performance. *Journal of Materials Chemistry* **2011,** *21* (34), 12910.

[176] Herman, H.; Slade, R. C. T.; Varcoe, J. R., The radiation-grafting of vinylbenzyl chloride onto poly(hexafluoropropylene-co-tetrafluoroethylene) films with subsequent conversion to alkaline anion-exchange membranes: optimisation of the experimental conditions and characterisation. *Journal of Membrane Science* **2003,** *218* (1-2), 147-163.

[177] Lu, W.; Shao, Z.-G.; Zhang, G.; Zhao, Y.; Yi, B., Crosslinked poly(vinylbenzyl chloride) with a macromolecular crosslinker for anion exchange membrane fuel cells. *Journal of Power Sources* **2014,** *248*, 905-914.

[178] Carter, R.; Wycisk, R.; Yoo, H.; Pintauro, P. N., Blended Polyphosphazene/Polyacrylonitrile Membranes for Direct Methanol Fuel Cells. *Electrochemical and Solid-State Letters* **2002,** *5* (9), A195.

[179] Xiong, Y.; Fang, J.; Zeng, Q. H.; Liu, Q. L., Preparation and characterization of cross-linked quaternized poly(vinyl alcohol) membranes for anion exchange membrane fuel cells. *Journal of Membrane Science* **2008,** *311* (1-2), 319-325.

[180] Nagarale, R. K.; Shahi, V. K.; Rangarajan, R., Preparation of polyvinyl alcohol–silica hybrid heterogeneous anion-exchange membranes by sol–gel method and their characterization. *Journal of Membrane Science* **2005,** *248* (1-2), 37-44.

[181] Xiong, Y.; Liu, Q. L.; Zhang, Q. G.; Zhu, A. M., Synthesis and characterization of cross-linked quaternized poly(vinyl alcohol)/chitosan composite anion exchange membranes for fuel cells. *Journal of Power Sources* **2008,** *183* (2), 447-453.

[182] Gil, M.; Ji, X.; Li, X.; Na, H.; Eric Hampsey, J.; Lu, Y., Direct synthesis of sulfonated aromatic poly(ether ether ketone) proton exchange membranes for fuel cell applications. *Journal of Membrane Science* **2004,** *234* (1-2), 75-81.

[183] Balster, J.; Krupenko, O.; Punt, I.; Stamatialis, D.; Wessling, M., Preparation and characterisation of monovalent ion selective cation exchange membranes based on sulphonated poly(ether ether ketone). *Journal of Membrane Science* **2005,** *263* (1-2), 137-145.

[184] Zhang, S.; Yin, C.; Xing, D.; Yang, D.; Jian, X., Preparation of chloromethylated/quaternized poly(phthalazinone ether ketone) anion exchange membrane materials for vanadium redox flow battery applications. *Journal of Membrane Science* **2010,** *363* (1-2), 243-249.

[185] Fang, J.; Shen, P. K., Quaternized poly(phthalazinon ether sulfone ketone) membrane for anion exchange membrane fuel cells. *Journal of Membrane Science* **2006,** *285* (1-2), 317-322.

[186] Gopi, K. H.; Bhat, S. D.; Sahu, A. K.; Sridhar, P., Quaternized poly(phenylene oxide) anion exchange membrane for alkaline direct methanol fuel cells in KOH-free media. *Journal of Applied Polymer Science* **2016,** *133* (29).

[187] Wang, G.; Weng, Y.; Zhao, J.; Chu, D.; Xie, D.; Chen, R., Developing a novel alkaline anion exchange membrane derived from poly(ether-imide) for improved ionic conductivity. *Polymers for Advanced Technologies* **2009**, n/a-n/a.

[188] Wang, G.; Weng, Y.; Zhao, J.; Chen, R.; Xie, D., Preparation of a functional poly(ether imide) membrane for potential alkaline fuel cell applications: Chloromethylation. *Journal of Applied Polymer Science* **2009,** *112* (2), 721-727.

[189] Wang, G.; Weng, Y.; Chu, D.; Xie, D.; Chen, R., Preparation of alkaline anion exchange membranes based on functional poly(ether-imide) polymers for potential fuel cell applications. *Journal of Membrane Science* **2009,** *326* (1), 4-8.

[190] Arges, C. G.; Ramani, V., Two-dimensional NMR spectroscopy reveals cation-triggered backbone degradation in polysulfone-based anion exchange membranes. *Proceedings of the National Academy of Sciences of the United States of America* **2013,** *110* (7), 2490-2495.

[191] Clarke, R. L.; Dougherty, B.; Harrison, S.; Millington, P. J.; Mohanta, S. CERIUM BATTERIES. US 7625663 B2, 2009.

[192] Xie, Z.; Liu, Q.; Chang, Z.; Zhang, X., The developments and challenges of cerium half-cell in zinc–cerium redox flow battery for energy storage. *Electrochimica Acta* **2013,** *90*, 695-704.

[193] Chen, R.; Hempelmann, R., Ionic liquid-mediated aqueous redox flow batteries for high voltage applications. *Electrochemistry Communications* **2016,** *70*, 56-59.

[194] Leung, P. K.; Ponce de León, C.; Walsh, F. C., An undivided zinc–cerium redox flow battery operating at room temperature (295 K). *Electrochemistry Communications* **2011,** *13* (8), 770-773.

[195] Leung, P. K.; Ponce-de-León, C.; Low, C. T. J.; Shah, A. A.; Walsh, F. C., Characterization of a zinc–cerium flow battery. *Journal of Power Sources* **2011,** *196* (11), 5174-5185.

[196] Nikiforidis, G.; Berlouis, L.; Hall, D.; Hodgson, D., Impact of electrolyte composition on the performance of the zinc–cerium redox flow battery system. *Journal of Power Sources* **2013,** *243*, 691-698.

[197] Chakrabarti, M. H.; Dryfe, R. A. W.; Roberts, E. P. L., Evaluation of electrolytes for redox flow battery applications. *Electrochimica Acta* **2007,** *52* (5), 2189-2195.

[198] Kim, K. J.; Park, M.-S.; Kim, Y.-J.; Kim, J. H.; Dou, S. X.; Skyllas-Kazacos, M., A technology review of electrodes and reaction mechanisms in vanadium redox flow batteries. *Journal of Materials Chemistry A* **2015,** *3* (33), 16913-16933.

[199] Jeon, J.-D.; Yang, H. S.; Shim, J.; Kim, H. S.; Yang, J. H., Dual function of quaternary ammonium in Zn/Br redox flow battery: Capturing the bromine and lowering the charge transfer resistance. *Electrochimica Acta* **2014,** *127*, 397-402.

[200] Lai, Q.; Zhang, H.; Li, X.; Zhang, L.; Cheng, Y., A novel single flow zinc–bromine battery with improved energy density. *Journal of Power Sources* **2013,** *235*, 1-4.

[201] Yang, H. S.; Park, J. H.; Ra, H. W.; Jin, C.-S.; Yang, J. H., Critical rate of electrolyte circulation for preventing zinc dendrite formation in a zinc–bromine redox flow battery. *Journal of Power Sources* **2016,** *325*, 446-452.

[202] Lopez-Atalaya, M.; Codina, G.; Perez, J. R.; Vazquez, J. L.; Aldaz, A., Optimization studies on a Fe/Cr redox flow battery. *Journal of Power Sources* **1992,** *39*, 147-154.

[203] Codina, G.; Perez, J. R.; Lopez-Atalaya, M.; Vazquez, J. L.; Aldaz, A., Development of a 0.1 kW power accumulation pilot plant based on an Fe/Cr redox flow battery Part 1. Considerations on flow-distribution design. *Jownal of Power Sources* **1994,** *48*, 293-302.

[204] CODINA, G.; ALDAZ, A., Scale-up studies of an Fe/Cr redox flow battery based on shunt current analysis. *Journal of Applied Electrochemistry* **1992,** *22*, 668-674.

[205] Zeng, Y. K.; Zhao, T. S.; An, L.; Zhou, X. L.; Wei, L., A comparative study of all-vanadium and iron-chromium redox flow batteries for large-scale energy storage. *Journal of Power Sources* **2015,** *300*, 438-443.

[206] Kear, G.; Shah, A. A.; Walsh, F. C., Development of the all-vanadium redox flow battery for energy storage: a review of technological, financial and policy aspects. *International Journal of Energy Research* **2012,** *36* (11), 1105-1120.

[207] Oh, S. H.; Lee, C. W.; Chun, D. H.; Jeon, J. D.; Shim, J.; Shin, K. H.; Yang, J. H., A metal-free and all-organic redox flow battery with polythiophene as the electroactive species. *J. Mater. Chem. A* **2014,** *2* (47), 19994-19998.

[208] Li, Z.; Li, S.; Liu, S.; Huang, K.; Fang, D.; Wang, F.; Peng, S., Electrochemical Properties of an All-Organic Redox Flow Battery Using 2,2,6,6-Tetramethyl-1-Piperidinyloxy and N-Methylphthalimide. *Electrochemical and Solid-State Letters* **2011,** *14* (12), A171.

[209] Song, H. K.; Palmore, G. T. R., Redox-Active Polypyrrole: Toward Polymer-Based Batteries. *Advanced Materials* **2006,** *18* (13), 1764-1768.

[210] Janoschka, T.; Martin, N.; Martin, U.; Friebe, C.; Morgenstern, S.; Hiller, H.; Hager, M. D.; Schubert, U. S., An aqueous, polymer-based redox-flow battery using non-corrosive, safe, and low-cost materials. *Nature* **2015,** *527* (7576), 78-81.

[211] Janoschka, T.; Morgenstern, S.; Hiller, H.; Friebe, C.; Wolkersdörfer, K.; Häupler, B.; Hager, M. D.; Schubert, U. S., Synthesis and characterization of TEMPO- and viologen-polymers for water-based redox-flow batteries. *Polymer Chemistry* **2015,** *6* (45), 7801-7811.

[212] BOVEY, F. A., Polymer NMR Spectroscopy. VI. Methyl Methacrylate-Styrene and Methyl Methacrylate-a-Methylstyrene Copolymers. *JOIJRNAL OF POLYMER SCIENCE* **1962,** *62*, 197-209.

[213] PANDEY, K. K., A Study of Chemical Structure of Soft and Hardwood and Wood Polymers by FTIR Spectroscopy. *Journal of Applied Polymer Science* **1999,** *71*, 1969–1975.

[214] Bruch, M., *NMR Spectroscopy Techniques, Second Edition*. 1996.

[215] Koenig, J. L., *Spectroscopy of Polymers*. 1999.

[216] Robertson, G. P.; Guiver, M. D.; Yoshikawa, M.; Brownstein, S., Structural determination of Torlon® 4000T polyamide–imide by NMR spectroscopy. *Polymer* **2004,** *45* (4), 1111-1117.

[217] Heikkinen, S.; Toikka, M. M.; Karhunen, P. T.; Kilpelainen, I. A., Quantitative 2D HSQC (Q-HSQC) via suppression of J-dependence of polarization transfer in NMR spectroscopy: application to wood lignin. *J Am Chem Soc* **2003,** *125* (14), 4362-7.

[218] Yuan, T. Q.; Sun, S. N.; Xu, F.; Sun, R. C., Characterization of lignin structures and lignin-carbohydrate complex (LCC) linkages by quantitative 13C and 2D HSQC NMR spectroscopy. *J Agric Food Chem* **2011,** *59* (19), 10604-14.

[219] Zhang, L.; Gellerstedt, G., Quantitative 2D HSQC NMR determination of polymer structures by selecting suitable internal standard references. *Magn Reson Chem* **2007,** *45* (1), 37-45.

[220] Schram, J.; Bellama, J. M., *Two dimensional NMR spectroscopy*. 1988.

[221] Dincer, I., Renewable energy and sustainable development: a crucial review. **2000,** *4*, 157-175.

[222] Turner, J. A., A Realizable Renewable Energy Future. *Science* **1999,** *285* (5428), 687-689.

[223] Johansson, T. B.; Kelly, H.; Reddy, A. K. N.; Burnham, L., *Renewable Energy: Sources for Fuels and Electricity*. 1993.

[224] Lund, H., Renewable energy strategies for sustainable development. *Energy* **2007,** *32* (6), 912-919.

[225] Wüstenhagen, R.; Wolsink, M.; Bürer, M. J., Social acceptance of renewable energy innovation: An introduction to the concept. *Energy Policy* **2007,** *35* (5), 2683-2691.

[226] Teleke, S.; Baran, M. E.; Bhattacharya, S.; Huang, A. Q., Rule-Based Control of Battery Energy Storage for Dispatching Intermittent Renewable Sources. *IEEE TRANSACTIONS ON SUSTAINABLE ENERGY* **2010,** *1*, 117-124.

[227] Park, M.; Ryu, J.; Wang, W.; Cho, J., Material design and engineering of next-generation flow-battery technologies. *Nature Reviews Materials* **2016,** *2* (1), 16080.

[228] Weber, A. Z.; Mench, M. M.; Meyers, J. P.; Ross, P. N.; Gostick, J. T.; Liu, Q., Redox flow batteries: a review. *Journal of Applied Electrochemistry* **2011,** *41* (10), 1137-1164.

[229] Cotton, F. A.; Kibala, P. A., Reactions of Iodine with Triphenylphosphine and Triphenylarsine. *J. Am. Chem. Soc.* **1897,** *109*, 3308-3312.

[230] Sasaki, S., Reaction of a sterically crowded triarylphosphine with iodine in the presence of oxygen. *Phosphorus, Sulfur, and Silicon and the Related Elements* **2016,** *191* (11-12), 1513-1514.

[231] Gu, S.; Sheng, W. C.; Cai, R.; Alia, S. M.; Song, S. Q.; Jensen, K. O.; Yan, Y. S., An efficient Ag-ionomer interface for hydroxide exchange membrane fuel cells. *Chemical Communications* **2013,** *49* (2), 131-133.

[232] Parrondo, J.; Wang, Z.; Jung, M. S.; Ramani, V., Reactive oxygen species accelerate degradation of anion exchange membranes based on polyphenylene oxide in alkaline environments. *Physical Chemistry Chemical Physics* **2016,** *18* (29), 19705-12.

[233] Jie, Z.; Haolin, T.; Mu, P., Fabrication and characterization of self-assembled Nafion–SiO2–ePTFE composite membrane of PEM fuel cell. *Journal of Membrane Science* **2008,** *312* (1-2), 41-47.

[234] Ramya, K.; Velayutham, G.; Subramaniam, C. K.; Rajalakshmi, N.; Dhathathreyan, K. S., Effect of solvents on the characteristics of Nafion®/PTFE composite membranes for fuel cell applications. *Journal of Power Sources* **2006,** *160* (1), 10-17.

[235] Carrasco, J. M.; Franquelo, L. G.; Bialasiewicz, J. T.; Galvan, E.; PortilloGuisado, R. C.; Prats, M. A. M.; Leon, J. I.; Moreno-Alfonso, N., Power-Electronic Systems for the Grid Integration of Renewable Energy Sources: A Survey. *Ieee Transactions on Industrial Electronics* **2006,** *53* (4), 1002-1016.

[236] Hammons, T. J., Integrating renewable energy sources into European grids. *International Journal of Electrical Power & Energy Systems* **2008,** *30* (8), 462-475.

[237] Aghaei, J.; Alizadeh, M.-I., Demand response in smart electricity grids equipped with renewable energy sources: A review. *Renewable and Sustainable Energy Reviews* **2013,** *18*, 64-72.

[238] Schwenzer, B.; Zhang, J.; Kim, S.; Li, L.; Liu, J.; Yang, Z., Membrane Development for Vanadium Redox Flow Batteries. *ChemSusChem* **2011,** *4* (10), 1388-1406.

[239] Arges, C. G.; Ramani, V., Investigation of Cation Degradation in Anion Exchange Membranes Using Multi-Dimensional NMR Spectroscopy. *Journal of the Electrochemical Society* **2013,** *160* (9), F1006-F1021.

[240] Bouchet, R.; Siebert, E., Proton conduction in acid doped polybenzimidazole. *Solid State Ionics* **1999,** *118*, 287-299.

[241] Wainright, J. S.; Wang, J.-T.; Weng, D.; Savinell, R. F.; Litt, M., Acid-Doped Polybenzimidazoles: A New Polymer Electrolyte. *J. Electrochem. Soc.* **1995,** *142*.

[242] Aili, D.; Hansen, M. K.; Pan, C.; Li, Q.; Christensen, E.; Jensen, J. O.; Bjerrum, N. J., Phosphoric acid doped membranes based on Nafion®, PBI and their blends – Membrane preparation, characterization and steam electrolysis testing. *International Journal of Hydrogen Energy* **2011,** *36* (12), 6985-6993.

[243] Dubarry, M.; Devie, A.; Stein, K.; Tun, M.; Matsuura, M.; Rocheleau, R., Battery Energy Storage System battery durability and reliability under electric utility grid operations: Analysis of 3 years of real usage. *Journal of Power Sources* **2017,** *338*, 65-73.

[244] Gong, K.; Ma, X.; Conforti, K. M.; Kuttler, K. J.; Grunewald, J. B.; Yeager, K. L.; Bazant, M. Z.; Gu, S.; Yan, Y., A zinc–iron redox-flow battery under $100 per kW h of system capital cost. *Energy & Environmental Science* **2015,** *8* (10), 2941-2945.

[245] Gong, K.; Xu, F.; Grunewald, J. B.; Ma, X.; Zhao, Y.; Gu, S.; Yan, Y., All-Soluble All-Iron Aqueous Redox-Flow Battery. *ACS Energy Letters* **2016,** *1* (1), 89-93.

[246] Yun, S.; Parrondo, J.; Ramani, V., Derivatized cardo-polyetherketone anion exchange membranes for all-vanadium redox flow batteries. *J. Mater. Chem. A* **2014,** *2* (18), 6605-6615.

[247] Jung, M.-s. J.; Parrondo, J.; Arges, C. G.; Ramani, V., Polysulfone-based anion exchange membranes demonstrate excellent chemical stability and performance for the all-vanadium redox flow battery. *Journal of Materials Chemistry A* **2013,** *1* (35), 10458.

[248] Li, Y.; Lin, X.; Wu, L.; Jiang, C.; Hossain, M. M.; Xu, T., Quaternized membranes bearing zwitterionic groups for vanadium redox flow battery through a green route. *Journal of Membrane Science* **2015,** *483*, 60-69.

[249] Germer, W.; Leppin, J.; Nunes Kirchner, C.; Cho, H.; Kim, H.-J.; Henkensmeier, D.; Lee, K.-Y.; Brela, M.; Michalak, A.; Dyck, A., Phase Separated Methylated Polybenzimidazole (O-PBI) Based Anion Exchange Membranes. *Macromolecular Materials and Engineering* **2015,** *300* (5), 497-509.

[250] Henkensmeier, D.; Cho, H.; Brela, M.; Michalak, A.; Dyck, A.; Germer, W.; Duong, N. M. H.; Jang, J. H.; Kim, H.-J.; Woo, N.-S.; Lim, T.-H., Anion conducting polymers based on ether linked polybenzimidazole (PBI-OO). *International Journal of Hydrogen Energy* **2014,** *39* (6), 2842-2853.

[251] Cho, H.; Hur, E.; Henkensmeier, D.; Jeong, G.; Cho, E.; Kim, H. J.; Jang, J. H.; Lee, K. Y.; Hjuler, H. A.; Li, Q.; Jensen, J. O.; Cleemann, L. N., meta-PBI/methylated PBI-OO blend membranes for acid doped HT PEMFC. *European Polymer Journal* **2014,** *58*, 135-143.

[252] Thomas, O. D.; Soo, K. J.; Peckham, T. J.; Kulkarni, M. P.; Holdcroft, S., A stable hydroxide-conducting polymer. *J Am Chem Soc* **2012,** *134* (26), 10753-6.

[253] Wright, A. G.; Weissbach, T.; Holdcroft, S., Poly(phenylene) and m-Terphenyl as Powerful Protecting Groups for the Preparation of Stable Organic Hydroxides. *Angew Chem Int Ed Engl* **2016,** *55* (15), 4818-21.

[254] Chang, Z.; Henkensmeier, D.; Chen, R., One-Step Cationic Grafting of 4-Hydroxy-TEMPO and its Application in a Hybrid Redox Flow Battery with a Crosslinked PBI Membrane. *ChemSusChem* **2017,** *10* (16), 3193-3197.

[255] HANSCH, C.; LEO, A.; TAFT, R. W., A Survey of Hammett Substituent Constants and Resonance and Field Parameters. *Chem. Rev.* **1991,** *91*, 165-195.

[256] Conley, R. T.; Kane, J. J.; Ghosh, S. *Mechanism of Thermal Oxidation of the Benzimidazole System*; Department of Chemistry, Wright State University: http://www.dtic.mil/dtic/tr/fulltext/u2/891598.pdf, 1971.

[257] Luo, Q.; Zhang, H.; Chen, J.; You, D.; Sun, C.; Zhang, Y., Preparation and characterization of Nafion/SPEEK layered composite membrane and its application in vanadium redox flow battery. *Journal of Membrane Science* **2008,** *325* (2), 553-558.

[258] Teng, X.; Zhao, Y.; Xi, J.; Wu, Z.; Qiu, X.; Chen, L., Nafion/organic silica modified TiO2 composite membrane for vanadium redox flow battery via in situ sol–gel reactions. *Journal of Membrane Science* **2009,** *341* (1-2), 149-154.

[259] Jia, C.; Liu, J.; Yan, C., A significantly improved membrane for vanadium redox flow battery. *Journal of Power Sources* **2010,** *195* (13), 4380-4383.

Appendix A

ABBREVIATIONS AND NOTATIONS

A.1 Abbreviations and notations

RFB	Redox flow battery
VRFB	Vanadium redox flow battery
HEMFC	Hydroxide exchange membrane fuel cell
IEM	Ion exchange membrane
AEM	Anion exchange membrane
CEM	Cation exchange membrane
^{1}H NMR	Proton nuclear magnetic resonance
^{31}P NMR	Phosphorus nuclear magnetic resonance
HSQC	Heteronuclear single quantum coherence
ATR-FTIR	Attenuated total reflectance Fourier transform infrared
SEM	Scanning electron microscope
MS	Mass spectrometry
TGA	Thermogravimetric analysis
TTMPP	Tris(2,4,6-trimethoxyphenyl)phosphine
TTMePP	Tris(2,4,6-trimethylphenyl)phosphine
F_6PBI	Hexafluoroisopropylidene polybenzimidazole
PBI	Polybenzimidazole

PS	Polystyrene
PSF	Polysulfone
PPO	Poly(2,6-dimethyl-phenylene oxide)
PTFE	Polytetrafluoroethylene
ePTFE	Expanded polytetrafluoroethylene
IEC	Ion exchange capacity
ADL	Acid doping level
ASR	Area specific resistance
SA	Sulfuric acid
CDCl3	Deuterated chloroform
DMSO-d6	Deuterated dimethylsulfoxide
TMS	Tetramethylsilane
DS	Degree of substitution
WL	Weight loss
WU	Water uptake
SR	Swelling ratio
CV	Cyclic voltammetry
WE	Working electrode
CE	Counter electrode
RE	Reference electrode

Appendix B

BROMINATION OF METHYL-TRIS(2,4,6-TRIMETHYLPHENYL)PHOSPHONIUM

B.1 Bromination of Methyl-tris(2,4,6-trimethylphenyl)phosphonium

Due to the high steric hindrance of tris(2,4,6-trimethylphenyl)phosphine (TTMePP), the direct quaternization of the center phosphorous was problematic at the beginning. Before the discovery of quaternization with alkyl iodide and Cu added as an inhibitor (details in section 3.3.2), another bromination strategy was investigated. The overall synthetic strategy is shown in Figure B1.

Since multiple brominations would cause crosslinking in the future functionalization step and cause the polymer to be insoluble and impossible to cast membranes, the key to achieving the linkage at outside methyl group was to obtain single bromination of the TTMePP cation.

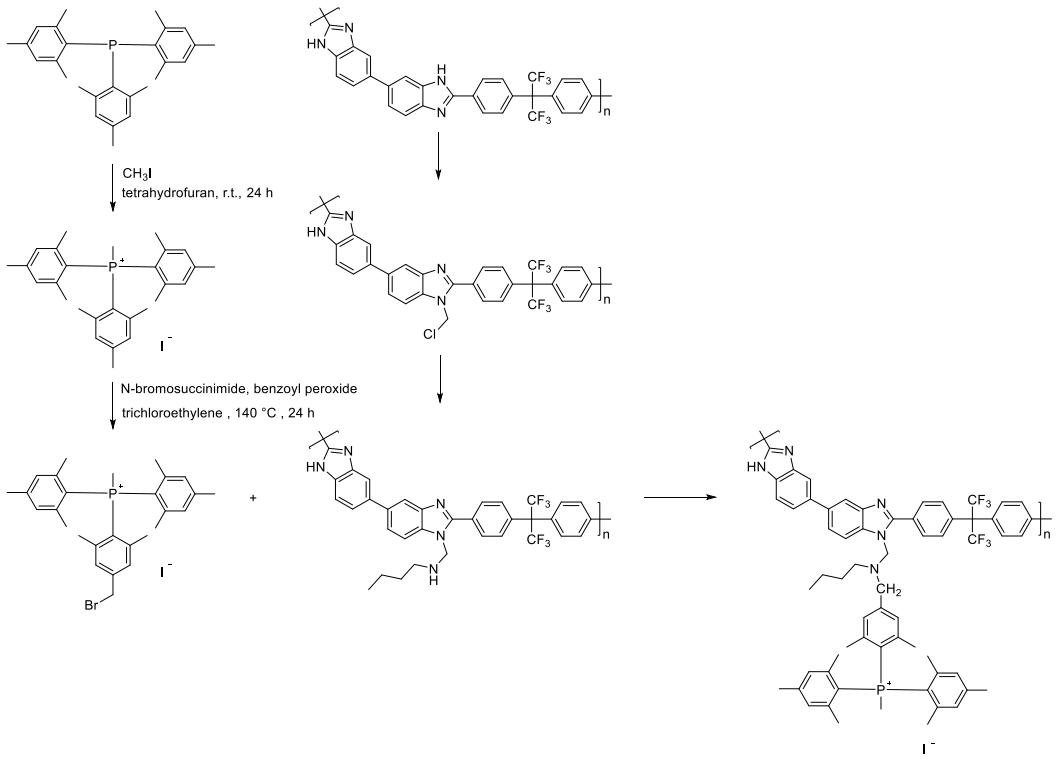

Figure B1: Proposed synthetic strategy of connecting TTMePP to a polymer backbone through bromination. F_6PBI polymer backbone was chosen as an example here. TTMePP cation must be single brominated to prevent crosslinking.

A series of reactions were taken to investigate the bromination (illustrated in Table B1). However, even though I achieved single bromination in a small-scale (mg scale) model reaction (condition of Entry 9), further amplifications always showed multiple bromination products.

Table B1: Partial list of investigated bromination conditions.

Entry	$TTMePP^+$ (mmol)	NBS[a] (mmol)	BPO[b] (mmol)	TCE[c] (ml)	T (°C)	Time (hour)	DB[d] (%)
1	1	1	0.05	10	80	24	0
2	1	1	0.05	10	140	24	5
3	1	1	0.05	10	140	48	5
4	1	1	0.1	20	100	20	0
5	1	1.5	0.15	20	100	20	0
6	1	1.5	0.15	20	80	20	0
7	1	2	0.2	12	140	24	25
8	1	3	0.3	10	140	24	30
9	1	3	0.3	3	140	24	33
10	1	5	0.5	12	140	24	40
11	1	5	0.5	10	140	24	50
12	1	5	0.5	3	140	24	100

a. N-Bromosuccinimide (NBS) was used as bromination reagent;
b. Benzoyl peroxide (BPO) was used as radical initiator;
c. Tetrachloroethane (TCE) was used as the solvent;
d. Degree of total bromination.

Figure B3 and Figure B4 show the ^{31}P NMR spectroscopy and mass spectrometry of products from amplified bromination reactions. Unfortunately, multiple bromination products were observed.

This bromination strategy was abandoned later after the discovery of successful center quaternization with Cu added as the inhibitor.

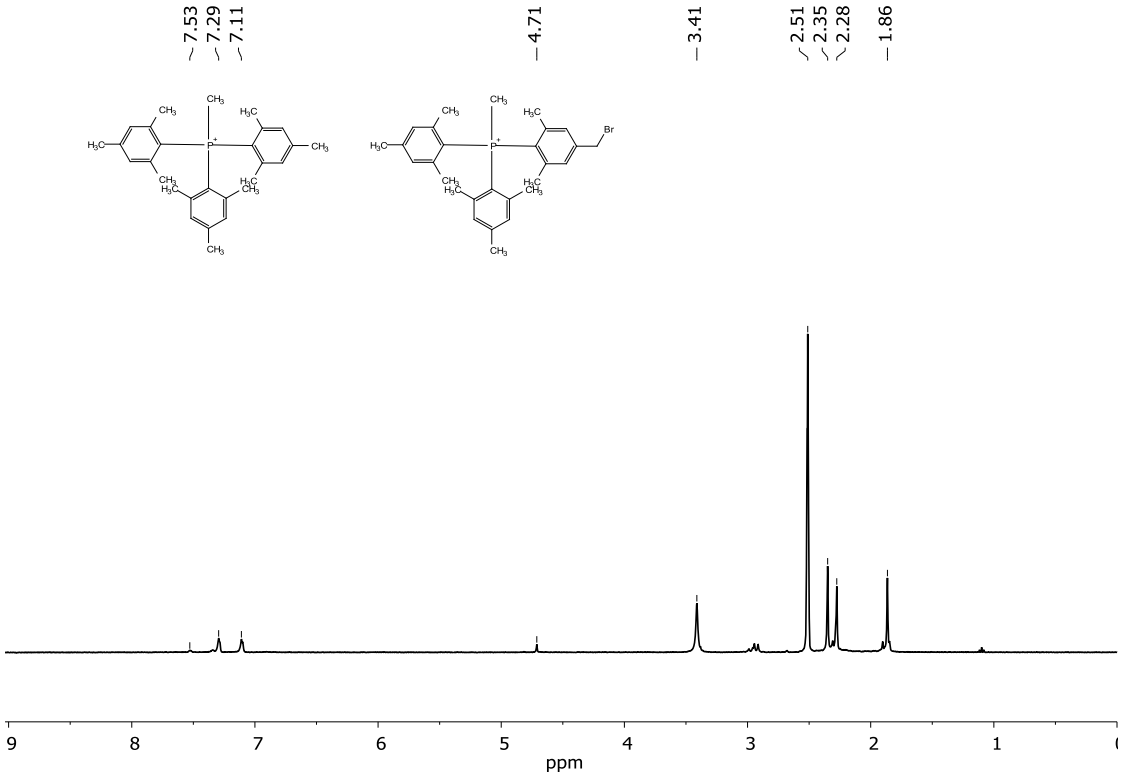

Figure B2: ^{1}H NMR spectroscopy of the products of entry 9 at a milligram scale. The peak at 4.71 ppm is attributed to the brominated methylene group.

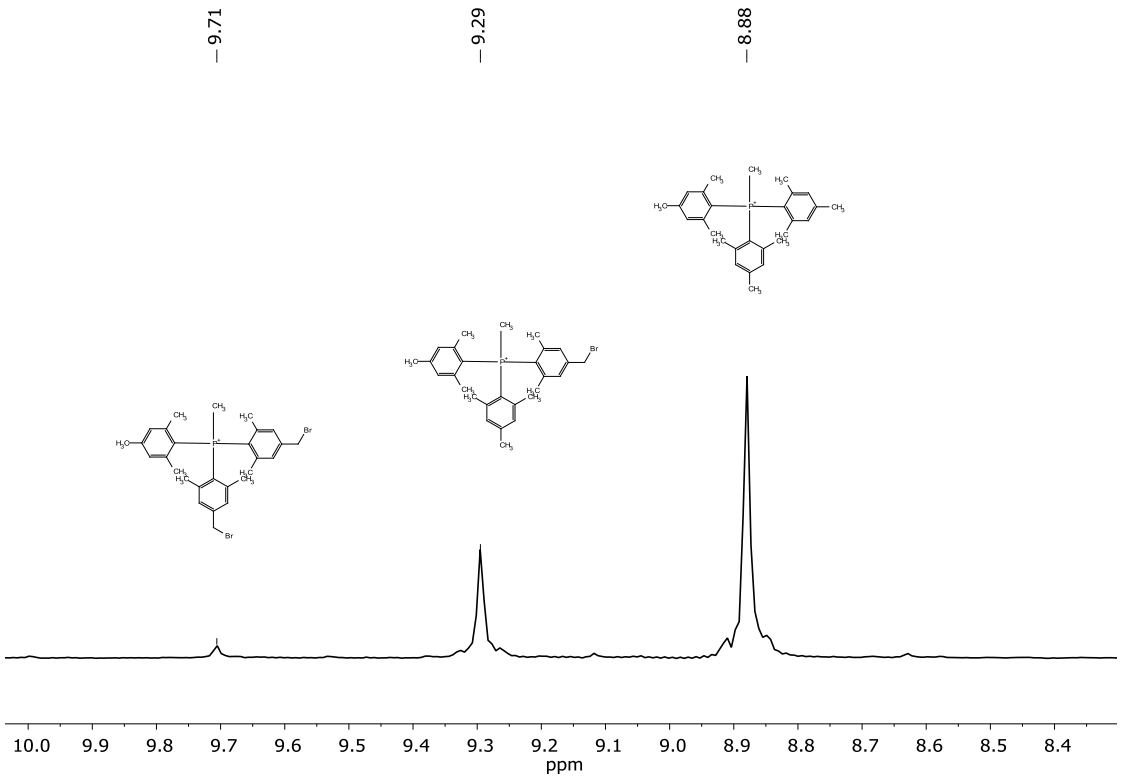

Figure B3: ^{31}H NMR spectroscopy of the products of entry 9 at a larger gram scale. The peak at 9.71 ppm indicates multiple bromination TTMePP^{+}.

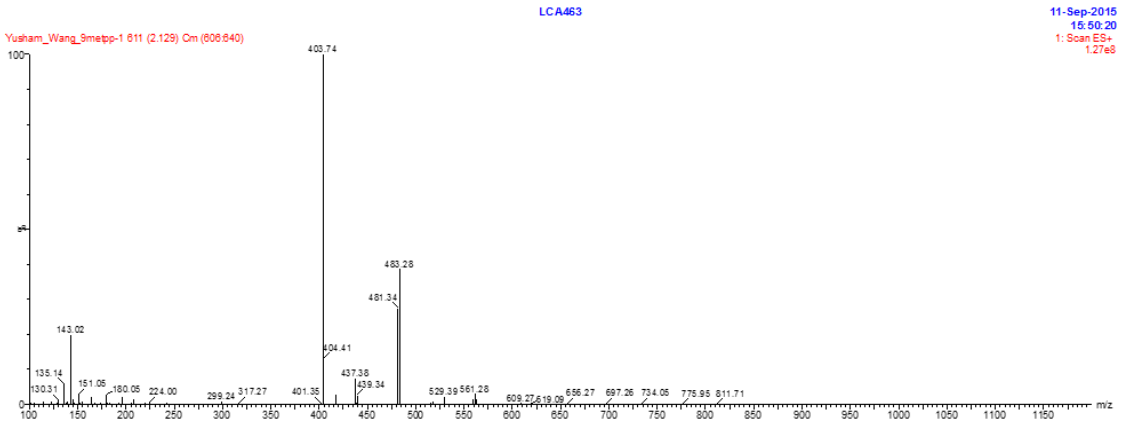

Figure B4: Mass spectrometry of bromination reaction products. m/z 403 was attributed to the non-brominated TTMePP^{+}, m/z 481 and 483 were attributed to the single brominated TTMePP^{+}, while m/z 561 was attributed the double brominated TTMePP^{+}.

Appendix C

SUPPLEMENTARY TABLES

C.1 Literature sources for Figure 4.4

Table C1: Literature sources for Figure 4.4. Area specific resistance (ASR) are measured in different electrolytes, and the cell configurations are different for different literature.

Membrane	**Area specific resistance (ASR) (Ω cm^2)**	**ASR test condition**	**Thickness (μm)**	**Vanadium permeability (cm^{2}min^{-1})**
Nafion 115*	0.26	3 S	125	1.09×10^{-6}
TTMPP-PBI-3/PTFE*	0.24	3 S	20	3.37×10^{-8}
F6PBI*	0.47	3 S	20	3.00×10^{-9}
SPEEK 40[126]	1.22	1.5 V & 3 S	90	3.6×10^{-8}
SPEEK 60[126]	1.23	1.5 V & 3 S	90	2.12×10^{-7}
Nafion 115[126]	0.95	1.5 V & 3 S	127	7.95×10^{-7}
N/S[257]	1.6	1.5 V & 3 S	100	1.928×10^{-7}
Nafion[258]	1.14	1 V & 2.5 S	215	3.69×10^{-6}
Nafion/Si/Ti[258]	1.26	1 V & 2.5 S	225	4.3×10^{-7}
Nafion 212[259]	0.6	1.5 V & 2 S	50	8.23×10^{-7}
SPEEK/TPA/PP[259]	1.3	1.5 V & 2 S	240	4.78×10^{-7}
porous PBI-18[104]	0.16	3 S	18	7.43×10^{-9}
porous PBI-34[104]	0.54	3 S	34	8.41×10^{-9}
porous PBI-68[104]	0.67	3 S	68	8.4×10^{-9}
Nafion 115[104]	0.95	3 S	125	7.01×10^{-7}
Nafion 115[128]	0.19	3 S	127	3.48×10^{-7}
mPBI[128]	0.46	3 S	27	2.86×10^{-9}

BIpPBI[128]	0.2	3 S	27	3.45×10^{-8}

*: data collected in this work.
S: sulfuric acid, for example, 1 S means 1 M H_2SO_4.
V: vanadium, for example, 1 V means 1 M vanadium.